ELECTRO-FLUORESCENCE CHARACTERIZATION OF OXIDATIVE AND REDUCTIVE

DESORPTON OF THIOL MONOLAYERS

by

Amanda   Musgrove

B.Sc., University of Alberta, 2003

A THESIS SUBMITTED IN PARTIAL FULFILMENT OF

THE REQUIREMENTS FOR THE DEGREE OF

MASTER OF SCIENCE

in

THE FACULTY OF GRADUATE STUDIES

CHEMISTRY

THE UNIVERSITY OF BRITISH COLUMBIA

December 2005

Abstract

The electro-fluorescence microscopy technique was used to characterize the oxidative and reductive desorption behavior of fluorescent-tagged thiol self-assembled monolayers on a polycrystalline gold electrode. Effects of pH and thiol alkyl chain length on desorption potential and fluorescence behavior were studied. The use of an alternating 'base-step' potential was established in order to eliminate uncertainty in capacitance measurements arising from charge-transfer reactions (H_2 evolution or gold oxidation) occurring at more extreme potential values. The potential of monolayer desorption, here defined as the potential at which the capacitance of the electrode interface begins to change rapidly with potential, was found to be affected by solution pH. Electrolyte solutions with a higher pH required a lower potential to desorb the thiol monolayers. An increase in fluorescence intensity at the electrode surface accompanied the change in capacitance, confirming that the thiol molecules are migrating away from the electrode. Evidence of oxidative readsorption following reduction of the monolayer was also observed, both by the associated decrease in capacitance and a dramatic decrease in fluorescence intensity. Fluorescence intensity during oxidative desorption was found to be linked to the pH of the environment surrounding the electrode surface. Lower fluorescence intensity was associated with a decrease in solution pH, and was also observed at the step (oxidizing) potential. The decrease in fluorescence at the step potential is believed to be linked to a local decrease in electrolyte pH at the electrode surface due to the oxidation of gold. The oxidation products are expected to be less soluble in acidic media, causing aggregation and self-quenching of the BODIPY fluorophore used. On return to the base potential, the local pH was returned to the bulk solution pH, and fluorescence was restored. At all pH values studied, a more extreme potential was required to desorb the thiol with the longer alkyl chain (16 carbon atoms) than the shorter-chain thiol studied (10 carbon atoms).

Table Of Contents

Table of Figures

Acknowledgments

No project as large as a thesis research project can be completed without support from others. I owe a debt of gratitude to many people who have helped along the way, by providing insight, guidance, skill, or simply by being there for moral support. Thanks to everyone who has been there for me.

I would like to recognize especially Professor Dan Bizzotto, my supervisor. Dan, your support and patience through this maze has been incredible. It would have been an even more difficult journey without your guidance. Thank you.

As well, to the members of the Bizzotto group I have had the pleasure of working with, past and present: Robin Stoodley, Aya Sode, Jeff Shepherd, John Agak, and Emily Chung, your assistance has been invaluable, and it has been a true pleasure working with you.

Thank you also to the staff of the electronic, mechanical, and glassblowing shops for their valued services.

Finally, a thank you to my family and friends, for their support and company throughout my studies, especially to my parents for their encouragement, and to my husband, Laurent, for supporting me through long hours in the working lab and writing.

1   Introduction

The technique of modification of metal surfaces with organic molecules has many uses, from model surfaces in research to control of surface wetting or chemical resistance. Though several methods for modifying metal surfaces exist, such as Langmuir-Blodgett deposition [1], or gas-phase deposition [2], self-assembly of thiol molecules from a solution is the most common method[3]. Though self assembled monolayers (SAMs) of thiols have been studied on such diverse surfaces as platinum[4], iron[5], copper and silver[6], mercury[7], and glassy carbon[8], gold is the most commonly used substrate. The stability of gold over a wide range of conditions, as well as its availability as a well-studied material combine with the strong affinity of the thiol molecules to make an ideal system for forming robust monolayers. The flexibility of the thiol molecules themselves also contributes to the popularity of this system, as virtually any organic moiety desired can be attached to the -SH group and therefore tethered to the substrate. This 'molecular glue' technique has been explored for the formation of biological receptors and enzymatic biosensors [9]. Gaining electrochemical control over the substrate and monolayer affords more opportunities, however. It has been found that application of potentials outside a certain window of stability for a given system will result in the removal of the thiol molecule[10]. Exploitation of this behavior to produce a sensor array has already been reported [11][12]. This was effected by creating an array of electrodes, each individually potential-controlled, in a flow cell. As a thiol solution was passed through the cell, any electrodes not desired to be coated in the thiol were held at a desorption potential, thus allowing only the selected electrodes to accumulate a thiol monolayer. The process is repeated until all electrodes are covered in thiol layers.

SAMs have also been explored for use in molecular electronics [3]. A thorough understanding of their behavior as electrical potentials are applied to them is obviously useful for design and control of such devices. Applications directly to electrochemistry include use of thiol SAMs for blocking of electron transfer, for example, in corrosion prevention[5]. The ability to selectively allow and block electron transfer reactions at the electrode surface via desorption and readsorption of thiol molecules would be a powerful tool as well. The uses of thiol SAMs under electrochemical control are many, and the studies of this thesis work towards a fuller understanding, and therefore a greater control of this system.

1.1 Objectives

The focus of work in our laboratory has been the spectroelectrochemical characterization of insoluble surfactants on electrode surfaces. This continues with the studies encompassed in this thesis, though the focus is on the study of a thiol self assembled monolayer, rather than a physically adsorbed monolayer. More and more attention in the literature is being drawn to studies of SAMs, due in part to their robustness and many immediate applications, as outlined previously. Previous work done in our lab [13][14] showed that the techniques used to study physically adsorbed systems carry over well to the chemically adsorbed SAMs. Observations on the selectivity of the reductive desorption of the thiol monolayers were also made, but the properties of the oxidative desorption were left unstudied. To that end, the studies in this thesis were carried out to characterize the response of the thiol SAMs to oxidizing potentials using the electro-fluorescence technique. Studies were performed on two

related thiols in order to assess changes related to chain length on oxidation, and at several solution pHs to study the effects of solubility and acidity.

1.2 Scope of the Thesis

The work presented in this thesis represents a large body of knowledge from several disciplines, including electrochemistry and microscopy. The second chapter of this thesis will endeavor to provide the fundamental theoretical background necessary to the understanding of the material presented herein. Required background in the electrochemical double layer, mechanisms of monolayer adsorption, and fluorescence are included, as well as a review of essential microscopy information. This leads to a brief review of some previous literature relevant to the topic of this thesis, including a more in-depth presentation of the electrochemical properties of thiol SAMs, fluorescence behavior near metal surfaces, and the electro-fluorescence technique.

After this background, the experimental procedures are reported in Chapter 4, followed by a presentation and discussion of the results obtained thereby. A summary and conclusions are given, as well as some suggestions for future work in this area.

2   Theoretical Background

In order to facilitate a more complete understanding of the research presented in this thesis, a brief theoretical background is provided in this chapter. Topics discussed include an introduction to the electrical double layer, adsorption of organics on electrode surfaces, and environmental factors affecting fluorescence of molecules.

2.1 The Electrical Double Layer

In many branches of chemistry, the reactions of interest take place at the boundary between two phases. In electrochemistry, the boundary of interest is the electrode-solution interface. Several theories have been developed over the years to describe the behavior of solvent and electrolyte molecules near this boundary, the most applicable of which is the Gouy-Chapman-Stern theory, introduced in the following sections.

2.1.1 Simple Capacitors

The most basic capacitor is simply two parallel metal plates separated by a fixed distance. The space between them may be vacuum, or be filled with a dielectric medium. When a voltage is applied across these plates, charge will accumulate on them according to the equation:

$$q = E \cdot C \qquad\qquad (2.1)$$

4

where q is the accumulated charge in coulombs (C), E is the applied potential in volts (V), and C is the capacitance of the capacitor, measured in farads (F). For a given capacitor, C depends on the distance between the plates (d, in m) and the relative permittivity of the material between them (ϵ, unitless), as well as the permittivity of free space (ϵ_o, 8.854 x 10^{-12} C^2/ Jm) in the following relation:

$$C = \frac{\epsilon \cdot \epsilon_o}{d} \qquad (2.2)$$

Altering the potential applied across a capacitor will cause a charging current to flow to compensate for this change:

$$C \left(\frac{dE}{dt}\right) = \frac{dq}{dt} = i \qquad (2.3)$$

where i is the *capacitive current*, measured in amperes (A). This current will be present at all times when the potential applied across a capacitor is changing, and is separate from the current arising from electron transfer through a circuit. The total capacitance of a group of capacitors connected in series is given by:

$$\frac{1}{C_{series}} = \frac{1}{C_1} + \frac{1}{C_2} + \frac{1}{C_3} + \dots \qquad (2.4)$$

where C_{series} is the representative capacitance of the capacitor series, and C_1, C_2, etc are the capacitances of the individual capacitors. For a set of capacitors connected in parallel, the total capacitance ($C_{parallel}$) is given by the sum of the individual capacitances:

5

$$C_{parallel} = C_1 + C_2 + C_3 + \ldots \tag{2.5}$$

In some sets of conditions, real electrodes exist in a state where no electron transfer reactions (oxidation/reduction) are taking place. An electrode in such a state is termed an *ideally polarized electrode*, or IPE. One example of such a situation is a clean Au electrode in a deoxygenated $KClO_4$ solution. Between the potentials at which hydrogen evolution and gold oxide formation occur, the behavior of the electrode may be approximated by that of an IPE. Since no charge is transferred, though potential is applied to the electrode, it behaves as a simple capacitor through this IPE region. Though no reactions occur at the electrode surface, changes such as the orientation of solvent molecules, or adsorption and desorption of molecules can occur, which can alter the capacitance of the IPE-solution interface and induce the flow of charging currents.

2.1.2 Capacitance of the Electrode-Solution Interface

At a given potential, there may be a charge associated with the metal side of the metal-solution interface, localized on the metal surface. Due to the field produced by this charge, and its electrostatic attractions of the mobile ions in solution, this charge will be balanced by an equal and opposite charge in solution. These two layers of charge in metal and solution, separated by a finite distance, act as a capacitor with capacitance C_{dl}, or the *double-layer capacitance*. The most accepted theories of the structure of the electrode-surface interface were developed successively by Helmholtz, Gouy, Chapman, and Stern [15]. Helmholtz noted the capacitor-like behavior of electrodes in

solution, and proposed that the charge in the solution was distributed in a thin layer at a fixed distance from the electrode surface. Gouy and Chapman extended this theory, stating that since the conductivity of the solution is much lower than that of the metal, the charge on the solution side would therefore be distributed through a larger area. Thus, rather than Helmholtz' thin layer of charge, the solution side of the interface would consist of a *diffuse layer* of ions beginning at the electrode surface and extending into the bulk of the solution.

Stern further refined this theory, taking into account the finite size of ions, suggesting that the minimum distance of a specifically adsorbed (desolvated) ion to the metal surface would be the radius of that ion, thus creating an *inner layer* between the diffuse layer and the metal surface. This arrangement is illustrated in Figure 2-1, where the charge on the metal, located on the left side of the diagram, is q_M. The inner layer is located at distance x_1 from the metal surface, and is designated the *inner Helmholtz plane*, or IHP. The outer Helmholtz plane (OHP), at distance x_2 from the metal surface, marks the inner edge of the diffuse layer and represents the center of the closest approach a solvated ion could make to the electrode surface. The potentials at the IHP and OHP are given by ϕ_1 and ϕ_2, respectively. In order for the interface as a whole to maintain a neutral overall charge, the excess charge density on the solution side (σ_s), as expressed as the sum of the charge densities of the inner and diffuse layers composing it ($\sigma_i + \sigma_d$), must be equal and opposite to the charge density on the metal surface (σ_m). Thus:

$$-\sigma_m = \sigma_s = (\sigma_i + \sigma_d) \tag{2.6}$$
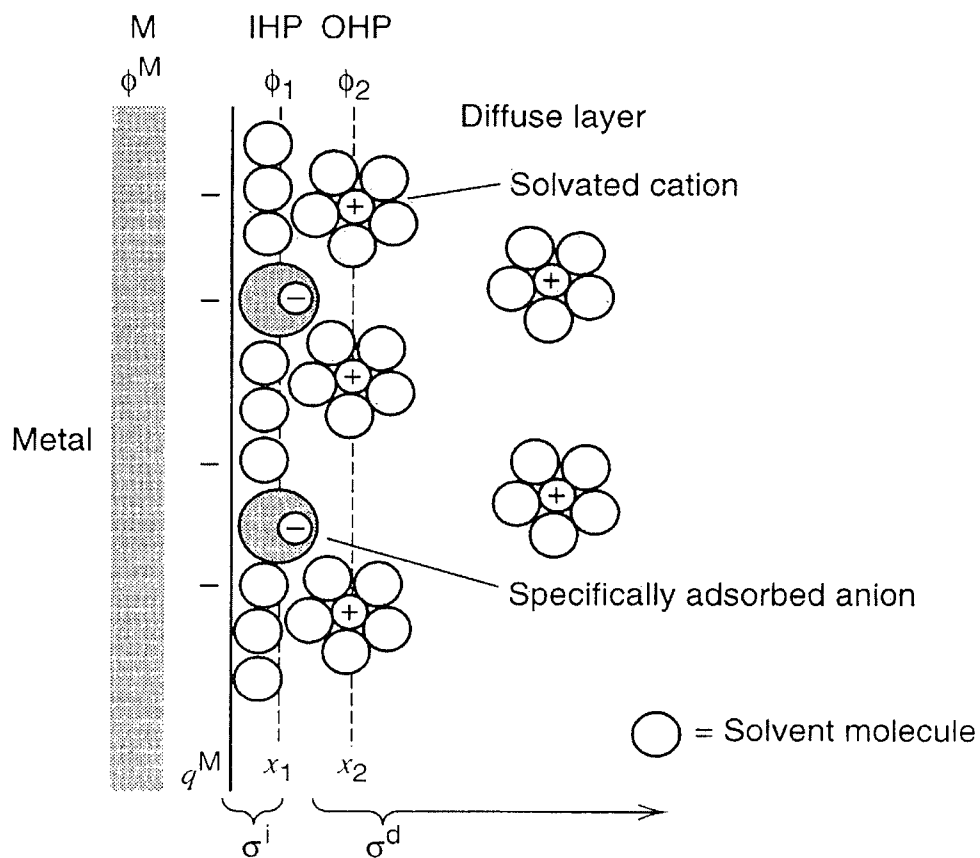
Figure 2-1 Model of the electrical double layer region, including specifically adsorbed anions. The inner Helmholtz plane (IHP) and outer Helmholtz plane (OHP), as well as the potential (ϕ), distance from the metal surface (x) and charge density (σ). Taken from [15].

The total capacitance of the interface can thus be represented by two capacitors in series, that of the inner layer and the diffuse layer.

2.1.3 Quantitative Description of the Electrical Double Layer

The GCS theory is derived fully in [15], considering the double layer in the case where there is no specific adsorption. By approximating the diffuse layer as sequential laminae of constant thickness, starting at the OHP and extending into the bulk of solution, κ, the inverse of the diffuse layer thickness can be calculated as:

$$\kappa = \left(\frac{2n^0 z^2 e^2}{\epsilon \epsilon_0 kT} \right)^{\frac{1}{2}} \tag{2.7}$$

where n^0 is the number concentration of the ions in the bulk (reference lamina), z is the signed charge of the ion, e is the charge on an electron (C), k is the Boltzmann constant (J K^{-1}), and T is the temperature (K). As the ion concentration decreases, κ will increase, implying a thicker diffuse layer. As the assumption has been made that there is no specific adsorption at the electrode, the volume between the beginning of the diffuse layer (the OHP), and the electrode surface is filled with solvent only, and the charge density in this region is zero. Therefore, the potential profile across the double layer is described by:

$$\phi_o = \phi_2 - \left(\frac{d\phi}{dx} \right)_{x=x_2} x_2 \tag{2.8}$$

where ϕ_o is the potential drop from the metal surface across the double layer. This relation is shown graphically in Figure 2-2. The potential drops linearly with distance
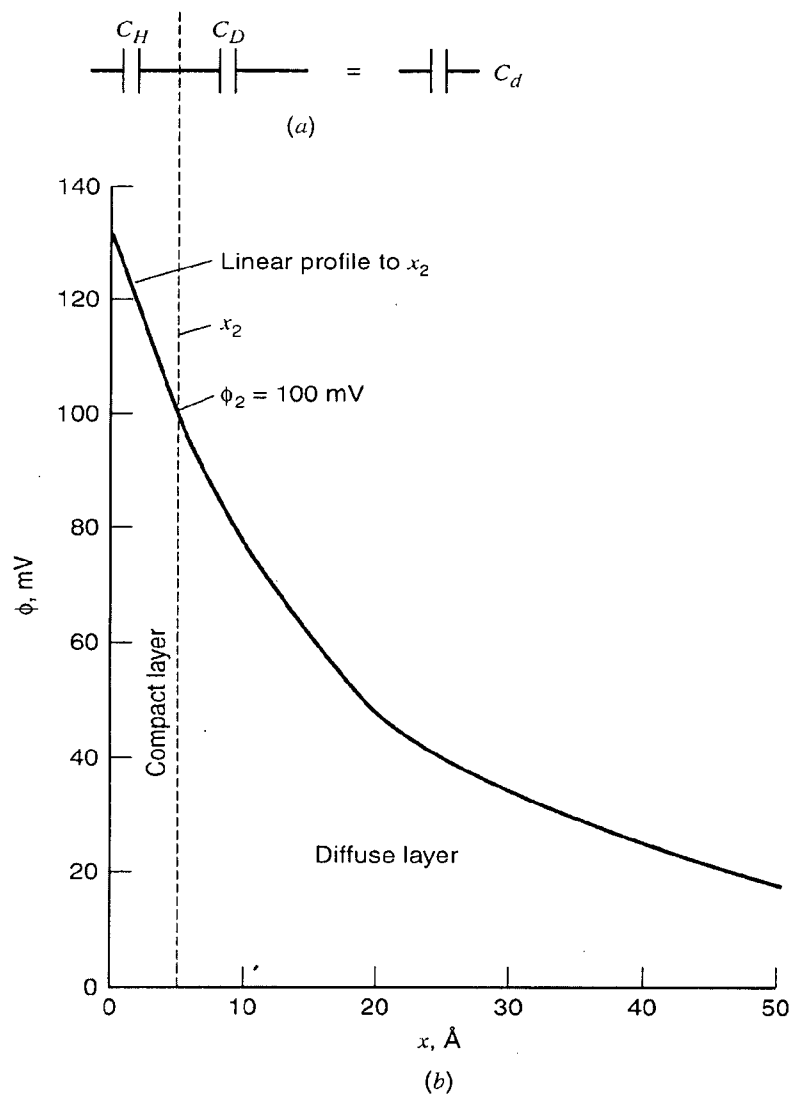
Figure 2-2 (a) Double layer capacitance as modeled by GCS theory, showing C_d as represented by the Helmholtz and diffuse layer capacitances in series. (b) Calculated potential profile of the double layer with a non-specifically adsorbing electrolyte in water at 25°C. Taken from [15].

from the electrode surface to the OHP, and from there declines exponentially into the bulk of solution. By approximating the laminae as a series of Gaussian enclosures, the charge density on the metal can be related to ϕ_o:

$$\sigma^M = \left(8kT\epsilon\epsilon_0 n^0\right)^{\frac{1}{2}} \sinh\left[\frac{ze}{2kT}\left(\phi_0 - \frac{\sigma^M x_2}{\epsilon\epsilon_0}\right)\right]$$ (2.9)

Differentiating σ with respect to ϕ_o, and simplifying yields the capacitance of the double layer:

$$\frac{1}{C_{dl}} = \frac{x_2}{\epsilon\epsilon_0} + \frac{1}{\left(2\epsilon\epsilon_0 z^2 e^2 n^0/kT\right)^{\frac{1}{2}}\cosh\left(ze\,\phi_2/2kT\right)}$$ (2.10)

which bears a strong resemblance to the expression describing two capacitors in series (Equation 2.4). As derived qualitatively in the previous section, the double layer capacitance (C_{dl}) is comprised of the inner layer capacitance (C_h) and the diffuse layer capacitance (C_d). The inner layer capacitance is not potential-dependant, and is essentially constant, behaving as a simple capacitor. For dilute electrolytes, C_d is roughly parabolic with respect to potential, with a minimum at the potential of zero charge (pzc) of the electrode. Because the potential (and charge density) of the metal at the pzc is zero, the charge present in the double layer will be nearly zero. Thus, the diffuse layer capacitance is lowered at this point. Due to the reciprocal nature of the relation between C_{dl}, C_h, and C_d, C_{dl} is dominated by the smallest individual capacitance. Thus, for low electrolyte concentrations, the double layer capacitance will show a minimum value at the pzc.

11

2.2 Self-Assembled Monolayers at the Electrode Surface

Much work in this lab has been dedicated to the study of physically adsorbed

surfactants such as octacedanol onto electrode surfaces [16][17]. A related area that

has been seeing much exposure in research today is that of self-assembled

monolayers (SAMs). Unlike physisorbed monolayers, whose formation is driven mainly

by the reduction of surface tension, SAM formation is additionally driven by the strong

interaction of a functional group in the molecule with the substrate. This interaction

allows the quick and simple formation of a stable, organized monolayer on the metal

surface, without the need for a Langmuir trough or other more difficult techniques. The

postulated mechanisms and theories for the formation and electrochemical destruction

of such layers follows.

2.2.1 Adsorption of alkanethiols

There are many classes of molecule that will form a SAM on a metal surface, such as

thiols, silanes, and organic acids [2]. However, during the course of the experiments

presented in this thesis, only thiol-based SAMs were studied. One of the simplest, and

therefore most studied, thiol molecules is the simple alkanethiol, an alkyl chain

terminated at one end with an S-H group. Figure 2-3 shows decanethiol (C10 thiol), a

molecule similar in structure to the thiols used in the thesis studies. Though other

substrates have been used, including glassy carbon,platinum, iron, silver and copper

[6][8], gold is typically used for such studies, primarily because gold forms a strong

12

bond with the thiols in the SAM, and generally does not undergo any undesirable reactions with the thiol under standard conditions [3].

The adsorption of a thiol molecule onto a gold substrate follows the general reaction:

$$R-SH+Au(0)\rightarrow R-S-Au+(H)$$

(2.11)
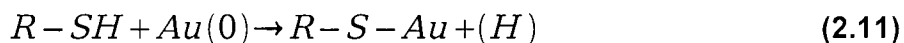
The fate of the hydrogen atom produced is disputed [10], however, It has been suggested that in the thiol solution used for SAM formation H_2O_2 is formed, presumably from a reaction of H_2 formed via the reaction of the thiol and gold with O_2 in solution:

$$2R-SH+2Au+O_2\rightarrow 2R-S-Au+H_2O_2$$

(2.12)
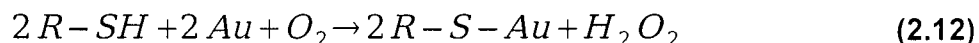
Previous studies have shown [18][19] that the growth of alkanethiol SAMs on gold involves at least two time scale domains in the growth mechanism. The first, fast step saw the contact angle and thickness of the thiol layer reach ~90% of its final value after the first minute of SAM growth. The much slower second step saw the final thickness and contact angle reached over a period of several hours. Figure 2-4 shows the evolution of the thickness of several thiol films with time, measured in-situ via surface plasmon resonance. Figure 2-4(a) shows the short-term development, 2-4(b) the longer term evolution of the layer. It is also postulated that the growth of the monolayers proceeds via an 'islanding' mechanism. In such a mechanism, the thiol molecules adsorb onto the gold surface in a disordered manner. As the surface coverage density increases, small areas of greater order form. These 'islands' grow as the coverage increases (and the number of poorly-ordered defects correspondingly decreases), until the entire surface is covered with a well-ordered layer. Figure 2-5
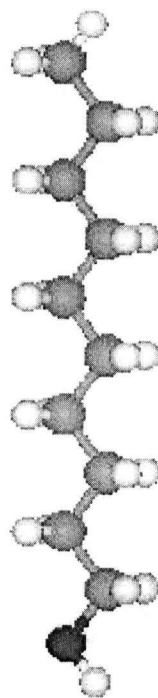
Decanethiol
(C10SH)

Figure 2-3 Ball and stick representation of decanethiol, a molecule similar to the BODIPY-C10-SH thiols used in the studies in this thesis.
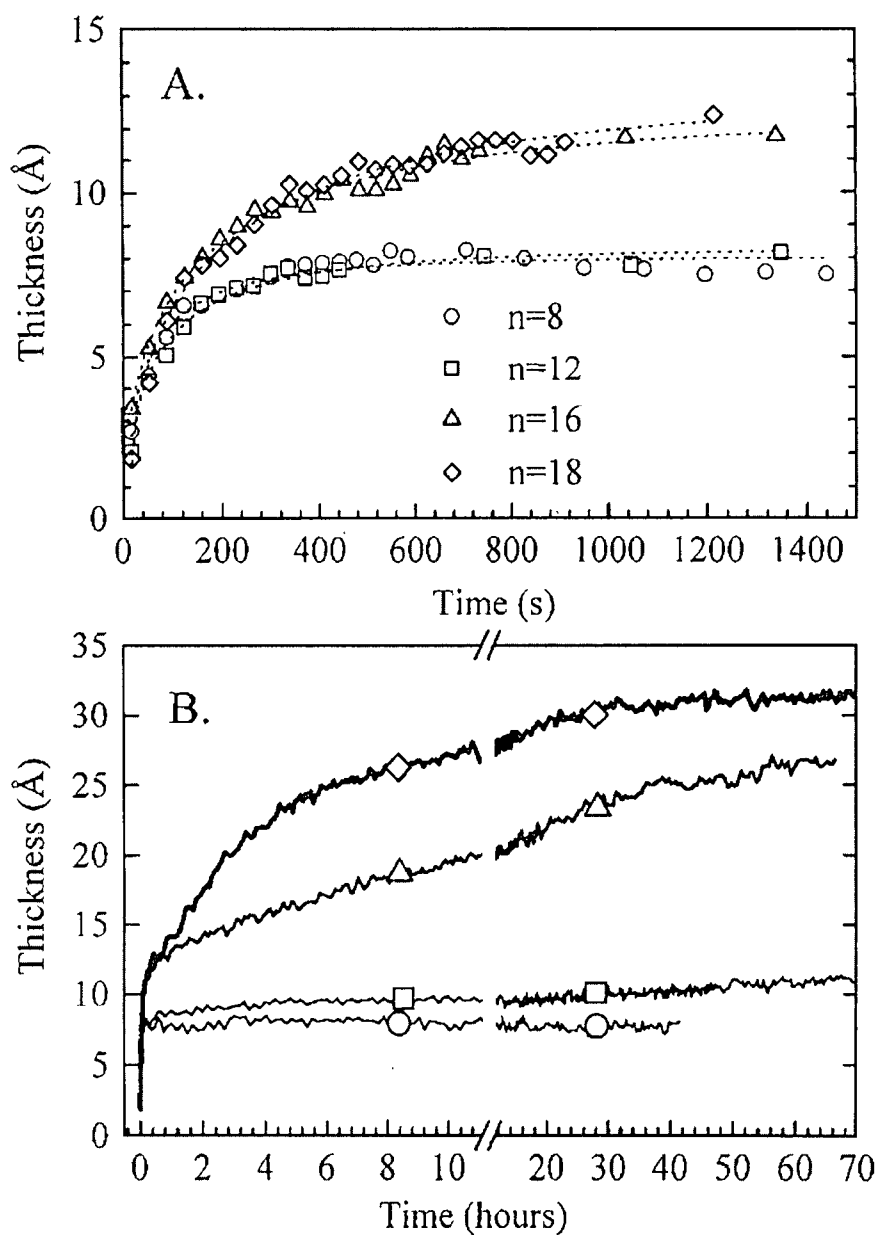
Figure 2-4 Chain-length dependence on formation kinetics for C8 – C18 thiols formed from solution in ethanol, as calculated with surface plasmon resonance measurements. (a) Kinetics at short times. (b) Kinetics on a larger time scale. Figure taken from [2].

shows one possible pathway to monolayer formation using this mechanism. It has also been suggested that the formation of the monolayer begins at high-energy regions of the substrate, such as facet and step edges and defects in the metal surface.

Several other factors can affect the formation of a thiol monolayer, including solvent choice, ambient temperature, and potential of the metal surface during desorption. For n-alkanethiols, use of a solvent in which the thiols are highly soluble, such as ethanol or long hydrocarbons, lowers the rate of monolayer formation, likely due to the strong interaction between the solvent and thiol interfering with adsorption. Conversely, polar liquids in which the alkanethiols are less soluble have been found to promote densely packed layers with fewer defects[20][21]. Again, this is likely due to the interaction between the thiol and the solvent encouraging segregation to the metal surface and enhancing layer formation. Ambient temperature can also play a role in the quality and speed of formation of the layer. Slightly elevated temperatures could encourage the desorption of impurities from the electrode surface as well as increasing the ability of the thiols to rearrange. Controlling the electrochemical potential of the metal during SAM formation is a more recent addition to the arsenal of methods to form more well-organized layers [22]. Weisshaar *et al* found that if the potential of the electrode onto which a thiol SAM was being formed was held at a slight oxidative potential, the SAM would form more quickly and with better order (for the timescale) than for a conventionally-formed SAM.

The presence of the thiol on the electrode surface will also affect the potential decay from the electrode surface and therefore the location of the IHP and OHP. In an ideal

16
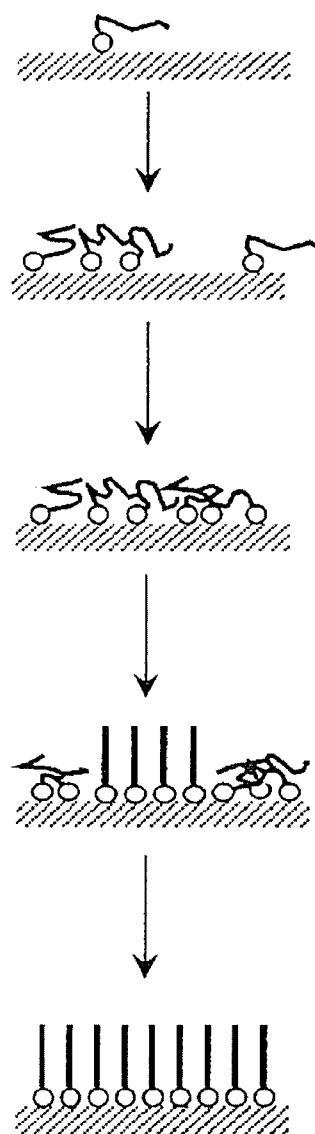
Figure 2-5 Schematic depiction of one possible 'islanding' mechanism of SAM formation, where thiol molecules pass through a 'gas-like' phase, a 'liquid-like' phase, phase where the 'liquid-like' and organized phases coexist, and the final, organized layer. Modified from [2].

situation where the electrode is covered with a perfect monolayer, the IHP will be determined by how close dehydrated ions in solution may approach the electrode surface. If the monolayer is impenetrable (the simplest situation, similar to potentials where the thiol is unperturbed [23]) then the location of the IHP and OHP will be shifted away from the electrode surface by the thickness of the monolayer. The potential drop across the double layer will also be affected by the properties of the molecules in the monolayer, with a more polarizable molecule contributing more to a decrease in potential at the "new" double layer than a less polarizable molecule, based on the model of the interface as a capacitor with the monolayer modelled as a simple dielectric.

2.2.2 Electrochemical Desorption of Alkanethiol SAMs

Both reductive and oxidative desorption of alkanethiol SAMs were first reported in 1991 by Widrig *et al* [10]. Based on the charge consumed, they estimated the reaction occurring at the electrode to be:

$$R-S-Au+1\ e- \rightarrow Au(0)+RS^-$$
(2.13)

forming the thiolate in solution, which is then able to diffuse into the bulk of the electrolyte. This thiolate is free to be oxidatively readsorbed via the reverse reaction. It was also observed that longer chain thiols more readily readsorbed in this way, presumably because they were less soluble in aqueous electrolyte solutions and thus did not diffuse as far from the electrode surface. This has become the generally

accepted form for the electrochemical reduction of thiol SAMs. The potential required to desorb a thiol monolayer was found to be directly related to the chain length of the thiols concerned. Figure 2-6 shows the relation between chain length and desorption potential required to effect reductive desorption.

More recent studies [24] have suggested that the kinetics of the reductive desorption follow two parallel paths: one of thiol removal from along the edges of domains in the monolayer, and one of nucleation and removal inside thiol adsorbate domains. At moderate potentials, both paths coexist relatively equally, but it is believed that at more extreme potentials, the path of domain edge removal is more dominant.

A mechanism for oxidative desorption of the thiol monolayer was also proposed in Widrig's paper. Based on charges integrated from cyclic voltammograms (CVs) recorded at 100mV/sec, the following reactions were proposed for electrochemical oxidation at pH < 4 and pH > 7, respectively:

$$R-S-Au+2H_2O \rightarrow Au(0)+RSO_2H+3e^- +3H^+ \qquad \textbf{(2.14)}$$

$$R-S-Au+2H_2O \rightarrow Au(0)+RSO_2^- +3e^- +4H^+ \qquad \textbf{(2.15)}$$
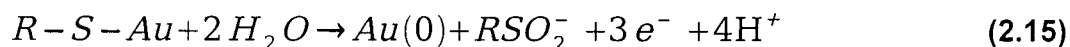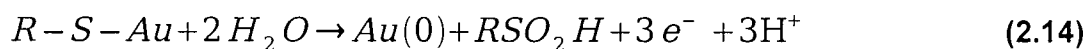
These reactions were supported by measurements of the potential required for oxidation at various pH for a single type of thiol. Figure 2-7 illustrates that there are two regions in which the relationship is roughly linear, pH < 4, with a slope of -52 mV/pH unit, and pH > 7, with a slope of -79 mV/pH unit. These slopes are roughly consistent with the change predicted by the Nernst equation for the 3-and4-hydrogen ion reactions
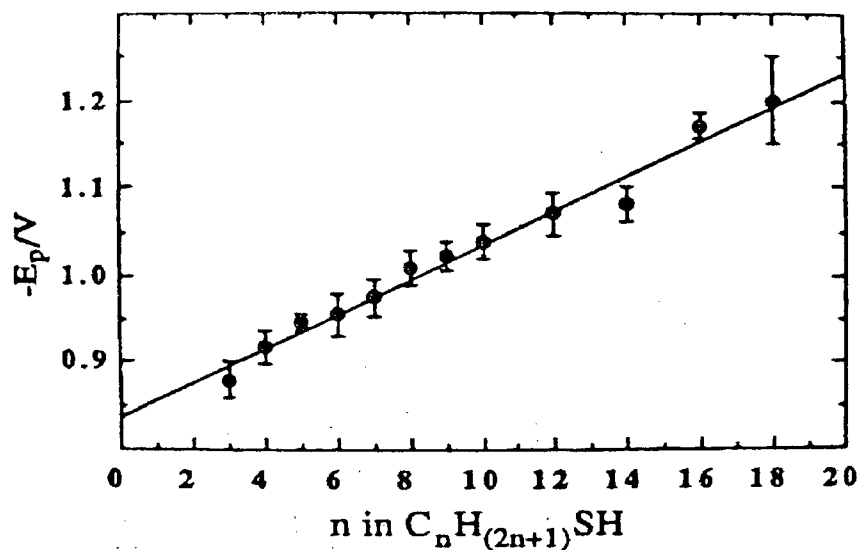
Figure 2-6 Peak potential (vs. Ag/AgCl) of reductive desorption versus thiol chain length for thiol SAMs on Au/mica electrodes, from cyclic voltammograms recorded at 100 mV/s in 0.5 M KOH. Modified from [10].
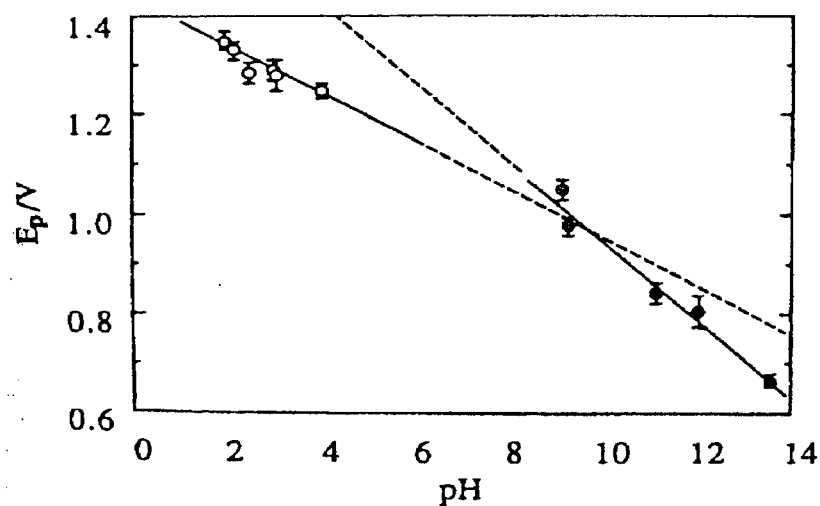
Figure 2-7 Peak potential (vs. Ag/AgCl) of oxidative desorption of n-propanethiol from Au/mica electrodes in H_3PO_4/KOH electrolyte of constant ionic strength. Taken from [10].

proposed above. However, more recent studies on alkanethiols by Morin et al. [25] have suggested that at slower CV scan rates (2mV/sec), the charge transferred in the reaction is more consistent with an 11-electron process. Thus, for a basic electrolyte solution, the following reaction was proposed for electrochemical oxidation:

$$R-CH_2-S-Au+14\,OH^- \rightarrow SO_4^{2-} +RCO_2^- +8H_2O+11\,e^- +Au(0) \qquad \textbf{(2.16)}$$
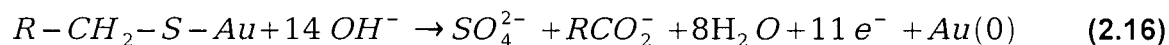
This data was supported by in-situ SNIFTIRS measurements showing the development of bands assigned to the CO stretching of an unprotonated carboxylate group immediately after the electrode potential was increased to the desorption range. Figure 2-8 shows the results of the SNIFTIRS study for oxidative desorption. Which, if either, reaction is most appropriate has not yet been firmly agreed upon in literature as yet[10][25][26][27].

2.3 Factors Affecting Fluorescence

Many variables, from molecular structure to the nature of nearby molecules, can affect the fluorescence of a particular molecule. A few of the factors most relevant to the thesis are summarized in the following sections, including basic fluorescence principles, and the effects of a nearby metal surface on fluorescence, especially relevant for electrochemical studies.
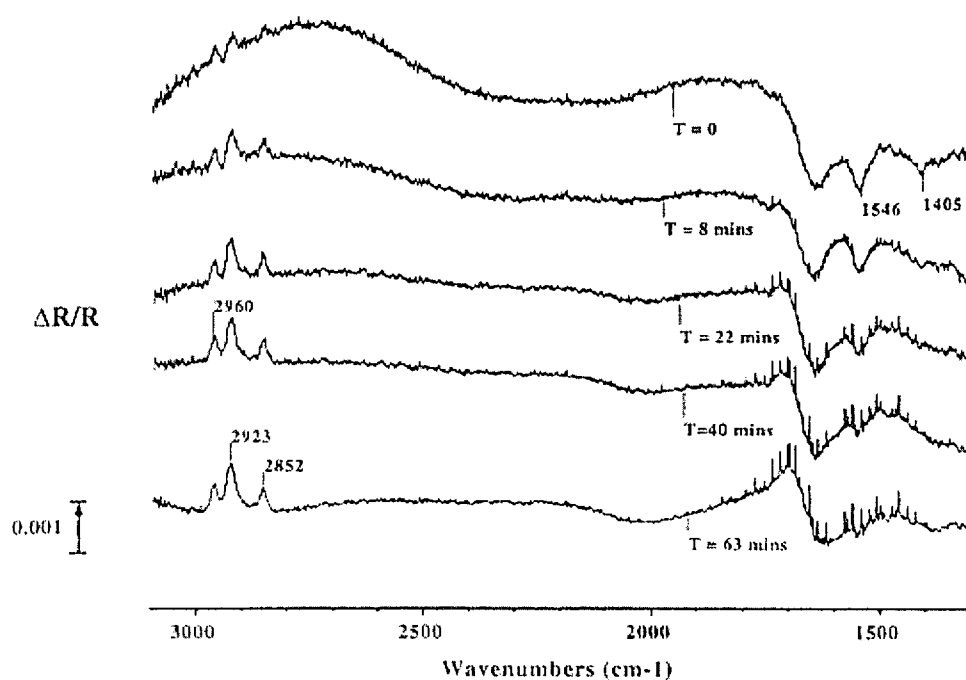
Figure 2-8 SNIFTIRS spectra of a nonanethiol monolayer formed on an Au electrode with time held at +0.60 V/Ag/AgCl. P-polarized light was used. The bands between 2850-2960 are assigned to C-H stretching modes of the adsorbed thiols, while the peaks at 1546 and 1405 cm^{-1} are assigned to the asymmetric and symmetric stretching modes of an unprotonated carboxylate group. Taken from [25].

22

2.3.1 Electronic Transitions and the Franck-Condon Principle

Chemical luminescence arises from the transfer of an electron from a ground state back to the ground state. For a molecule to fluoresce, this excitation is effected by the absorption of light, most commonly in the visible or ultraviolet wavelengths, and the relaxation proceeds via the release of a photon.

The *Franck-Condon Principle* describes which types of transitions are 'allowed', or highly probable, and which are 'forbidden', or highly unlikely to occur. The central assumption of this theory is that, since the nuclei of atoms are much more massive than the electrons, the electronic transition from the ground state to excited state will occur faster than the nuclei can move. This implies that in order for a transition to be favorable, the conditions regulating its probability will be those present in the initial spatial configuration of the molecule, rather than in any new arrangements of the atoms that may occur as a result of the excitation.

The probability of any electronic transition occurring is:

$$|\langle \psi_f^0 | \hat{\boldsymbol{d}} | \psi_i^0 \rangle|^2 \tag{2.17}$$

where Ψ_i and Ψ_f are the wavefunctions of the initial (ground) and final (excited) electronic states, and **d** is the dipole moment operator. The *transition dipole moment*, d_{fl}, is given by:

$$\boldsymbol{d}_{fl} = \langle \psi_{f_\epsilon}^0(r) | \hat{r} | \psi_{i_\epsilon}^0(r) \rangle \langle \psi_{f_v}^0(R) | \psi_{f_v}^0(R) \rangle \tag{2.18}$$

23

where ε and ν represent electronic and vibrational states, and r and R represent electronic and molecular coordinates, respectively. The transition being considered is forbidden when d_{fi} is zero, and transitions for which d_{fi} are non-zero are allowed. The second factor in the equation describes the initial and final vibrational states. Since the intensity of the transition varies with the square of the transition dipole, by the above equation, it can be seen that a stronger intensity will correspond to the strongest overlap in the vibrational states, termed a 'vertical transition' because of its appearance when expressed graphically, as in Figure 2-9.

2.3.2 Fate of the Excited State Molecule

Once a molecule has been raised to an excited state, there are several pathways for the subsequent relaxation to the ground state. A Jablonski diagram is reproduced in Figure 2-10, illustrating several of the possible relaxation pathways. Through the absorption of a photon, an electron is raised from the ground state to an excited state. Due to the quantum mechanical selection rules for electronic excitation, excitations from energy states of the same multiplicity are allowed, while excitation to a differing multiplicity is forbidden. Upon excitation to one of the vibrational levels of an electronic energy level, the molecule may relax to a lower-energy vibrational level through collisions with other molecules. If a fluorescence photon is then emitted, it will be of a lower energy than the excitation photon. This difference in the excitation versus emission photon energy is termed the *Stokes shift*. An alternate path for the relaxation of the molecule is through intersystem crossing, where the molecule transitions from

24
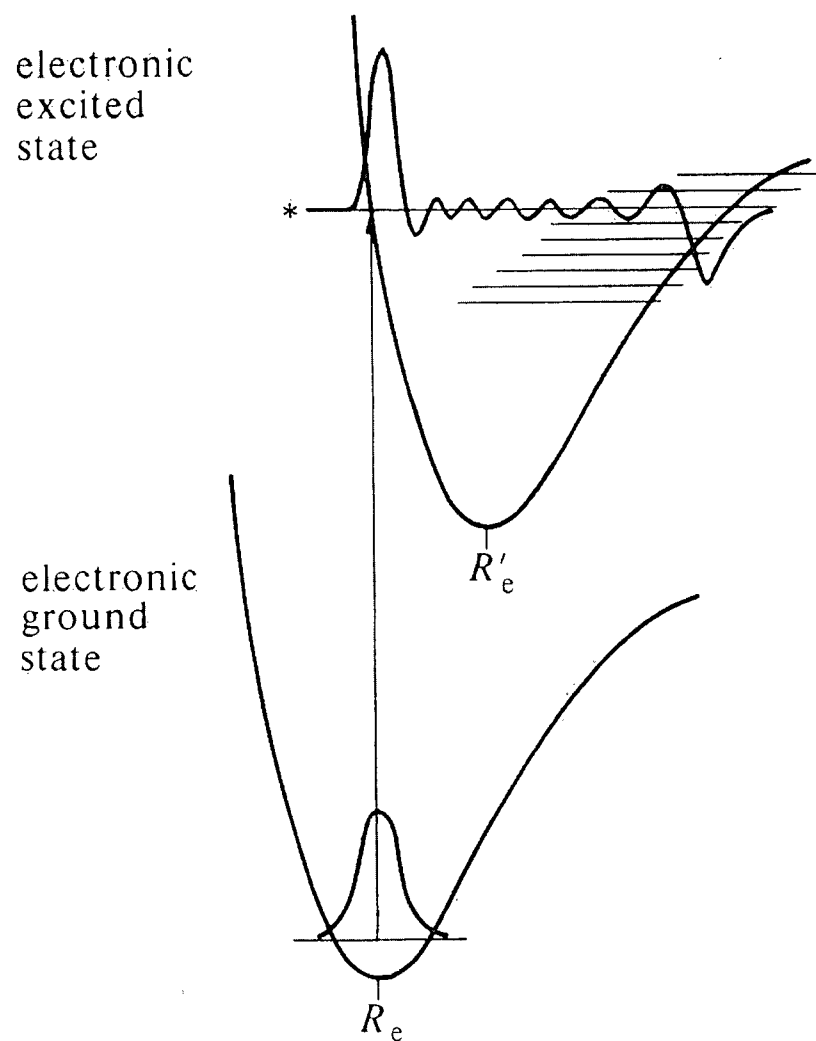
Figure 2-9 Depiction of the vertical transition from the ground electronic state to the excited state. The wavefunctions of the two states must overlap for a transition to be allowed. Taken from [28].
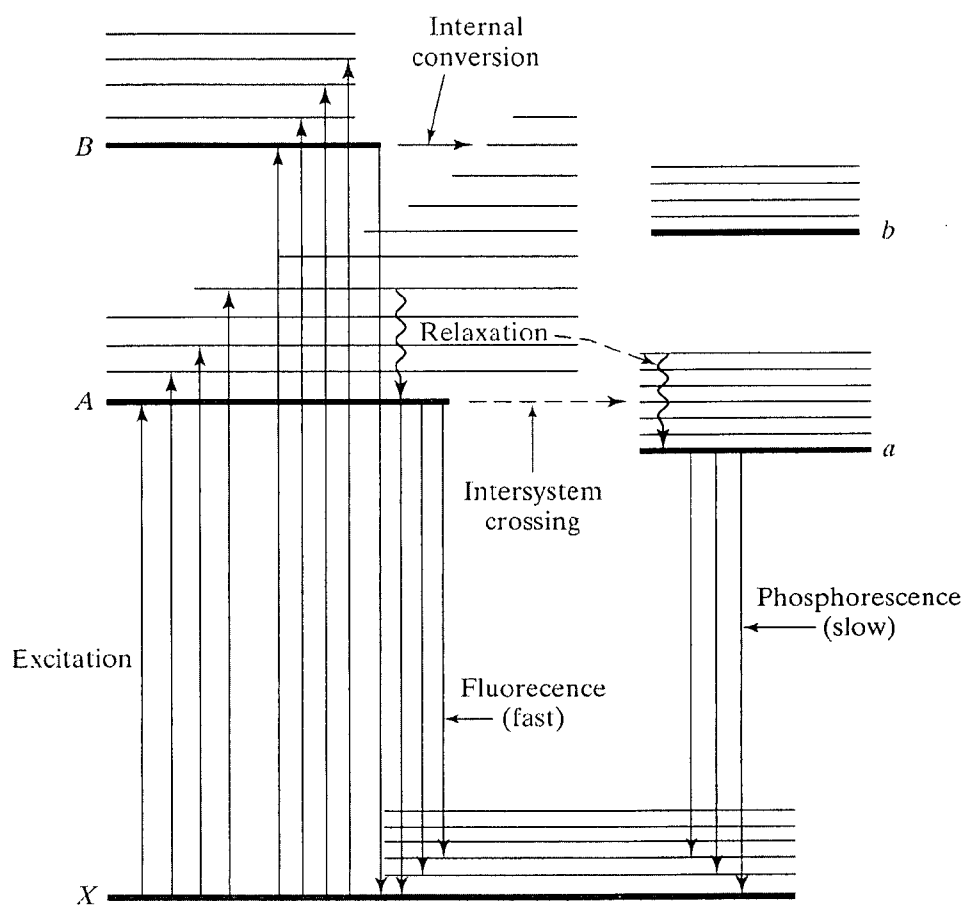
Figure 2-10 A Jablonski diagram depicting some of the possible emission and relaxation processes for electronic excitations. Electronic states A, B, and X have the same multiplicity, while levels a and b share a multiplicity that differs from X. Taken from [29].

26

the singlet to triplet excited state. The molecule may then relax radiatively from this triplet excited state, or phosphoresce. Phosphorescence is a much slower process than fluorescence, taking seconds, minutes, or even hours after excitation before releasing a photon.

Many nonradiative relaxation pathways exist as well. For example, excited molecules are less stable and therefore more reactive than when in their ground states. By extension, it is possible for a fast chemical reaction to occur on a shorter timescale than a slow phosphorescent relaxation. Photobleaching is another, related fate, where fluorescence intensity decreases with increasing exposure to the excitation wavelength. It is believed that photobleaching results from a photochemical reaction of the excited molecule to form a nonfluorescent product [30]. Most other nonradiative relaxation pathways are included in the general category of quenching. Variables such as temperature, collisions with other molecules, and resonance energy transfer all will cause quenching of fluorescence. Resonance energy transfer in particular is important to the work reported in this thesis, as it can take place between a fluorophore and a nearby metal surface.

2.3.3 Förster Energy Transfer

As mentioned in the previous section, it is possible for one molecule (the sensitizer, S) to transfer electronic excitation energy nonradiatively to another molecule (the acceptor, A). In order for this to occur, there must be significant overlap between the fluorescence spectrum of the sensitizer and the absorbance spectrum of the acceptor, and the

distance between the molecules must be larger than their Van der Waals radii. Additionally, the orientation of their dipoles must be appropriate, as accounted for by an orientation factor. It is believed that the energy transfer takes place between a single donor-acceptor pair, and so dipole-dipole interactions are used. For separation distances from 10-100 Å, the following relation generally holds:

$$k_T = \left(\frac{1}{\tau_s}\right)\left(\frac{R_O}{R}\right)^6 \qquad (2.19)$$

where τ_s is the normal fluorescence lifetime of the sensitizer in the absence of the acceptor, and R is the center-to-center distance between the chromophores. R_o, the *Förster critical distance*, marks the separation at which it is equally likely that the sensitizer will relax through energy transfer with or without the acceptor, that is, 50% of the excitation energy is transferred to the acceptor.

This effect was demonstrated by Drexhage's group, using two cyanine dyes with complimentary fluorescence and absorbance spectra [31]. The first dye, which absorbed in the ultraviolet region and fluoresced in the blue, was deposited onto a glass slide, and covered with layers of a fatty acid as a spacer. The second dye, absorbing in the blue and fluorescing in the yellow, was then deposited onto this coating. Upon exposure to ultraviolet light, it was found that the intensity of the fluorescence from the yellow-emitting dye was proportional to the square of the strength of the 'near-field' electric field produced by the blue-emitting dye. The result of this effect was that while when the dye separation distance was very small, the yellow dye accounted for almost all of the fluorescence intensity, and for separation distances

greater than about 100 Å the yellow dye was essentially non-fluorescing.

2.3.4 Fluorescence Near the Metal Surface

Drexhage and his group performed several other groundbreaking experiments investigating the effect of a metal mirror very near to electronically excited molecules [31][32][33]. For emitter-mirror separations on the order of the emission wavelength, damped oscillation in the fluorescence lifetime was present, which corresponded to simple interference from reflection of the emitter's field. However, at much smaller separations, the lifetime drops sharply, indicating a more complicated interaction with the metal. Figure 2-11 depicts a representative experiment of these effects during an experiment examining Eu^{3+} ions near an Ag mirror.

The quenching of emission at small distances from the mirror arises from a combination of two energy transfer possibilities: lossy surface waves, and surface plasmon polaritons (SPPs). Lossy surface waves, a shortlived and non-radiative excitation, correspond to electron-hole pair excitations in the metal, with scattering of the excited electron. [34] Weber and Egen demonstrated [35] that significant numbers of emitters will decay to form SPPs when adjacent to the metal, and that the relation between distance and energy transfer to SPPs is exponential. The probability of decay through each of the three modes (radiative, lossy waves, and SPPs) varies not only with distance, but also with orientation of the dipole to the metal surface. Image dipoles will form on the surface when the emitter's dipole is in close proximity, and can enhance or subtract from the overall dipole strength, depending on the orientation. Figure 2-12
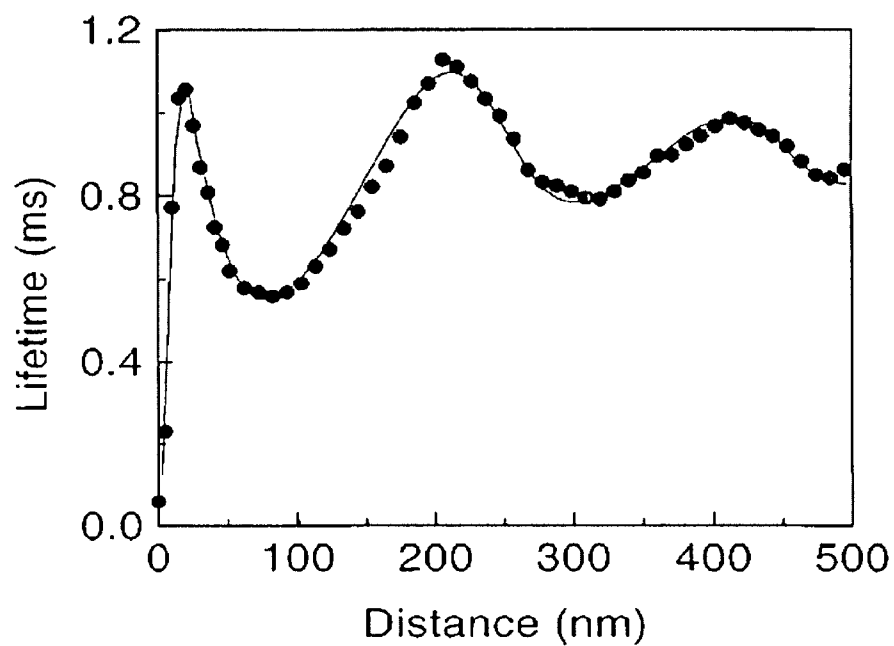
Figure 2-11 Calculated and experimental values for fluorescence lifetime of Eu3+ atoms at varying distances from an Ag mirror. The excited lifetime drops sharply at small metal-ion distances. Taken from [36].
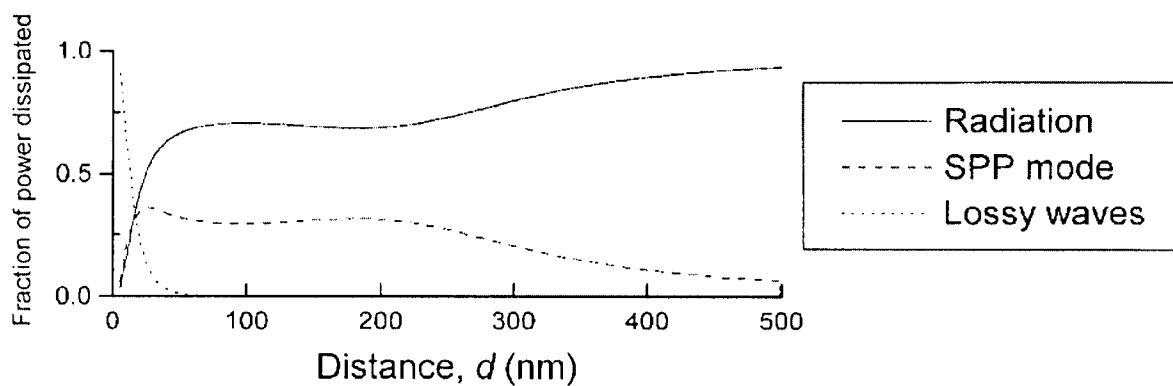
Figure 2-12 Calculated fraction of power dissipated in for an emitter in vacuum above an Ag mirror for an isotropic combination of dipole orientations. Taken from [37].

shows the relative amounts of power dissipated in the three modes by an isotropic combination of dipole orientations, at varying distance. The relation of the lifetime to separation distance (d) has been experimentally and theoretically found to be close to d^{-4} [37], implying that the quenching process arises from the metal surface, eg. by formation of an electron-hole pair. In order to accommodate this, either a continuously varying dielectric for the metal or a selvedge region, where the properties near the surface are different from the bulk, must be assumed. The d^{-4} dependence of the energy transfer is similar to the dependence based on a Förster transfer from a single donor to a 2-dimensional array of acceptors [37]. The type of metal and its surface properties, especially roughness, will also affect the decay behavior of the emitter, to a degree.

As demonstrated briefly here, there are many factors that can affect fluorescence in the electrochemical environment. Chemical factors, such as nearby molecules can donate or accept electronic excitation energy, or a photobleaching reaction can reduce the detectable fluorescence. As well, the presence of a metal surface such as an electrode can reduce fluorescence lifetime by up to a factor of up to $\sim 10^6$ when the emitter is located at the electrode surface, with the quenching decreasing with increasing separation from the metal.

2.4 Fluorescence Microscopy

The factors described in the previous section can be manipulated and controlled so that fluorophores behave in a reasonably well-defined manner. Fluorescence microscopy is

the incarnation of this technique, and is most frequently used in biological laboratories, where fluorescently tagging a cellular structure or product has been in practice for many years. This section will review an application of the fluorescence microscopy technique as an in-situ monitoring technique for electrochemistry.

2.4.1 The BODIPY fluorophore [38]

BODIPY (4,4-difluoro-4-bora-3a,4a-diaza-s-indacene) is a versatile fluorophore that has an absorption maximum at ~500 nm and an emission wavelength of ~510 nm, both of which can be easily altered by adding substituents to the core fluorophore. An entire range of BODIPY-based fluorophores are currently commercially available from Molecular Probes, Inc., with emission wavelengths from 503-616 nm.

The attractive characteristics of the BODIPY fluorophore are its narrow absorption and emission bandwidth, high extinction coefficient ($>80\ 000$ cm^{-1} M^{-1}), stability, and the ease of controlling the absorbance and emission maxima simply by controlling the substituents on the fluorophore. The fluorophore itself has been previously reported to be insensitive to changes in solution pH [39][40], however, many "on-off" fluorescent pH probes have been fashioned based on the BODIPY fluorophore by choosing a substituent that is itself pH sensitive and will control the fluorescence properties of the BODIPY moiety itself through a shift in the frontier molecular orbital energies that encourages nonradiative relaxation over fluorescence. [41][42][43]
BODIPY dyes have also been shown to interact with other nearby BODIPY molecules. In high local concentrations, the fluorophores form excimers with a red-shifted

fluorescence wavelength. [44] This behavior has been explored for use in microsphere-contained probes, where quenching interactions between the dye molecules and environment outside the sphere environment are small, though the proximity of the dye molecules can cause shifting of their spectra. [45] The fluorophores can also 'self-quench' through fluorescence resonance energy transfer (FRET) [46][47][48]. This property is usually used in cellular studies, where the dye aggregates in specific regions within the cell and is quenched, and fluorescence is restored as the dye is freed by transport within the cell or destruction of the organelle in which they were held. Da Poian *et al* observed a 97% decrease in the BODIPY fluorescence, attributed to FRET, in their study of viral disassembly in cells. [49]

2.5 Epi-Fluorescence Microscopy

2.5.1 Anatomy of the Epi-Fluorescence Microscope

Epi-Fluorescence Microscopy uses a microscope in the inverted configuration, with the objective as well as the light source below the sample. Excitation is through a lamp or laser generally mounted at the rear of the microscope. The excitation light, typically visible or UV wavelengths, is passed through a filter cube consisting of three major filters. The exciter filter allows the excitation wavelength to pass through to a dichroic filter, which then reflects it through the objective lens and onto the sample. Fluorescence from the sample is gathered through the objective, and passes through the dichroic filter, and through a barrier filter, which removes any excitation light not reflected by the dichroic filter, allowing only the fluorescence light to pass through. The

fluorescence light is then directed to the detector, usually a camera or charge coupled device (CCD) array. A coupler is frequently used between the filter cube and detector in order to maximize the use of the detector's photosensitive area. A schematic of the light pathway is included in Figure 2-13, and an example of the transmission spectra for a typical filter cube is shown in Figure 2-14.

2.5.2 Resolution

Resolution, as related to microscopy, is defined as the ability of the microscope to render two features in close proximity on the sample distinguishable from each other (ref. OED). The microscope allows the user to distinguish the features in two ways, the most basic being simple magnification. The lenses in the objective and eyepieces allow a closer view of the sample through the simple magnification of the sample image. At high magnifications, however, the second method becomes more important. When light from a source, such as a small slit, passes through the objective, there is some diffraction of the light, resulting in a diffraction pattern called an *Airy disk*. The Airy disk diffraction pattern is shown in Figure 2-15, and consists of a central circle of intensity surrounded by rings of decreasing intensity. The maximum resolution of an objective is determined by its ability to separate two Airy disks from sources in close proximity to each other. Figure 2-15(d) shows two Airy disks at the limit of resolution, while 2-15(e) shows two disks that are too close together to be resolved. The resolving power of a microscope may be improved by decreasing the diameter of the disks such that the centers of the patterns may be closer together, while the edges of the central circles are far enough apart to remain separate. This is generally done by choosing objectives with

a large *numerical aperture* (NA), as defined by the following:

$$NA = n(\sin\theta)$$ (2.20)

where n is the refractive index of the material between the sample and the objective, and θ is the angle formed between the objective lens normal and the most oblique light ray captured by the objective. The effect of an increasing NA on resolution is illustrated in Figure 2-15(a-c), where the Airy disks resulting from objectives with increasing NA are depicted. The Airy disk from (c), resulting from the objective with the highest NA, has the sharpest profile and thus the smallest size and will give the highest resolution.
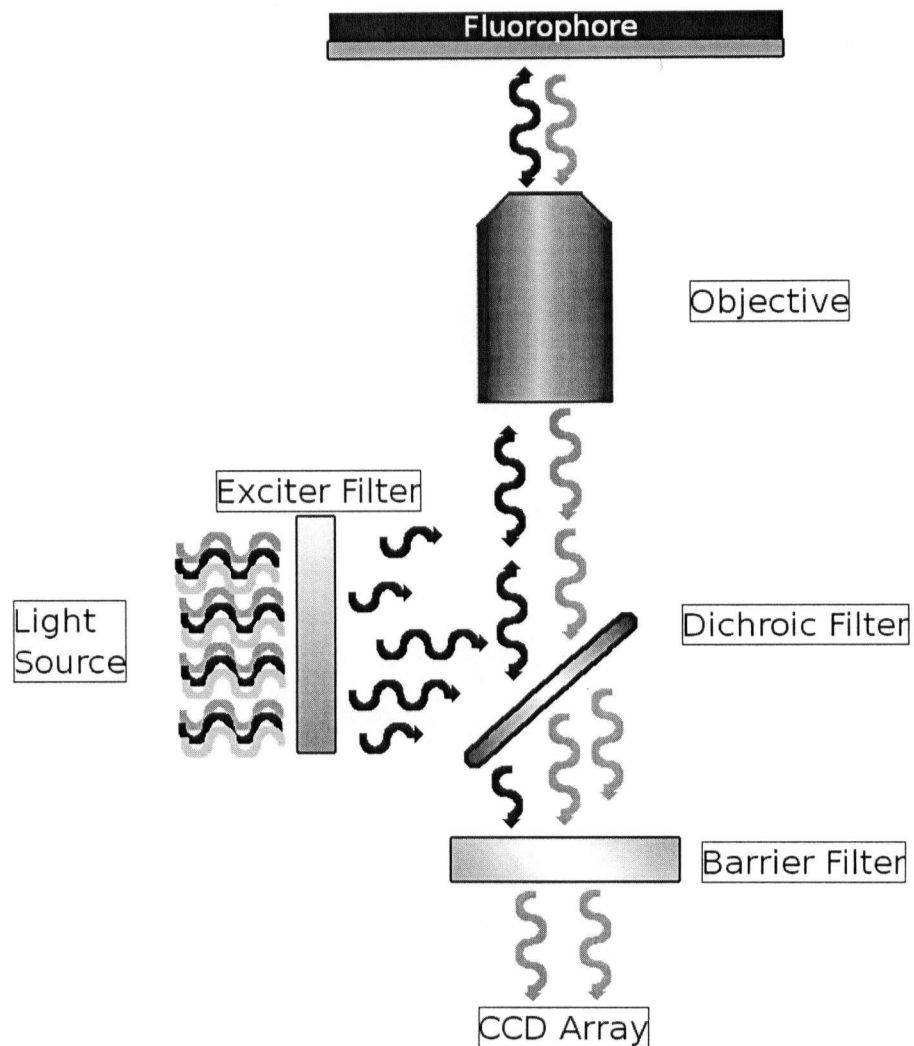
Figure 2-13 Schematic of pathway of light through an epi-fluorescence microscope. The light is passed through an exciter filter selecting the desired wavelength. The light is then reflected from a dichroic filter through the microscope objective and onto the sample. Fluorescence wavelengths are gathered through the objective, passed through the dichroic filter, which reflects the excitation wavelength, and through a final barrier filter to further isolate the fluorescence wavelengths. The light is then directed onto the CCD.
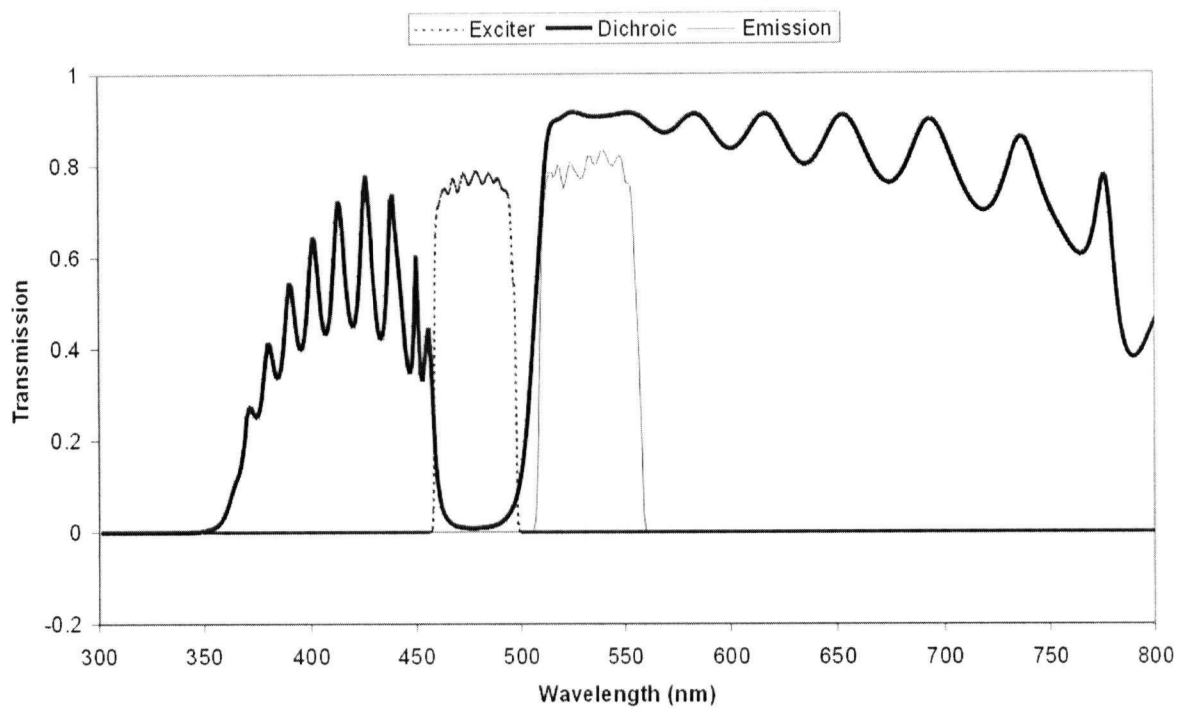
Figure 2-14 Transmission spectra for a filter cube with an exciter, dichroic, and emission filter. Taken from [50].
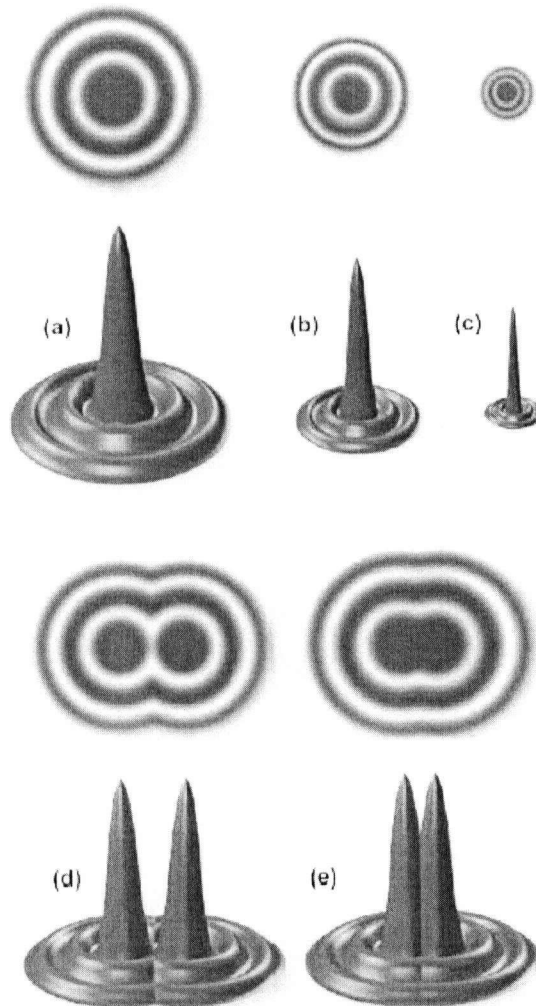
Figure 2-15 (a-c) Airy discs and their corresponding intensity profile (point spread function) with increasing numerical aperture. (d) Two Airy discs (and their intensity profiles) at the limit of resolution. (e) Two Airy discs too close together to be resolved. Taken from [51].

3. Literature Review

The work embodied in this thesis represents a range of topics related to the electrochemistry and desorption of thiol self assembled monolayers (SAMs). The ease of formation and stability of SAMs compared to traditional methods, such as use of Langmuir troughs, opens the way for industrial uses of thiol-modified surfaces, and thus research in the area has been intense. Though many types of SAMs exist, including those formed from silanes, carboxylates, amines and others [3], the most studied system is that of thiols on noble metals, especially gold. The electrochemical behavior of this system has been studied by many researchers, highlights of which are included in this chapter as background to the work presented in this thesis. As well, works on the properties of fluorescent molecules near metal interfaces, and the development of the electro-fluorescence technique are described within.

3.1 Electrochemistry of Thiol SAMs

3.1.1 Desorption Behavior

The electrochemical characterization of thiol monolayers has been of considerable interest to the research community, perhaps because of the control that the modification of the electrode surface can give to the researcher. Finklea *et al.* [23] found that the presence of a SAM of alkanethiols (C_{12} to C_{18}) on an Au electrode strongly inhibited electron transfer reactions on the modified surface. Based on electrochemical oxidation of the gold and electron transfer to a redox pair in solution, it

39

was suggested that electron tunneling through a well-formed monolayer was unlikely, and any Faradaic current would arise at defect sites and 'collapsed' areas in the monolayer.

Though it was known that alkanethiol monolayers could be disrupted thermally, the first report of the electrochemical oxidation and reduction of an alkanethiol monolayer was made by Widrig et al in 1991 [10]. In this study, the electrochemical reduction of alkanethiol monolayers on Au and Ag was observed via cyclic voltammetry as a reduction peak located positive of the potential for solvent reduction. The charge of the reduction, determined by integration of this peak, was determined to be 90 ± 7 $\mu C/cm^2$, and led to the proposed single-electron reaction of the adsorbed thiol to the thiolate anion.

Oxidative desorption was also observed in the same study. From cyclic voltammetry at 100 mV/s, the oxidation of the gold electrode was suppressed, followed by thiol oxidation and partial oxidation of the Au surface at a more positive potential. The effect of pH on the oxidation was studied, leading to the observation of two regions where the potential of thiol oxidation was linear with solution pH, pH < 4 and pH > 7. The slope of these linear regions was approximately consistent with the 3 electron oxidation of the adsorbed thiol to RSO_2H or RSO_2^- at pH < 4 and >7, respectively. A comparison of the charges for oxidation and reduction for thiol monolayers ($\sigma_{OD}/\sigma_{RD} = 3.1 \pm 0.5$) is also consistent with the proposed 3e$^-$ reaction. This proposed reaction has since found support in at least one other study [27]. In this study, Yu et al used Fourier Transform Infrared Reflection-Adsorption Spectroscopy (FTIR-RAS) to examine the oxidation of

azobenzene-alkanethiols. Upon oxidation, peaks assignable to CO_2 and SO_2 stretching modes were developed, in agreement with the predictions from [10] for the solution pH used. The CO_2 produced was believed to be from further oxidation of the products in solution.

Another study by Morin's group focused on both the reductive and oxidative desorptions of thiol monolayers on Au electrodes, using Subtractively Normalized Interfacial Fourier Transform Infrared Spectroscopy (SNIFTIRS) to probe the properties of the electrode-solution interface during the desorptions[25]. The results from the reductive desorption showed an increase in the C-H stretching intensity after desorption, which would imply that the desorbed thiolates are in an organized form, supporting the proposition that hydrophobic structures, such as micelles, are formed upon desorption. In the chosen electrolyte of 0.1M KOH, no S-H stretching was observed, confirming that the desorbed molecules are indeed thiolates at this pH.

The SNIFTIRS and voltammetric studies of the oxidative desorption open room for debate of the mechanism of oxidation, however. Using scan rates of 3 mV/sec and 5 mV/sec, Morin's group determined by integration of cyclic voltammogram peaks that at the slower scan rate, the reduction proceeded by an 11 electron mechanism. At the faster scan rate, the data varied from 3-7 electrons per thiol molecule, suggesting that there may be two mechanisms for oxidation of thiol monolayers. One mechanism may apply for fast potential scan rates, and another for slower rates, where further oxidation may take place at the electrode. As well, from the SNIFTIRS measurements, two bands were observed which were assigned to the stretching modes of COO^-, indicating that

the C-S bond had been broken. This behavior was attributed to a possible two-step process, first breaking the S-Au bond, then involving further oxidation of the product, with the overall result producing SO_4^{2-} and R-COO⁻ from each alkanethiol and using 11e⁻. The authors supported this proposition with previous experimental evidence [52] wherein CO_2 had been produced, suggesting that further oxidation of the desorbed products had occurred. The electrochemical studies of Esplandiú [53] provided a charge associated with the oxidation of roughly 6-9 electrons at 10 mV/s, which agrees more closely with Morin's proposed mechanism of oxidation.

3.1.2 Adsorption and Other Electrochemical Properties

Desorptions are not the only areas of thiol SAM electrochemistry that have attracted attention, however. One of the more interesting aspects of the reductive desorption is the oxidative readsorption that can take place after the initial desorption. Widrig, Chung, and Porter observed partial recovery of the reductively desorbed monolayer via oxidation of the thiolate on the positive scan of their voltammograms, though this re-formed layer was more easily desorbed, and reduced at a slightly higher potential than the original layer [Widrig]. In their 1996 paper, Calvente *et al* [54] studied the interaction between the reductive desorption and subsequent oxidative readsorption of thiol monolayers on gold electrodes. Based on the potential of desorption, they found that the original, spontaneously formed monolayers were more stable than the oxidatively formed ones, suggesting that a reorganization step that occurs during the spontaneous formation is missing in the oxidative reformation of the layers.

42

Further examination by Morin and coworkers explored the effects of pH on the reductive desorption and oxidative readsorption[55]. At pH values greater than the pK_a of the thiol (approximately 10-11 for alkanethiols) , up to 90% of the initial monolayer was oxidatively readsorbed. This high level of recovery was suggested to be the result of high interaction between the desorbed thiolate molecules, such as the formation of a hydrophobic structure inhibiting movement into solution, keeping the desorbed thiolates close to the electrode surface. At pH less than the pK_a of the thiols, where the thiolates would begin to become protonated, the degree of layer recovery is dependent on the solubility of the thiol itself. For example, layers formed from butanethiol had essentially no layer recovery, while hexadacanethiol layers remained at ~90% when pH was decreased from 13.5 to 10.5.

Oxidative deposition has attracted attention for its usefulness in reproducibly modifying electrode surfaces. Lennox and Ma studied the oxidative adsorption of single-component and mixed monolayers formed under potential control in ethanol solution[56]. Layers formed by their method of maintaining the electrode at a favorable potential for the adsorption of thiol resulted in a monolayer that reached optimum order in a short time (15 minutes compared with hours for spontaneous formation). These layers also showed a three-fold lower current when exposed to a redox probe in the electrolyte versus the spontaneously formed monolayers. Though the capacitances for the two types of layers were similar, this decrease in the current passing through the monolayer suggests that the electrochemically-formed layer has a more compact structure. In the studies with the mixed monolayers, the test system of $C_{16}SH$ and $HSC_{15}COOH$ in ethanol was shown to form monolayers where the composition was

43

directly related to the composition of the thiol solution. This is in contrast to the typical spontaneously formed SAM, where one thiol will typically displace another on the electrode surface, making the monolayer composition related not only to the solution composition, but to the deposition time as well. Thus, using electrochemical control when forming thiol monolayers can produce a more reproducible, and possibly superior, monolayer to spontaneously formed layers.

The desorption and adsorption of thiol SAMs have been examined in a number of scanning tunneling microscopy (STM) studies. The formation and structure of adsorbed layers has been extensively studied at many pH and potential conditions [57][58][5][59]. Oxidative and reductive desorption has been studied as well, with several groups examining the reductive behavior of thiol monolayers. [60][61][62] Yang *et al* observed the behavior of a thiol monolayer with changes in potential [4], and noted a change in structure of the adsorbed monolayer between +0.15 and _0.2 V/SCE, and a loss of most long-range order in the monolayer at 0.45 V/SCE, believed to be due to further deposition of thiol molecules from solution into the monolayer.

Oxidative desorption has also been studied, though less thoroughly. Hagenström *et al* [63] observed the oxidative desorption of ethanethiol monolayers with STM, and noted the "extreme" pitting of the electrode surface after desorption. Though small, usually monomolecular pits had been observed previously [57][64], this study confirmed the extent of the damage to electrode surfaces caused by the combination of surface oxidation of the electrode and oxidation of the thiol layer.

The oxidative readsorption of thiol molecules after a reductive desorption has also been observed via STM imaging. Hobara *et al* [62] imaged the reductive desorption, and found that after desorption the more water-soluble thiol (3-mercaptopropionic acid) diffused away from the electrode surface, while less-soluble thiols (1-propanethiol and 1-hexadecanethiol) formed aggregates at the electrode surface. Uosaki [61] also observed the formation of surface aggregates from monolayers of hexanethiol, and additionally noted that the number and size of the aggregates increased in H_2SO_4 vs KOH, corresponding with the decrease in thiol/thiolate solubility in acidic media. Hagenström, Schneeweiss, and Kolb [63] observed the oxidative readsorption as well, arranged in small islands of ordered thiol.

In addition to the adsorption and desorption of thiol monolayers at electrode surfaces, there exists at least one other region of electrochemical interest. Lennox *et al*, in their recent study [65], observed that there are 2 distinct regions of thiol monolayer stability in aqueous electrolyte. Above a certain critical potential, the SAM as formed is an ionic insulator, but at potentials negative of this potential, ion penetration into the monolayer is activated. The value of this critical potential was found to be dependent on the hydrophobicity of the tail groups of the thiols, with more hydrophilic thiols being more easily transformed into the penetrable form. For SAMs terminated with hydrophobic end groups, the transformation was reversible upon return to a potential above the critical potential. However, the hydrophilic layers did not fully return to their original state.

The electrochemical properties of thiol SAMs have been combined with scanning tunneling microscopy to form controlled structures formed by oxidatively desorbing a

localized region of the monolayer by control of tip proximity and bias potential [66]. Gorman and coworkers [67][68] also found that if the desorption was carried out in a solution of a different thiol, the new thiol would adsorb on the exposed surface, creating precise regions of different thiols. The scanning electrochemical microscope can be used in a similar way[69], though the features it creates are larger and subject to distortion from bubbles forming on the probe tip.

3.2 Fluorescence near Metal Surfaces

The science of altering the decay properties of fluorophores by controlling their proximity to a metal surface has been referred to as "radiative decay engineering" [70]. The pioneering work of Drexhage's team in this area [31][32][33] examined for the first time the effect that a nearby metal surface had on an electronically excited molecule located a fixed distance away. By using multiple Langmuir-Blodgett monolayers as spacers, it was shown that, for distances on the order of the emission wavelength, the excited-state lifetime oscillates with distance from the surface. The oscillating behavior can be adequately explained with simple interference resulting from reflection of the emitter field off the metal. At certain separations, fluorescence can even be enhanced [71]. However, for spacings very close to the metal surface, the lifetime drops sharply, a behavior not predicted by the interference theory [72]. This unexpected decline in excited state lifetime near the metal surface has sparked a great deal of study since, summarized in several reviews [37][34][73][74]. The close-range quenching is believed to arise from coupling to a combination of two energy transfer possibilities: lossy surface waves, and surface plasmon polaritons (SPPs).

46

3.3 Electro-Fluorescence Technique

The quenching property of metal on fluorophores can be exploited, and a technique to use fluorescence quenching and dequenching near electrode surfaces has been developed. Used to study the desorption of 12-(9-anthroyloxy) stearic acid (12-AS) from single-crystal gold electrodes [75], this technique allows the fate of electrochemically desorbed molecules to be determined in-situ. Vibrational methods such as SNIFTIRS [25] or FTIR-RAS [27] allow the determination of the nature of the products formed from an electrochemical desorption to be probed, but provide little information as to the location of the products after formation. Thus, the electro-fluorescence technique has developed, to provide a greater degree of knowledge about the fate of desorbed species. When a surfactant monolayer containing fluorophore is adsorbed on a metal surface, the fluorescence is quenched due to the processes described previously. If the monolayer is desorbed from the electrode surface, for example by application of a suitable electrical potential, as the molecules of the layer move away from the metal surface, they will no longer be quenched, and fluorescence will reappear as a function of separation from the electrode. This property has been used to probe the behavior of physically adsorbed monolayers of dye-containing octadecanol [76][17][16], dioleoyl phosphatidylcholine [77], and 2-(2'-thienyl)pyridine [78], as well as for a thiol SAM[14]. The technique was refined for octadecanol and thiol SAM monolayers in a recent thesis [13].

For the octadecanol system, it was discovered through use of the electro-fluorescence

technique that the monolayer desorbed from an Au(111) electrode in a coherent layer, with visible features that were reproduced over several cycles of desorption and readsorption. In the case of the thiol SAM, the selective desorption of thiol from regions of different crystallinities on the electrode was observed, confirming electrochemical evidence which suggested that the thiol would desorb at different potentials from different crystal faces.

3.4 Summary

The electrochemical behavior of alkanethiol SAMs has been characterized by many groups, and although some debate remains on the mechanism of the oxidative removal of the SAMs, the existence of the phenomenon has been thoroughly documented. Several scanning probe microscopy techniques have been undertaken which show the reductive and oxidative desorptions, oxidative adsorption, and the ability to create controlled structures by localized desorption of thiol SAMs. By exploiting the behavior of fluorescent molecules near metal surfaces, an electro-fluorescence technique has been developed, and will be used in this thesis alongside traditional electrochemical techniques to explore the oxidative behavior of a fluorescent-tagged thiol monolayer.

4   Experimental Methods

Details of the experimental methods, instrumentation, and materials are collected in this chapter. Where especially relevant, important passages will be noted again in the Results section. In brief, this chapter will describe the materials and methods used for the electrochemical and spectroelectrochemical characterization of the desorption of fluorescent thiols from an Au bead electrode. The procedures for ex-situ measurement of the fluorescence spectrum of the thiols in solution under various pH conditions are also included, as are details of the instrumentation used.

4.1 Electrochemical Measurements

All electrochemical measurements were carried out on a polycrystalline Au bead. The bead was formed by heating an Au wire with a torch to melting point such that it formed a bead, and then slowly removing it from the flame so that the metal cooled gradually, allowing the formation of several small facets on the bead. The bead was then electropolished in perchloric acid according to an established procedure [79]. Pt or Au wires were used for the counter electrodes, and a saturated calomel electrode (SCE) was used for reference, connected to the electrolyte solution via a salt bridge. For all experiments, the electrolyte was a 50 mM solution of $KClO_4$, made using Millipore water (>18 MΩ·cm) and triply recrystallized $KClO_4$. Alterations to the pH of the system were made by adding a small amount of diluted $HClO_4$ (Seastar Chemicals Inc.) or NaOH solution (Fluka suprapure, used as received) until the pH reached the desired value. pH was measured using colorpHast pH 0-5 indicator strips (Fluka, accuracy ± 0.5 pH unit)

or Duotest pH 1-12 indicator paper (accuracy ± 1 pH unit).

All glassware and teflon pieces used were cleaned in a heated 1:1 (v:v) mix of H2SO$_4$ and HNO$_3$ for at least 2 hours, followed by a thorough rinse in Millipore water. The cell pieces were filled with or soaked in (depending on the size of the piece) Millipore water overnight. The working and counter electrodes were individually flame annealed and quenched in Millipore water several times to clean the metal surface before introduction into the electrolyte solution. The bead electrode was placed in the solution such that the bead portion of the electrode that was under the surface of the electrolyte solution was maximized, while minimizing the contact with the wire portion of the electrode. This was to allow a more reproducible area interacting with the electrolyte solution during measurements. Figure 4-1 shows a schematic of the bead in solution as it would be set up for an experiment.

After filling the cell with electrolyte (vol ~70 mL), the electrodes were introduced and the electrolyte solution in the cell was purged of oxygen by bubbling with Ar (Praxair, cleaned with charcoal filter, Supelco). A constant blanket of Ar was maintained over the electrolyte surface during experiments to prevent reoxygenation of the electrolyte solution. After deoxygenation of the electrolyte solution, the salt bridge (see Figure 4-3) was filled by suction, filling first the cell side of the bridge with electrolyte, then the reference electrode (RE) side of the bridge with saturated KCl solution. The central stopcock prevented mixing of the chloride solution with the electrolyte, while the thin electrolyte layer surrounding the loose-fitting stopcock maintained ionic connectivity.
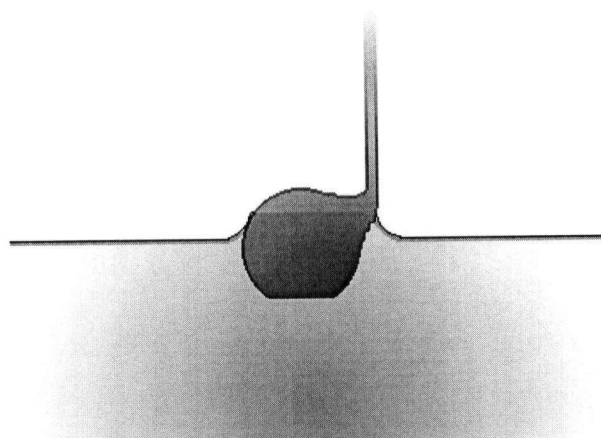
Figure 4-1   Diagram of electrode placement in solution. The large facet on the electrode was tilted to face towards the microscope objective.
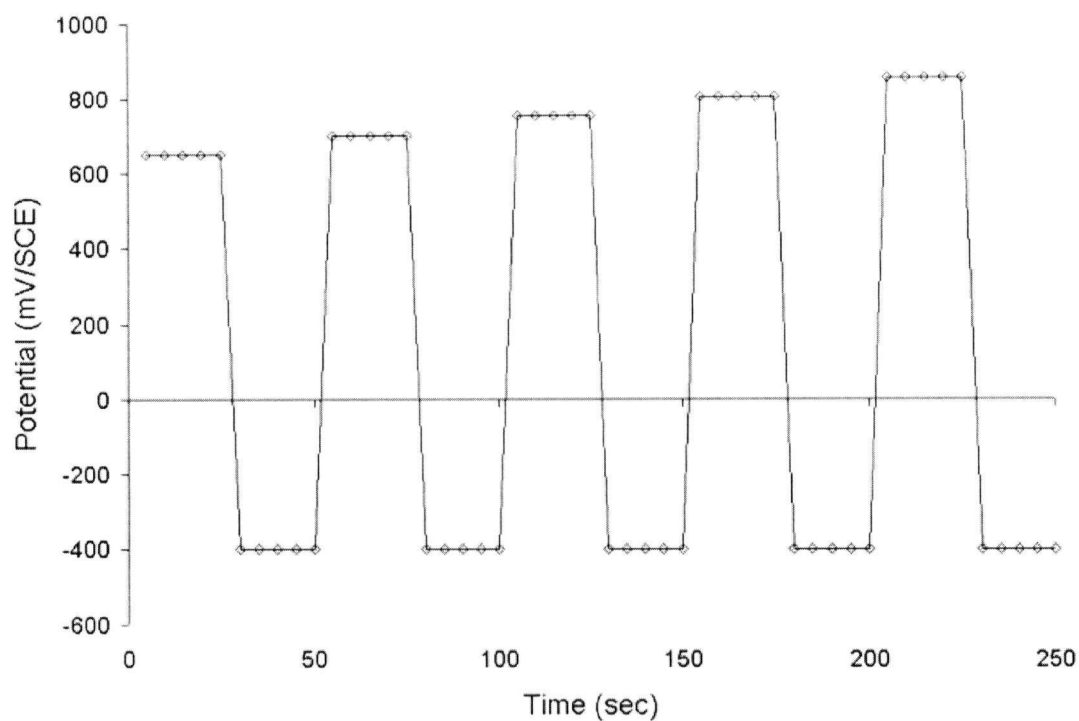
Figure 4-2 Sample potential profile for an oxidation experiment. Potential cycles between the incremented 'step' potential, and the 'base' potential, constant at -400 mV/SCE. At each marked point on the profile, a capacitance measurement (and fluorescence, if applicable) would be recorded.
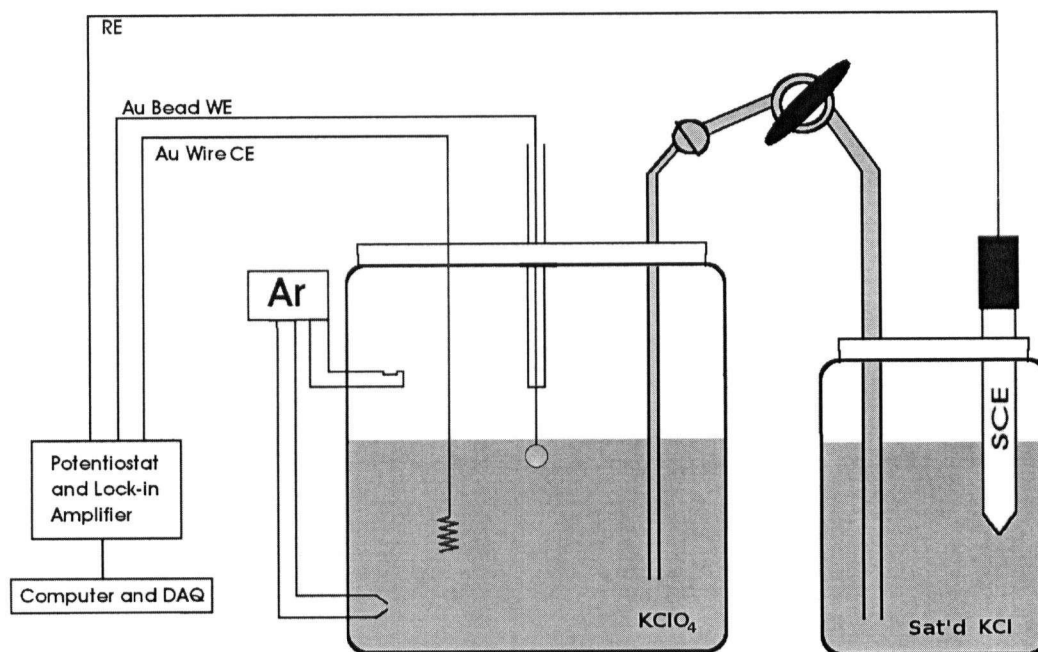
Figure 4-3 Schematic of the three-electrode cell used in the electrochemical studies. The working electrode (WE) is a polycrystalline Au bead, the counter electrode (CE) is a coiled Pt or Au wire, and the reference electrode (RE) is a saturated calomel electrode. The RE is connected to the cell via a salt bridge.

Cleanliness of the electrochemical experimental setup was verified at the start of each experiment by recording cyclic voltammogram (CV) and differential capacitance (DCap) measurements over a large potential range, from H_2 evolution to Au oxidation (-800 mV to +1250 mV) and the double-layer region (-800 mV to +650 mV) and comparing them to literature [10][14].

At this point, if the pH was to be adjusted, the $HClO_4$ or NaOH solution was added dropwise using a clean Pasteur pipette, and Ar was bubbled through for several minutes to ensure both sufficient mixing and deoxygenation of the solution. The pH was tested by withdrawing a small amount of solution via another clean pipette and applying it to a pH strip. The process was repeated until the desired pH was attained. To ensure the continued cleanliness of the solution, the CV and DCap measurements were repeated in the modified solution.

Once cleanliness was established, a potential step program was used. The program alternated the potential between the step potential (E_{step}) and a base potential (E_{base}, -400 mV/SCE). The step potential was incremented by 50 mV each cycle. At each step, a DCap measurement was taken every five seconds, and the potential was held to allow three or five such measurement periods before moving to the next step. Figure 4-2 shows an example of the potential profile for an oxidative desorption experiment.

These electrochemical measurements were repeated after deposition of a SAM for each thiol, though a full-scale cyclic voltammogram was not recorded in order to avoid moving into a potential region which might damage the monolayer.

4.1.1 Spectroelectrochemical Measurements

Spectroelectrochemical measurements were carried out using the same procedure as the electrochemical measurements, with a few exceptions. The design of the spectroelectrochemical cell (Figure 4-4) necessitated a different method for connecting the reference electrode. The salt bridge was filled by sealing the cell and increasing the Ar pressure to raise the electrolyte level into the reference electrode holder. The stopcock was then closed, ensuring that the fit was sufficiently loose to maintain ionic contact between the RE reservoir and working solution. Only then was the SCE introduced into the reference electrode reservoir, thereby reducing the chance of chloride ions from the SCE traveling back into the working portion of the cell.

The potential step program was carried out as in the electrochemical measurements, with the addition that concurrently with each DCap measurement, a fluorescence image of the bead was taken. For the C10 thiol, an exposure time of 0.5 seconds was used, and for the C16 thiol, an exposure time of 1.5 or 2 seconds was used, as this species had a weaker fluorescence signal. A fluorescence image of the bare Au bead was taken using the appropriate exposure time to provide the background signal.

4.1.2 Self Assembled Monolayer Formation

The fluorescent molecules used in this work were synthesized by A. Kell and M. Workentin at the University of Western Ontario [14]. They were used in deposition solutions of 3 mg/mL BODIPY-C10-SH and 0.3 mg/mL BODIPY-C16-SH,
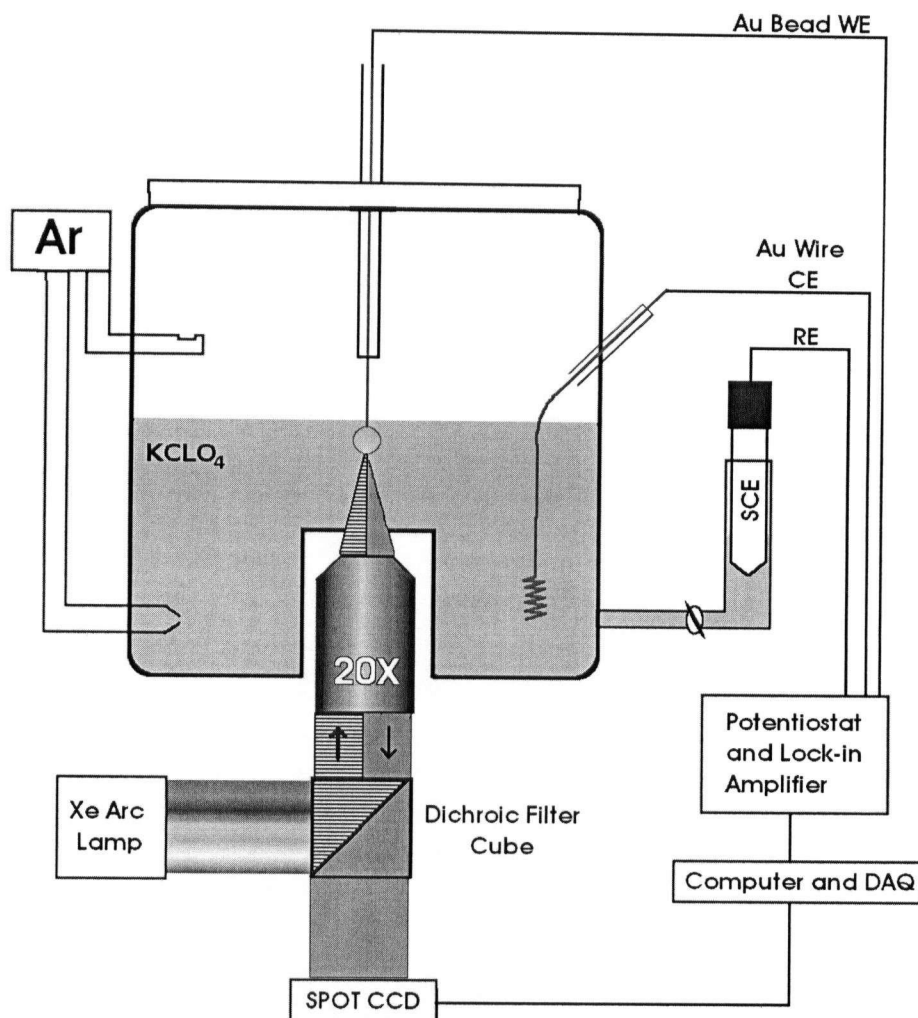
Figure 4-4 Schematic of the spectroelectrochemical cell used for in-situ fluorescence measurements. The optical glass window above the objective is 0.17 mm thick. The RE reservoir is filled with electrolyte solution and separated from the cell by a stopcock salt bridge.

respectively, and both in HPLC grade chloroform (Fluka, used as received).

To form the self assembled monolayer (SAM), the bead electrode was immersed in the desired thiol solution for 20 minutes. The bead was then rinsed with chloroform (HPLC, Fluka), and sonicated in fresh chloroform for 2 minutes, followed by a final rinse in chloroform. This procedure was based on previously published procedures [14][26] and was modified empirically to minimize the amount of physically adsorbed thiol molecules present after SAM formation. The sonication time used was found to eliminate most of the physically adsorbed thiols while leaving a good quality SAM on the bead as determined by capacitance values.

4.1.3 Electrochemical Techniques

4.1.3.1   Cyclic Voltammetry

Measurement of a cyclic voltammogram (CV) involves sweeping the electrode potential linearly between two boundary potentials and recording the current passing through the electrode. The Labview program used to record the CVs was developed in house. At the beginning of each experiment, a CV was recorded from H_2 evolution to Au oxidation (+1250 to -800 mV/SCE in pH 5) as well as in the double layer region (+650 mV to -800 mV/SCE in pH 5). For solutions more acidic or basic, the potential windows were shifted by 100-200 mV positively or negatively, respectively. CV measurements were recorded using a potential sweep rate of 20 mV/s .

4.1.3.2   Differential Capacitance

As established in Chapter 2, the metal-solution interface can be approximated as a simple capacitor, and the electrode-solution interface as a capacitor and resistor in series. One important difference, however, is that a real capacitor has a capacitance that is independent of the potential applied, while the capacitance of the electrode-solution interface will vary with potential due to changes taking place at the interface. The simplest way to measure an accurate capacitance of the interface is the differential capacitance technique, wherein a small intensity sinusoidal perturbation is introduced over a DC potential profile (either scanning or constant current). The current from the electrode was analyzed by a lock-in amplifier, and the in- and out-of-phase components (real and imaginary currents) measured. Using the approximation of a capacitor and resistor in series, the capacitance of the interface can be calculated using:

$$C = \frac{i_{im}}{V_{ac}\omega}\left[1+\left(\frac{i_{re}}{i_{im}}\right)^2\right]$$

(4.1)

where C is the capacitance of the interface (μF), V_{ac} is the RMS amplitude of the AC voltage (mV), ω is the perturbation frequency, and i_{im} and i_{re} are the imaginary and real currents (μA). The term "differential capacitance" arises from the determination of capacitance through the differentiation of σ, the charge density, with respect to potential, as measured using small perturbations in potential:

$$C = \left(\frac{\delta\sigma}{\delta E}\right)$$

(4.2)

At the beginning of each experiment, following the CV measurements, the differential capacitance of the electrode in the double layer region was measured. The Labview program used to gather the data and make the capacitance calculations were developed in house for a previous thesis [80].

Capacitance measurements were performed at 5 mV/s with an AC perturbation of 200 Hz. This frequency value is higher than the usual value used for solid electrodes (around 25 Hz), however this frequency was used in order to minimize the time required for the lock-in amplifier to acquire the signal during stepping experiments, reducing the minimum step time. Measurements of the differential capacitance of the bare gold electrode at 25 and 200 Hz showed no difference in measured capacitance, indicating that the higher frequency is acceptable for use in this system.

4.1.4 *Ex-situ* fluorescence measurements

In order to determine the effect of pH on the BODIPY compounds being used in these experiments, measurements of the fluorescence of both thiols in solution at various pHs were obtained. Solutions consisting of 2mL $CHCl_3$, 10 mL CH_3OH, and 0.1 mL of a 0.3 mg/mL solution of the thiol were diluted to volume with Millipore water in 50 mL volumetric flasks. A blank was also made with the same composition, minus the thiol. A glass cuvette was used, and acid-washed according to the previously described procedure between measurements of each thiol. Monochromated light at 495 nm was used as the excitation wavelength. In order to eliminate any variances in fluorescence intensity due to differing amounts of water present at different pH values (due to the

addition of $HClO_4$ or NaOH solution), the 'added water' volume was kept constant for all cuvettes. That is, if 0.03 mL of $HClO_4$ was required to achieve pH 1, and 0.06 mL of NaOH was required to reach pH 10, 0.06 mL of water would be added to the blank cuvette, and an additional 0.03 mL of water would be added to the pH 1 cuvette. All pH values were again determined by application of a small sample to a colorpHast pH strip.

Fluorescence spectra were measured with an integration time of 200 ms, averaged over 250 points. Five such spectra were then averaged to obtain the final spectrum.

4.2 Instrumentation
4.2.1 Electrochemical Instrumentation

For electrochemical measurements, a potentiostat (FHI ELAB) was used to control the potential, connected to a EG&G Princeton 5204 lock-in amplifier for DCap measurements. Data was recorded using the LabView suite on a PC equipped with a 12-bit data acquisition board (National Instruments PC-MIO-16E-1, 12.5 MHz). A LabView program, through the data acquisition board, was also used to control the potential remotely when required.

4.2.2 Epi-fluorescence Microscope

An epi-fluorescence microscope in the inverted configuration (Olympus IX70) was used to take fluorescence images viewing the electrode from below while in the electrochemical cell (Figure 4-4). The microscope was equipped with a 20x objective (Olympus LMPlanFL, numerical aperture 0.40), and light from an Xe short-arc lamp (75

59

W DC, UXL-S75XE) was used to illuminate and excite the sample. The light was directed through a filter cube (Olympus UM-WIBA) with three filters: excitation (455-480 nm), dichroic (500 nm), and emission (515-500 nm). The transmission and emission range is overlaid onto the BODIPY-C10-SH excitation and emission spectra in Figure 4-5. The emitted light was collected through the microscope objective and directed through the filter cube and into the monochromatic digital camera (SPOT RT, Diagnostic Instruments) containing a Kodak interline transfer charged coupled device (CCD) (model KAI-2092). To reduce dark noise, the CCD is Peltier cooled to 37° C below ambient temperature, and contains a pixel array of 1520x1080 pixels, each 7.4μm x 7.4μm in size. The emitted light was focused onto the CCD with a 0.76x coupler (Diagnostic Instruments) to maximize the use of the CCD area. All image were acquired with SPOT software with either 2x2 binning and a 12-bit image depth (4096 gray levels) or 1x1 binning , acquired in 12-bit and saved with a 16 bit image depth (65536 gray levels). All fluorescence measurements were carried out in a light-tight enclosure.

4.2.3 *Ex-situ* Fluorescence Instrumentation

Light from a quartz-tungsten-halogen lamp source (Oriel, model 66814, controlled by a radiometric power supply with photofeedback, Oriel, model 68831) was directed through a monochromator (Oriel Cornerstone 74000), controlled by a LabView program on a PC via a data acquisition board (National Instruments PC-MIO-16E-1, 12 bit, 12.5 MHz). The acquisition was made with LabView using an Ocean Optics S2000 fibre-optic spectrometer. All *ex-situ* fluorescence measurements were carried out in a light-tight enclosure.
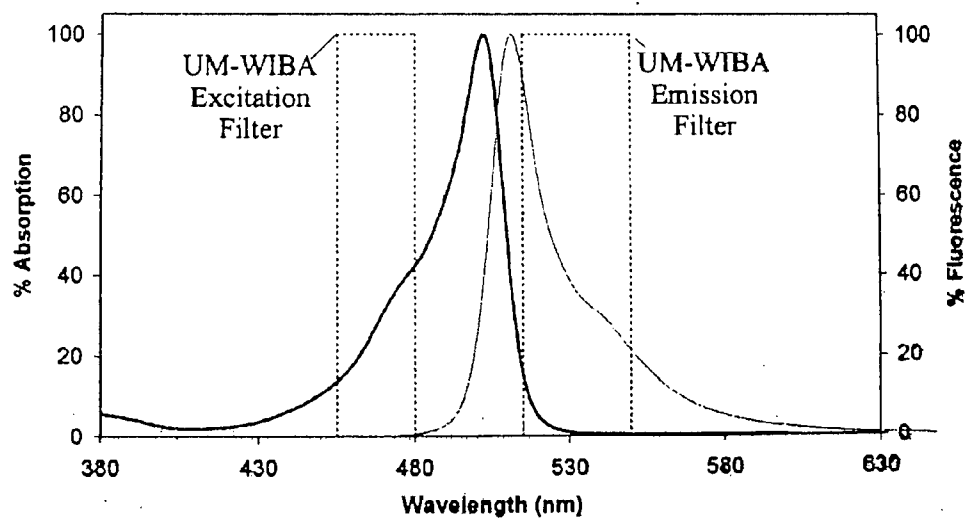
Figure 4-5   Absorption and emission spectra for BODIPY-C10-SH overlaid with the transmission windows for the UM-WIBA excitation and emission filters. Taken from [13].

5 Results and Discussion

In this chapter are presented the body of the results of the experimental work done for this thesis, including ex-situ fluorescence measurements, and electrochemical and electro-fluorescence observations of the oxidative and reductive desorption of thiol SAMs from the gold bead electrode. A summary and suggestions for future work related to the work presented in this thesis is also included.

5.1 Ex-Situ Fluorescence of C10-BODIPY-SH and C10-BODIPY-SH

Since electrochemical investigations were being done at several pH values, fluorescence measurements of the BODIPY-tagged thiols were carried out at a range of pH values in order to investigate any possible effects of pH on the fluorescence of the thiol, and by extension, the oxidation and reduction products.

5.1.1 Collection and Treatment of Data

All data was acquired using an excitation wavelength of 495 nm, and the fluorescence was collected with an Ocean Optics S2000 spectrometer. The solvent mix, (6:2:1) methanol:water:chloroform, was determined empirically and was designed to reduce the cloudiness of the thiol solution in the presence of water due to the insolubility of the thiols. Analysis was carried out using Matlab, by subtracting the spectrum obtained with a blank and the dark signal to ensure all baselines started at zero, and then determining the maximum height of the fluorescence peak.

5.1.2 Fluorescence Response to pH Changes

Both the C10 and C16 thiols responded similarily to the changes in solution pH. Figure 5-1 (A) and (B) show plots of the fluorescence spectrum for the C10 and C16 thiols at each pH. The data is summarized in Figure 5-1 (C), as a plot of the maximum intensities at each pH. Both thiols showed a relative insensitivity to the changes in solution pH, exhibiting changes in fluorescence intensity no greater than 15%, which is within the error inherent in the homemade fluorescence equipment used. This corresponds with reports from the literature [39][40] claiming that the BODIPY fluorophore is pH-insensitive.

5.2 Reductive Desorption of Thiols

Previous studies [13][14] have examined the behavior of the C10-BODIPY-tagged thiol using electro-fluorescence measurements and a sweeping potential scan. In order to ensure that the behavior of the thiol investigated in this thesis correlates with the base-and-step potential profile described in Chapter 4, the experiments were replicated using stepping potential profiles.

5.2.0.1   Collection and Treatment of Images

All fluorescence images were acquired with the 20x microscope objective with the field of view roughly centered on a specific facet on the electrode surface. Repeating all
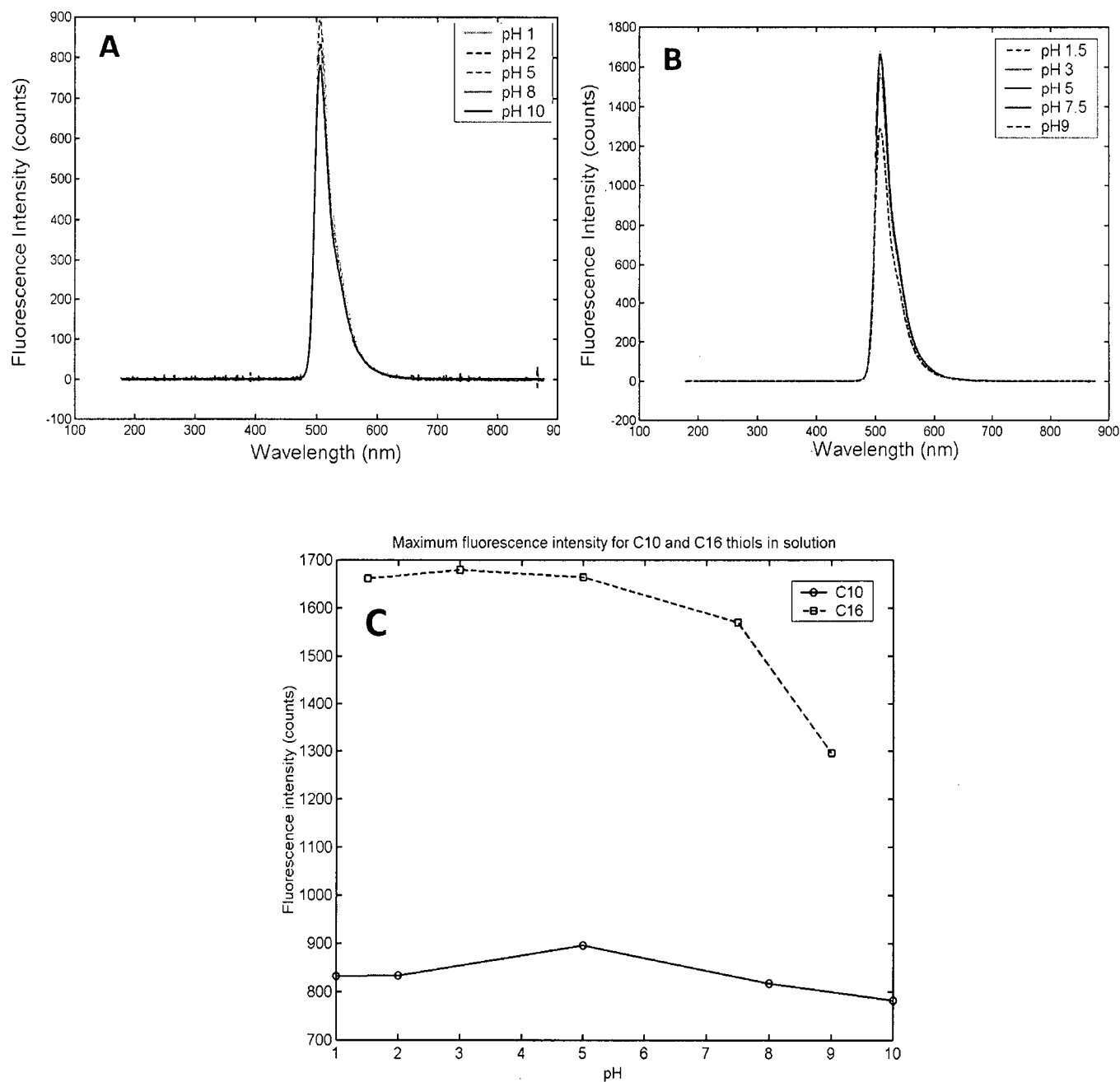
Figure 5-1 Fluorescence spectra and maximum fluorescence intensities for C10 and C16 thiols. A: Fluorescence spectra for C10 thiol at pH 1,2,5,8, and 10. B: Fluorescence spectra for C16 thiol at pH 1,3,5,7, and 9. C: Maximum fluorescence intensity vs. pH for C10 and C16 thiols at all pH values. All measurements were done with the Ocean Optics S2000 spectrometer at an excitation wavelength of 495 nm, an integration time of 200 ms, and averaged 5 spectra over 200 points.

64

experiments with the electrode in the same position eliminates the uncertainty arising from recording measurements using different portions of the electrode. The exposure time for all C10 images was 0.5 sec, and the exposure time for the C16 thiol was 1.5 sec, as noted in figure captions. Fluorescence intensity was calculated from the average grayscale value of the image, after subtraction of a background image taken with an unmodified electrode.

5.2.1 Electrochemical Characterization

5.2.1.1 'Sweeping' Potential Profile

The first studies were carried out with the 'sweeping' potential profile, as it is the most similar to the documented studies. The potential was stepped from -400 mV/SCE to -1450 mV/SCE in 50 mV increments, and a minimum of five 5 second measurement periods were taken at each potential value. Figure 5-2 shows the capacitance measurements taken using the electrode modified with the C10 or C16 thiol under the potential perturbations. Part A of this figure, describing the C10 thiol, shows that the initial capacitance of the thiol-covered bead is substantially lower than that of the clean, bare gold bead (0.3 µF vs. 4.3 µF at -400 mV/SCE). This capacitance behavior is expected for a surface modified with an organic layer. Since the electrode in solution is modeled as a simple capacitor, replacing the electrolyte at the interface, which has a high dielectric value, with a low-dielectric organic layer will decrease the interfacial capacitance. As the potential is stepped beyond -1000 mV/SCE in the negative direction, there is a region of increasing capacitance (approx. 0.3 µF per 50 mV step), leveling off at -1350 mV/SCE. In this region, the rapid increase in capacitance indicates
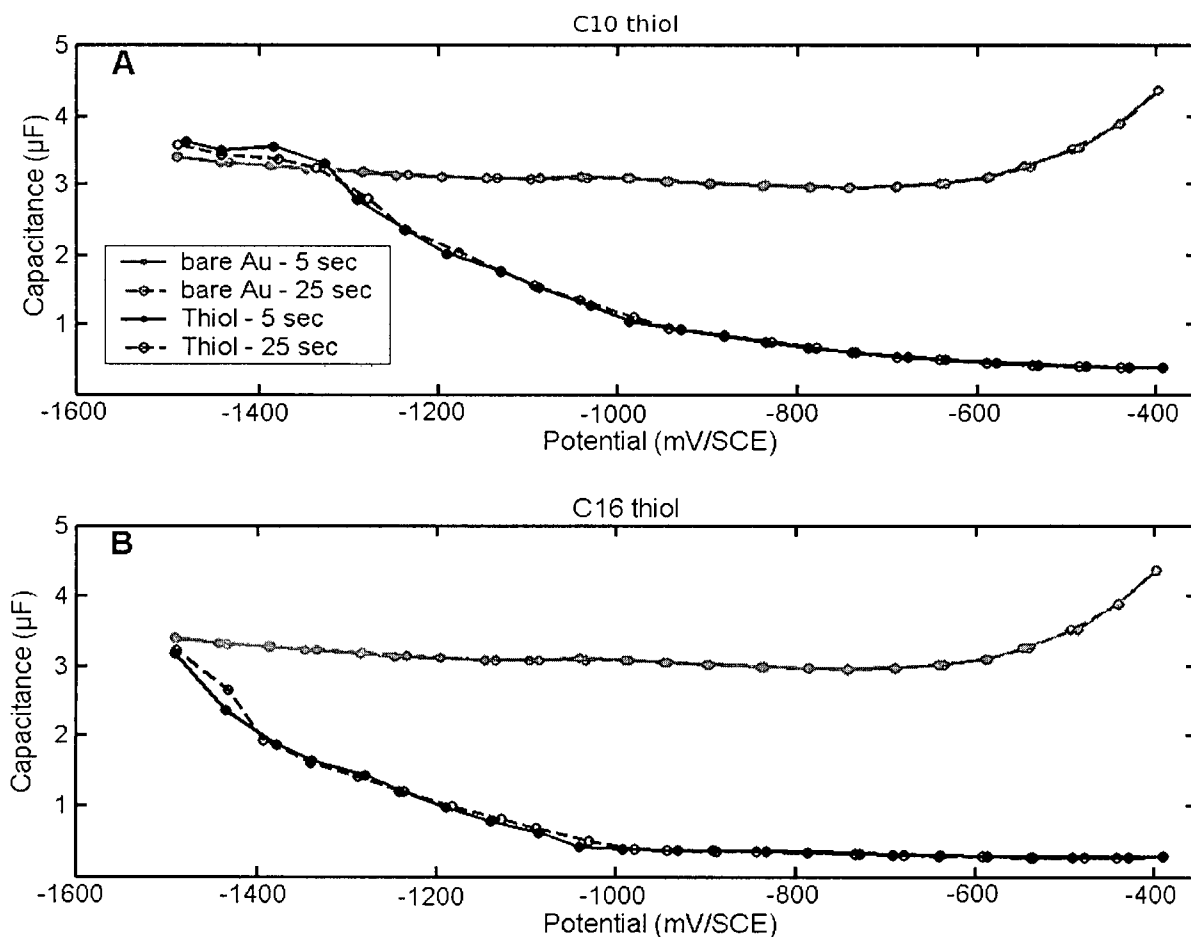
Figure 5-2 Capacitance for reductive desorption of C10- and C16-BODIPY-SH thiols, using 'sweeping' potential profile. Black lines are for thiol-modified electrode. For reference, capacitance of an unmodified Au electrode is shown in gray. Solid line represents capacitance after 5sec, dashed line represents capacitance after 25 sec.

Figure 5-3 Fluorescence intensity from reductive 'sweeping' potential profile, represented by average greyscale value of image (max= 65536) for C10 (A) and C16 (B) thiol in pH 10(±1) electrolyte. C10 images used a 0.5 sec exposure time, C16 images used 1.5 sec exposure time. All images were acquired with a gain of 2 and 1x1 binning. Solid lines represent intensities after 5 sec at the potential, dashed lines after 25 sec. See Appendix A for the images from which these measurements were derived.

67

that the organic material present at the electrode surface is desorbing. Negative of -1350mV/SCE, the capacitance of the thiol-modified electrode levels off at approx. 3.3 μF, slightly higher than the value recorded for the bare electrode. This discrepancy is most likely due to a small difference in the area of the electrode in contact with the electrolyte between the two measurements.

Using the description of the electrode surface developed in Chapter 2, the surface can be represented as two capacitors in parallel; one with the dielectric of the electrolyte, and one with the dielectric of the thiol. The total capacitance would be the sum of the two capacitances, weighted by the fractional area occupied by each. As thiol is removed from the surface, the area exposed to the electrolyte increases, and thus the total capacitance of the electrode surface will also increase. Based on this model, after application of the -1500 mV/SCE potential, ~105% of the C10 thiol-modified electrode monolayer had been desorbed. This value is likely higher than the actual coverage due to the previously mentioned difference in electrode area causing the actual bare Au capacitance to be underestimated.

The C16 thiol (Figure 5-2 B) shows a similar behavior, though the capacitance is initially more stable, with an essentially flat profile from -400 mV/SCE to -1050 mV/SCE, where the capacitance begins to increase (approx. 0.3 μF per 50 mV step). The capacitance does not plateau as it did for the C10 thiol, suggesting that though the capacitance was approaching that of the bare electrode at -1450 mV/SCE, there was still some thiol being removed from the electrode. At the final potential, approximately 95% of the thiol had been desorbed (as estimated using the capacitances). The potential was not

stepped to further negative potentials so as to prevent damage to the electrode by an excess of hydrogen evolution. That the C16 thiol shows evidence of requiring a larger desorption potential is not unexpected, as the longer-chain thiol is expected to have stronger Van Der Waals chain-chain type interactions which will need to be overcome in order to desorb thiol molecules from the surface or create pores for electrolyte to reach the electrode surface. As well, the C16 thiol is less soluble in the aqueous electrolyte, due to the increased hydrophobic nature of the molecule, and this could also contribute to the larger desorption potential required.

For both thiols, the values of the capacitance at 5 seconds (the first measurement) and at 25 seconds (the 5th measurement) are very similar, suggesting that the reaction happening at the electrode surface (i.e. the desorption of thiol) is rapid, and little to no further reaction is taking place after the 5 second mark.

It is also worth noting that, although the pH of the system was 11($\pm$1), which drives reduction of water to form H_2 at the electrode surface to a more negative potential regime, some hydrogen evolution was present at the electrode surface at the more extreme negative potentials investigated. Since during the calculation of capacitance, it is assumed that the electrode-solution interface can be modeled as a simple RC circuit (see Section 2.1), the addition of another resistance term (charge transfer resistance) can introduce an error into the calculations. For this reason, in both the bare and thiol-modified experiments, there is a degree of uncertainty to the capacitance measurements at the negative limits of the potential window used.

A summary of the fluorescence images taken concurrently with the capacitance measurements is given in Figure 5-3, but discussion of this data is reserved for Section 5.2.2.

5.2.1.2   'Base-Step' Potential Profile

In order to avoid the situation where a charge transfer reaction clouds the capacitance measurements, a potential profile of alternating 'base' and 'step' potentials was used. The base potential was selected such that there were no reactions expected at the electrode surface, and the capacitance of the bare electrode was essentially stable. This provides a baseline to compare the capacitance of the thiol-modified electrode against conditions when the accuracy of the capacitance at the step potential may be suspect.

Figure 5-4 shows the results of a set of experiments using the alternating step/base potential profile. A base potential of -400 mV/SCE was used, and the step potential was stepped from -400 mV/SCE to -1500 mV/SCE in 50 mV increments. Examining the results from the C-10 thiol monolayer first, the capacitance at the step potential exhibits a behavior similar to that with the scanning potential profile, with a stable, low-capacitance region from -400 mV/SCE to -1000 mV/SCE, followed by a region of dramatic increase, which slows near -1400 mV/SCE. The capacitance, in this case, increases to only about 75% of the bare gold capacitance. This suggests that the thiol monolayer is incompletely removed, even at the negative limit of the potential perturbation.

70
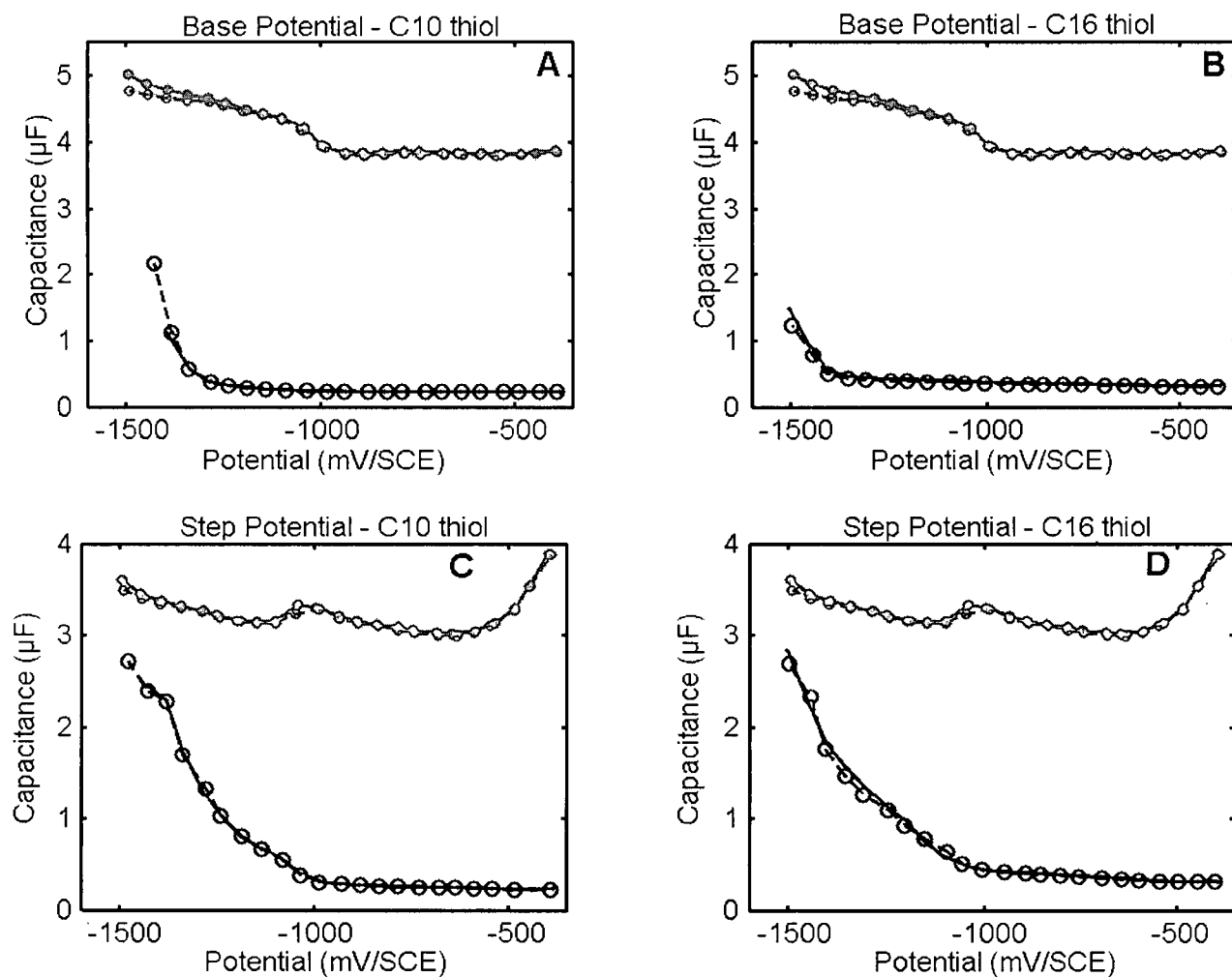
Figure 5-4 Capacitances from reductive desorption of C10 (A,C) and C16 (B,D) thiols, using the 'base-step' potential profile. Black lines are capacitances from the thiol-modified electrodes, gray lines are from bare Au electrode. Solid lines and circles represent capacitance values from 5 seconds held at the potential, dashed lines with hollow circles represent capacitance values from 25 seconds.
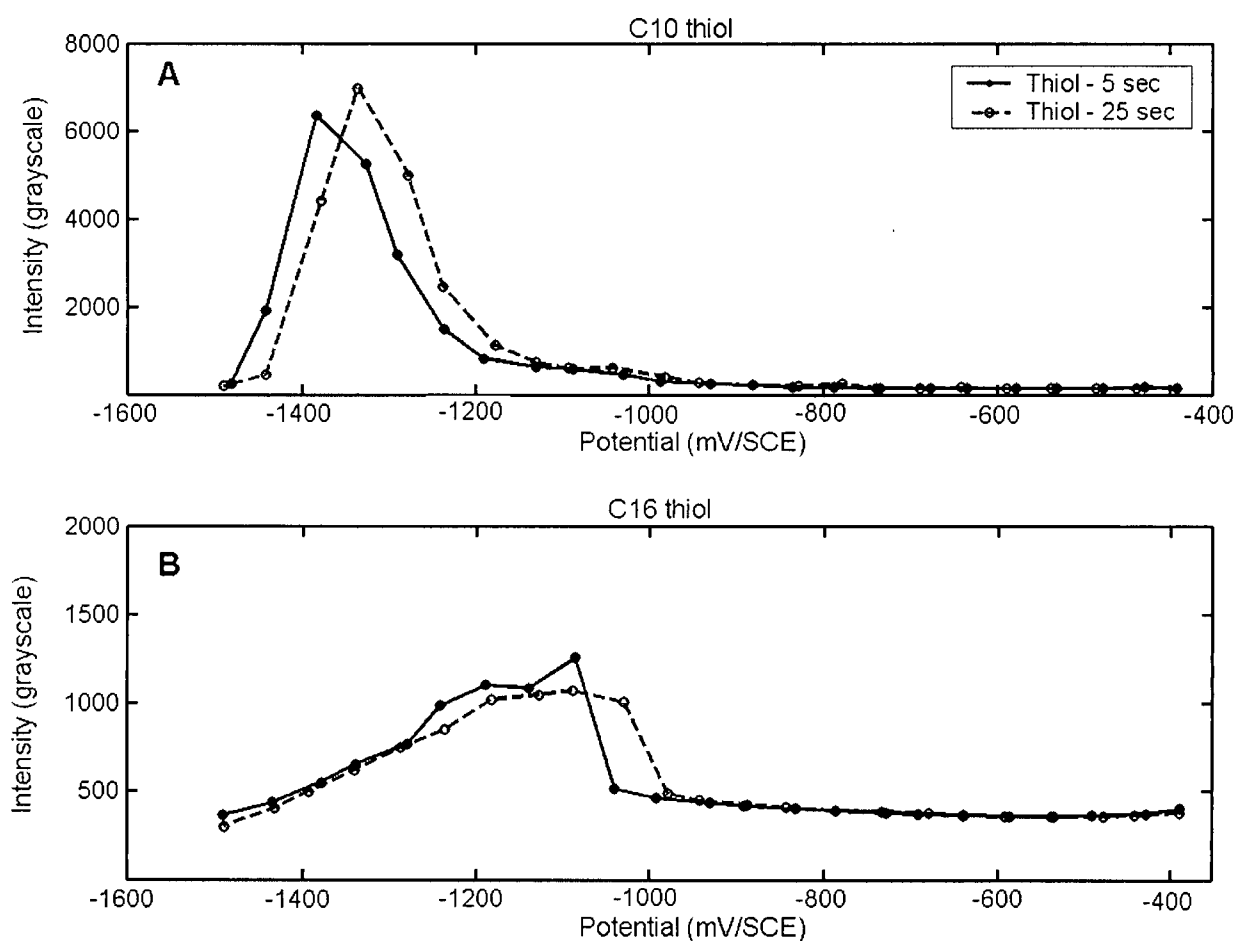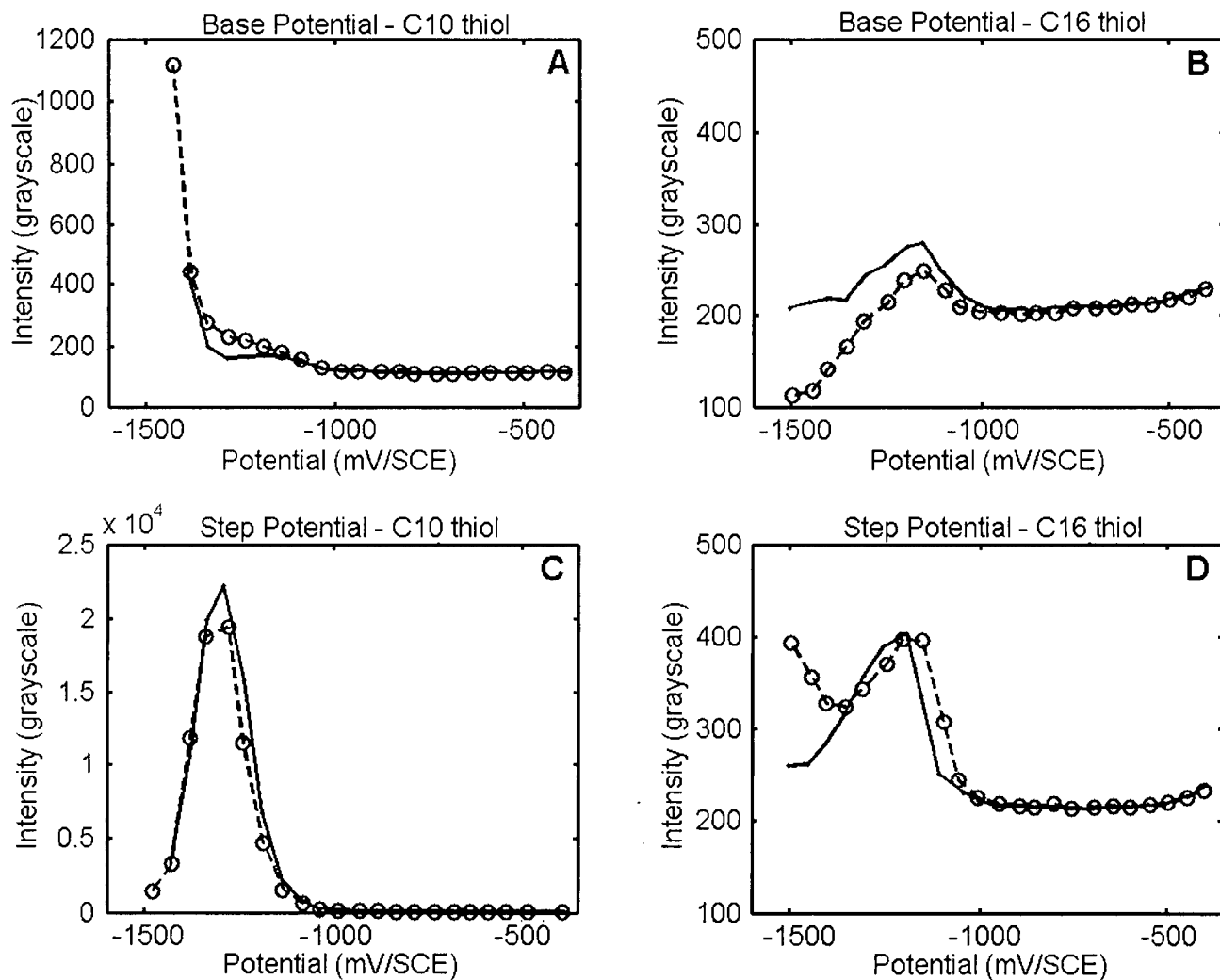
Figure 5-5 Fluorescence intensity from the 'base-step' potential profile, represented by average greyscale value of image (max= 65536) for C10 (A,C) and C16 (B,D) thiol in pH 10(±1) electrolyte. C10 images used a 0.5 sec exposure time, C16 images used 1.5 sec exposure time. All images were acquired with a gain of 2 and 1x1 binning. Solid lines represent intensities after 5 sec at the potential, dashed lines after 25 sec. See Appendix A for the images from which these measurements were derived.

An examination of the capacitance at the base potential (Figure 5-4A) shows that it is stable over a much larger potential region, with the region of rapid capacitance increase occurring when the potential has been stepped beyond -1350 mV/SCE. When the capacitance does begin to increase, it reaches less than half the capacitance of the bare gold. Using the same approximation as previously, that the capacitance is an area-weighted sum of the capacitance of the organically modified area and the electrode area exposed to the electrolyte, it is apparent that some material (~55% of the original layer) remains on the electrode surface at the base potential, even after a step to a potential at which much of the thiol appeared to be desorbed.

It has been noted in the literature [55][25][54] that the thiolate produced by the reductive desorption of a thiol SAM is able to oxidatively readsorb if the potential is changed to a suitable value, and if the thiolate has not diffused too far into the bulk of solution. This plays out in the capacitance data gathered from the step profile experiments, as the capacitance at the reducing potential indicated the removal of much of the SAM, while upon return to the more moderate base potential, the capacitance was nearly returned to the value when fully covered. It is probable that in the time scale of the step profile, the majority of the thiol desorbed remained close to the electrode, and readsorbed at the base potential. The swift increase in the capacitance at the base potential beginning at -1350 mV/SCE could be the result of the thiol either diffusing far enough away from the electrode that it cannot be readsorbed at the base potential, or possibly from the thiol being further reduced in such a way that it cannot be oxidatively readsorbed at the base potential.

As in the previous study, the C16 thiol (Figure 5-4B and D) behaves in essentially the same manner, with the exception of the onset of the change in the base potential capacitance (and the corresponding alteration in the rate of change at the step potential) beginning at a more negative potential, around −1450 mV/SCE vs. −1350 for the C10 thiol. Though the capacitance at the step potential begins at approximately the same potential as the C10 thiol, the rate of increase is slightly lower for the C16 thiol, suggesting that higher energy is required to remove the C16 monolayer from the surface, perhaps due to the presumably lower solubility and more dominant chain-chain interactions of the longer alkyl group.

5.2.2 Epi-Fluorescence Investigations

Fluorescence images of the electrode surface were taken concurrently with the capacitance measurements discussed in the previous section. These measurements should aid in elucidating the behavior of the thiol molecules as the SAM is perturbed by the changing the electrode potential.

5.2.2.1 'Sweeping' Potential Profile

For the measurements taken with the 'sweeping' potential profile (where no base potential was used), plots of the fluorescence intensity, calculated as the average grayscale value of the image, are shown in Figure 5-5. Corresponding fluorescence images are collected in Figure A-1. The fluorescence resulting from the reductive removal of the C10 SAM, Figure 5-5A, is initially quite low, showing a slight increase

starting at approximately -1000 mV/SCE. This corresponds roughly with the initial change in capacitance of the interface (Fig. 5-4A). The initial fluorescence intensity increases rapidly from -1200 mV/SCE to -1400 mV/SCE, then drops sharply, returning to near the initial value by -1500 mV/SCE. The evolution of the fluorescence intensity with time is also interesting during this potential region with rapid change. From -1200 to -1400 mV/SCE, on the increasing side of the peak, the fluorescence intensity increases as time passes during each step, suggesting that the thiolate product is moving slowly away from the electrode, from a region where the fluorescence is quenched (at or near the electrode surface) to one where fluorescence is visible (further from the electrode). The diffusion of the thiolate is also slow enough to observe the accumulation of fluorescent thiolates in the viewing area during the time of a 25s potential step. From -1400 mV to -1500 mV/SCE, however, the fluorescence decreases with time, indicating that the thiolate is diffusing out of the visible area more rapidly than it can be replaced by more thiolate from the electrode, and the fluorescence decreases. The capacitance does not decrease with time, so no thiolates are being readsorbed onto the electrode surface. This corresponds roughly with the plateau region of the capacitance plot, where the rate of change in the capacitance slows dramatically, suggesting that most of the thiol has been removed from the electrode surface by this potential.

The lag between the onset of the more rapid change in capacitance and the increase in fluorescence could be due to the kinetics of the thiol migration from the electrode surface. It is also possible that it is an artifact arising from the limited viewing area on the bead, focusing on a single facet on the surface. The thiol may preferentially desorb

from this facet at a more negative potential than from areas outside the viewing area. The change in capacitance is a property of the whole electrode, and would reflect changes not only in the area visible to the fluorescence measurements.

The fluorescence from the C16 thiol (Figure 5-5B) is about five times less than that of the C10 thiol (a maximum grayscale value of ~1300 vs. ~7000 for C10), though the exposure time was four times as long. Starting at -1000 mV/SCE, the fluorescence increases by about the same amount as that of the C10 thiol, then begins to drop gradually from -1100 mV/SCE to -1500 mV/SCE. It is possible that the lower overall fluorescence intensity from the C16 thiol arises from the insolubility of the thiol, or from the increased chain-chain interactions holding the fluorophores close enough together that the BODIPY groups self-quench, reducing the fluorescence intensity.

5.2.2.2   'Base-Step' Potential Profile

Examination of the fluorescence data for the experiments with a potential profile including the base step shows that for the step potential, beginning at -1050 mV/SCE, the fluorescence intensity increases sharply, reaching a maximum at -1250 mV/SCE. , then falling back to near the original value by -1500 mV/SCE. The onset of the increase in fluorescence corresponds to the beginning of the long increase in capacitance for the C10 thiol. The onset of the decrease corresponds to the 'kink' in the capacitance plot at the step potential. The shape of the plot suggests that an increasing amount of thiol is being desorbed with each step until -1250 mV/SCE, at which point a change occurs, and from then on decreasing amounts of thiol are released. At the base potential, there

is a small increase in fluorescence from -1100 mV/SCE, then a sharp increase beginning at -1350 mV/SCE. This increase is much smaller than that at the step potential, approximately 10 times less. The fluorescence at the base potential supports the proposition that the thiol is being readsorbed, as the fluorescence intensity drops dramatically on return to the base potential, much faster than the diffusion-related decreases seen in the previous measurements. The increase in the fluorescence starting at -1350 mV suggests that the thiol is no longer being completely readsorbed, and is freed from the electrode, even at the potentially oxidizing potential. It is possible that this change in the fluorescence at -1300 to -1350 mV/SCE is related to the onset of hydrogen evolution at the electrode surface either disturbing the monolayer and encouraging increased desorption of the thiol, or displacing the thiol farther into solution, where it is not able to readsorb oxidatively on the timescale of the experiment, allowing the thiol to diffuse away.

The C16 thiol, as previously, has a significantly lower increase (~5-56 times less) in fluorescence intensity although the exposure time is longer. At the step potential, the intensity increases beginning at -1050 mV/SCE, about the same potential as the beginning of the increase of capacitance. At -1300 mV/SCE, the intensity begins to decrease, however, negative of -1400 mV/SCE, the intensity at 25 seconds begins to increase once again. This corresponds with the change in slope of the capacitance plot. This may be the result of hydrogen evolution disturbing the electrolyte volume near the electrode surface and moving the thiol away from the electrode, where it can fluoresce and be detected. The fluorescence at the base potential also exhibits unusual behavior. After a slight increase in fluorescence starting at -1050 mV/SCE, the intensity begins to

drop negative of -1050 mV/SCE. The initial fluorescence remains at or above the initial intensity, however, the intensity after 25 seconds decreases even further, below the initial intensity. The dip below the original intensity could be due to the loss of aggregates on the electrode surface that were able to fluoresce at the initial potentials,

Previously, it was reported that the BODIPY-tagged thiol reductively desorbs selectively from certain crystal faces at specific potentials[14]. This phenomenon was not as strongly observed in this set of experiments, as the viewing area was dominated by a large facet, presumably of one crystal structure. Additionally, the effects would be masked by the thiol not fully diffusing out of the viewing area before a change in the potential, or by readsorption of the thiol at the base potential. Some evidence of the selective desorption occurring may be seen as additional regions of fluorescence are added as the reducing potential becomes more extreme, indicating that thiol is being desorbed from previously inactive areas of the electrode. See the sequence of images in Appendix A-1 at 10s for an example.

5.2.3 Summary

The reductive desorption of thiol was observed by use of capacitance and electro-fluorescence measurements. The use of the alternating 'base-step' potential profile was introduced and shown to be an effective method for measuring the reductive desorption and eliminating the uncertainty of measuring capacitance when charge-transfer reactions are present. The oxidative readsorption of the thiols was also observed when using the base step. Though the images were clouded by thiol remaining at the electrode, the selective reductive desorption of the thiol was also observed.

78

5.3 Oxidative Desorption of Thiols

5.3.0.1 Collection and Treatment of Images

Fluorescence images were acquired in the same manner as for the reductive desorption experiments. The exposure time for all C10 images was 0.5 sec, and the exposure time for the C16 thiol was either 1.5 or 2 seconds, as noted in figure captions. Fluorescence intensity was calculated from the average grayscale value of the image, after subtraction of a background fluorescence image taken with an unmodified electrode. Since not all images were taken at the same exposure time, all calculated fluorescence intensities for the C16 thiol were normalized to simulate the 2 second exposure time. To normalize the intensities, the dark signal was subtracted, and the intensity values were multiplied by a correction factor.

5.3.1 Oxidative Desorption in Alkaline Electrolyte

5.3.1.1 Electrochemical Measurements

Investigations in alkaline electrolyte were carried out at the same pH as the reductive desorption measurements (pH 10 ± 1). The potential profile used was the 'base-step' profile, with the base step remaining at -400 mV/SCE, and the step potential increasing from 0 to +800 mV/SCE in 50 mV increments. The potential was held for five measurement increments of 5 seconds each, for a total of 25 seconds at each potential. Differential capacitance measurements were taken every 5 seconds for the duration of the experiment.

A plot of the capacitance at the step potential for the oxidative desorption of the C10 thiol is presented in Figure 5-6 (C). The capacitance of the thiol-covered electrode is initially much lower than that of the uncovered electrode, as expected since the thiol has a lower dielectric constant than water. The capacitance increases gradually from ~0.75 μF to ~1.5 μF at +600 mV/SCE, then the rate of change increases slightly, and the capacitance rises to ~2.0 μF at 800 mV/SCE. This is approaching the value of the unmodified gold capacitance (~2.8 μF), however, it should be noted that at potentials above approximately +300 mV/SCE, oxidation of Au exposed to the electrolyte will occur at this pH. This will introduce a charge transfer current into the system which is not completely compensated for by the calculation of the differential capacitance. Thus, there will be some error associated with the capacitance measurements at the step potentials.

In order to eliminate this problem, the same strategy was used as in the reductive desorption measurements: After each 25s potential step, capacitances were also measured at -400 mV/SCE, a potential where the electrode is stable, and no undesirable reactions with the thiol occur. Figure 5-6 (A) shows the capacitance of the bead electrode both uncoated and coated with C10-thiol. The increase in the capacitance of the uncoated electrode above +300 mV/SCE is likely due to a residual amount of gold oxide remaining on the electrode, as gold oxide formation occurs beginning at ~+300 mV/SCE at this pH. The uncoated electrode again has an initial
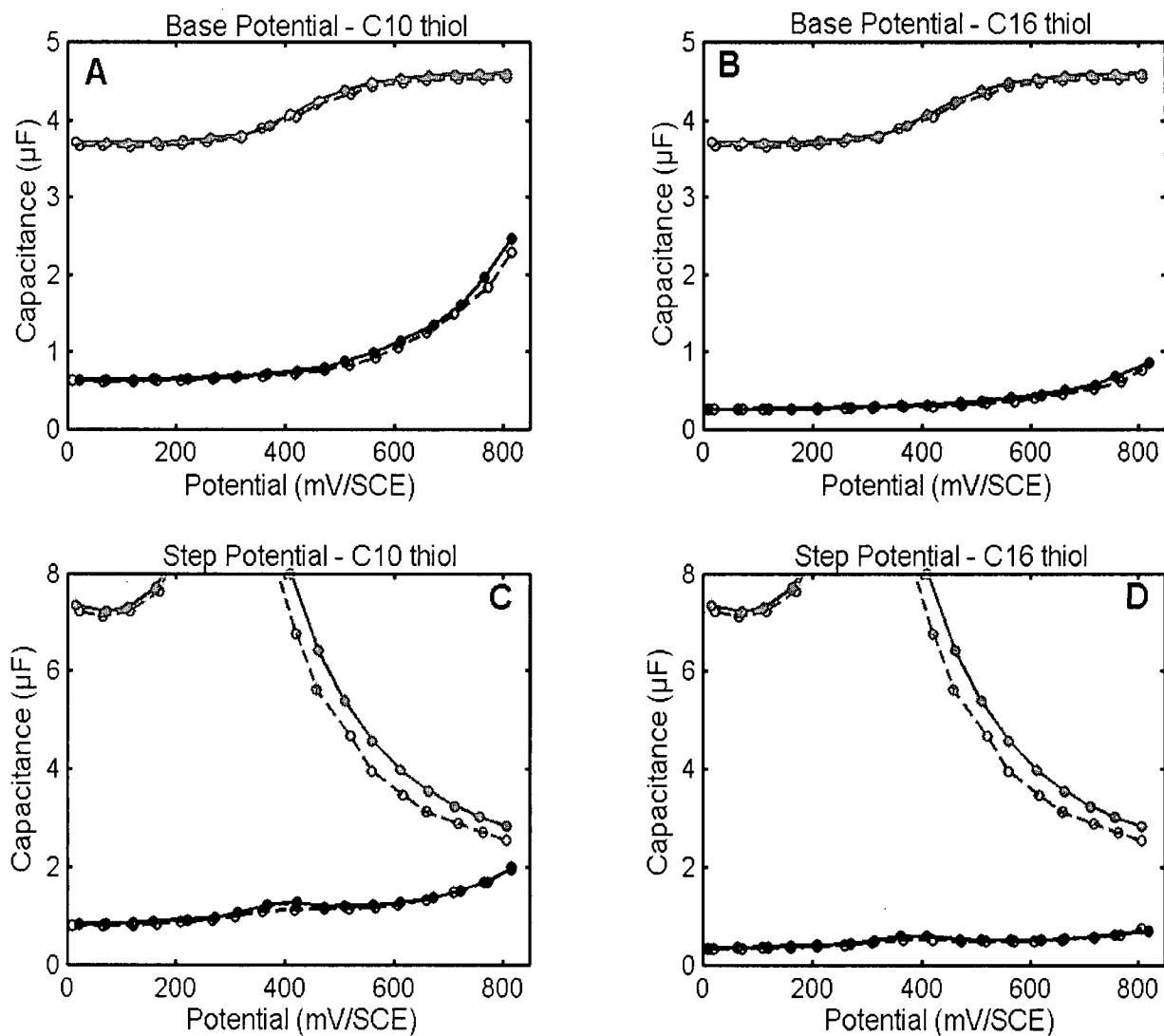
Figure 5-6 Capacitances from oxidative desorption of C10 (A,C) and C16 (B,D) thiols using pH 10±1 electrolyte. Black lines are capacitances from the thiol-modified electrodes, gray lines are from bare Au electrode. Solid lines and circles represent capacitance values from 5 seconds held at the potential, dashed lines with hollow circles represent capacitance values from 25 seconds.

81
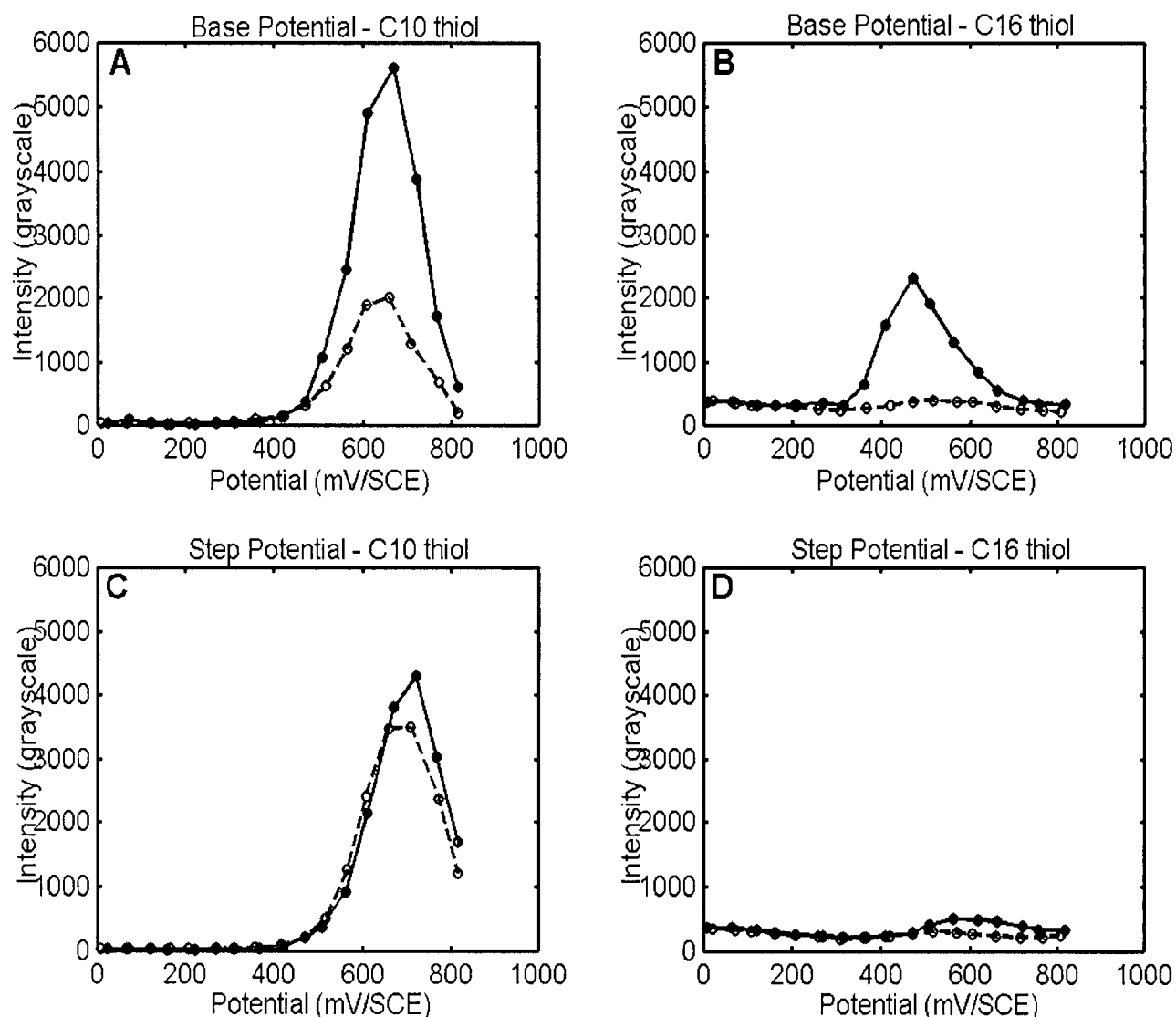
Figure 5-7 Fluorescence intensity from oxidative desorption of C10 (A,C) and C16 (B,D) thiol in pH 10(±1) electrolyte, represented by average greyscale value of image (max= 65536). C10 images used a 0.5 sec exposure time, C16 images used 1.5 sec exposure time, which has been normalized to a 2-second exposure time for comparison purposes. All images were acquired with a gain of 2 and 1x1 binning. Solid lines represent intensities after 5 sec at the potential, dashed lines after 25 sec. See Appendix A for the images from which these measurements were derived.

capacitance much higher than the C10-thiol coated capacitance. The coated electrode capacitance is relatively stable at ~0.75 µF until +450 mV/SCE, where a gradual increase in the capacitance begins, reaching ~2.5 µF by +800 mV/SCE. The final capacitance value is well below the uncoated capacitance value of ~4.7 µF, indicating that some organic material is still adsorbed on the electrode surface. By the parallel-capacitor approximation, about 45% of the monolayer remains on the electrode. It is possible that either the thiol has not fully desorbed from the electrode surface or that the oxidation product is physically adsorbed to the electrode surface at this potential, lowering the dielectric constant of the interface and reducing the capacitance.

The C16 thiol, Figure 5-6 (B and D), behaves in a similar manner to the C10 thiol. The initial capacitance is lower than that of the C10 thiol, suggesting that either the C16 thiol monolayer has greater surface coverage, or a decreased dielectric constant when compared to the C10 thiol. The capacitance of the C16 thiol remains relatively constant in both the step and base potentials, with the only major change being a rise from ~0.3 µF to ~0.9 µF at the base potential, in the 600-800 mV/SCE step potential range. A much greater fraction of the monolayer remains on the bead (~85%) for the C16 thiol, indicating that the factors working against desorption are greater in this system versus the C10 thiol monolayer.

5.3.1.2   Epi-Fluorescence Investigations

Fluorescence measurements were taken according to the procedures and conditions outlined above. The fluorescence from the C10 thiol, represented as the average

grayscale value of the image, is shown for the base and step potentials in Figure 5-7 (A and C). At the step potentials, the fluorescence intensity begins to increase at +400 mV/SCE, increasing with each step until +700 mV/SCE. Though the fluorescence does decrease, it does not return to zero fluorescence by the maximum potential. The non-zero fluorescence indicates that there is still fluorophore moving away from the electrode surface at this potential. In agreement with the capacitance data, it may be concluded that the thiol monolayer has not been fully removed from the electrode at this potential, as fluorophore is still being released from the electrode surface at the maximum potential of +800 mV/SCE.

Data from the base step, where the thiol is not being further removed from the electrode, also show a large peak in fluorescence, beginning after the step to +400 mV/SCE and returning nearly to the baseline value after return from the step to +800 mV/SCE. As there should be no new thiol being removed from the electrode at the base potential (-400 mV/SCE), fluorescence at this potential must result from thiols oxidized from the electrode at the step potential. This is supported by the evolution of the fluorescence with time, at each potential, the fluorescence intensity is at a maximum at the beginning of the step, and substantially lower (up to 60% lower) at the end of the 25 seconds held at that potential. A model where the fluorophore is present in a large amount at the beginning of the measurement time, and is depleted by diffusion away from the visible area, or by readsorption onto the electrode surface would produce such a trend in the fluorescence intensity. However, the intensity at the beginning of the base potential measurements are higher than the intensity at the end of the preceding step potential measurement, indicating that new fluorophores are being dequenched,

though none are being oxidized.

The fluorescence at the step potential is consistently lower than that at the base step, especially for the C16 thiol. The most likely explanation for this lies with the solubility of the oxidation products upon desorption. Though the exact product of the thiol oxidation is unknown, it is likely to be predominantly a carbonyl or sulfonyl terminated entity[10][25]. Either of these groups would have similar solubility properties, notably that when in the charged form (in basic media), solubility is significantly enhanced compared to the uncharged form (in acidic media). The charged molecules interact more strongly with water, and the electrostatic repulsions counter close-range attractions such as chain-chain interactions between molecules, causing the charged groups to spread out. This interaction will increase the solubility of the products, either by increasing the solubility of individual molecules or increasing the likelihood of forming micelles. The transition from charged to uncharged occurs between pH 2 for short-chained carboxylic acids and pH 6 for longer-chained acids, such as stearic acid $(C_{17}H_{35}COOH)$.[81]

It is possible that, though some of the oxidized thiol moved away from the electrode at the step potential, some of the oxidized thiol was held near the electrode by low solubility in a region of decreased pH immediately surrounding the electrode surface. The step potentials in the oxidation experiment go well above the potential at which the oxidation of gold occurs on the unmodified electrode (+300 mV/SCE at this pH). The electrochemical reaction of gold to form gold hydroxide:

$$Au^0 + 3H_2O \rightarrow Au(OH)_3 + H^+ + e^-$$ (5.1)
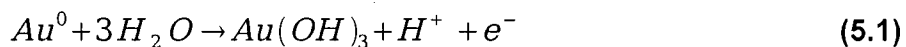
results in the formation of hydrogen ions in the region surrounding the electrode surface, lowering the pH in the immediate area. This reaction is reversed on return to the base potential, returning the pH at the interface to that of the bulk solution. As the thiol is expected to be less soluble in the lower-pH solution, it is possible that a portion of the thiol oxidized from the electrode at the step potential was unable to migrate far enough away from the metal surface to be dequenched from the metal. Upon return of the region to higher pH, the thiol was more able to move away from the electrode surface and fluoresce.

As the C16 thiol is generally less soluble than the C10 thiol, it would be expected that this effect would be stronger with the C16 thiol. Though this is hard to judge, as the overall fluorescence intensity is lower, the difference between the fluorescence at the base and step potentials is certainly greater than for the C10 thiol, supporting this hypothesis.

The increase in fluorescence from the C10 thiol occurs at a slightly lower potential than the beginning of substantial change in the capacitance. This could be due to selective desorption from the facet which occupies much of the visible area in the fluorescence images, which would skew the fluorescence data towards the properties of the facet. The electrode itself is polycrystalline, and it is possible that the visible facet desorbs at a potential more negative than that required to desorb the thiol from the remainder of the electrode.

The C16 thiol has a much lower maximum fluorescence intensity than the C10 thiol, even though the exposure time is longer. One possible cause for this phenomenon is the self-quenching of fluorophores held inside their Förster distance by chain-chain interactions of the thiol. It may be also simply due to less fluorophore being released from the electrode surface. The capacitance data shows that the change in capacitance of the C16 thiol is much less than that of the C10 thiol, suggesting that the adsorbed layer remains more intact for the longer-chain thiol, thus resulting in a lower amount of measured fluorescence.

5.3.2 Oxidative Desorption in Neutral Electrolyte

Investigations were also carried out on the oxidative desorption of the C10-and C16-BODIPY-SH thiols in neutral electrolyte (pH 5±0.5), unmodified by adding acid or base. Examining the oxidative behavior in lower pH environments provides the benefit of being able to observe the oxidation of the thiol monolayer in a potential regime where the oxidation of gold has been shifted to a larger positive potential, allowing the potential to be stepped farther positive without damaging the surface.

5.3.2.1   Electrochemical Investigations

Electrochemical investigations of the oxidation of the thiol SAMs were carried out in the same manner as for the basic electrolyte in the previous section, except that the step potentials ranged from +650 mV/SCE to +1350 mV/SCE to accommodate the shift in

the gold oxidation potential. Capacitance measurements taken during the investigations are summarized in Figure 5-8. Figure 5-8 (C), the capacitance of the C10-thiol modified electrode at the step potential, shows that the initially low capacitance begins to rise sharply beginning at +900 mV/SCE, reaching a maximum of ~2.75 µF at +1100 mV/SCE. The capacitance positive of +1100 mV/SCE is near the value of the bare gold capacitance, but slightly lower. This difference in capacitance is likely due to a convolution of the error inherent in capacitance measurements when a charge-transfer reaction is taking place, and a slight difference in electrode area exposed to the electrolyte between the two measurements.

The capacitance at the base potential for the oxidation of the C10 thiol has a similar profile, starting at ~0.3 µF and increasing after +900 mV/SCE. At the base potential, however, the capacitance does not reach a plateau, but continues to rise to a maximum of ~3.5 µF by +1350 mV/SCE. This value is again lower than the capacitance of the unmodified electrode (~4.5 µF), suggesting that ~80% of the surface is exposed to the electrolyte. The capacitance did not reach a steady maximum value, indicating that there is still some organic material being removed from the surface between each potential step. This could be due to incomplete removal of the thiol monolayer, or readsorption of oxidation products onto the electrode surface. The C16 thiol has a similar behavior, with the onset of the increase in capacitance beginning at +1000 mV/SCE for both the base and step potentials. The capacitance at the step potential also reaches a plateau value of ~2.5 µF beyond +1200 mV/SCE. The capacitance at the base potential is still increasing at +1350 mV/SCE, achieving a maximum value of
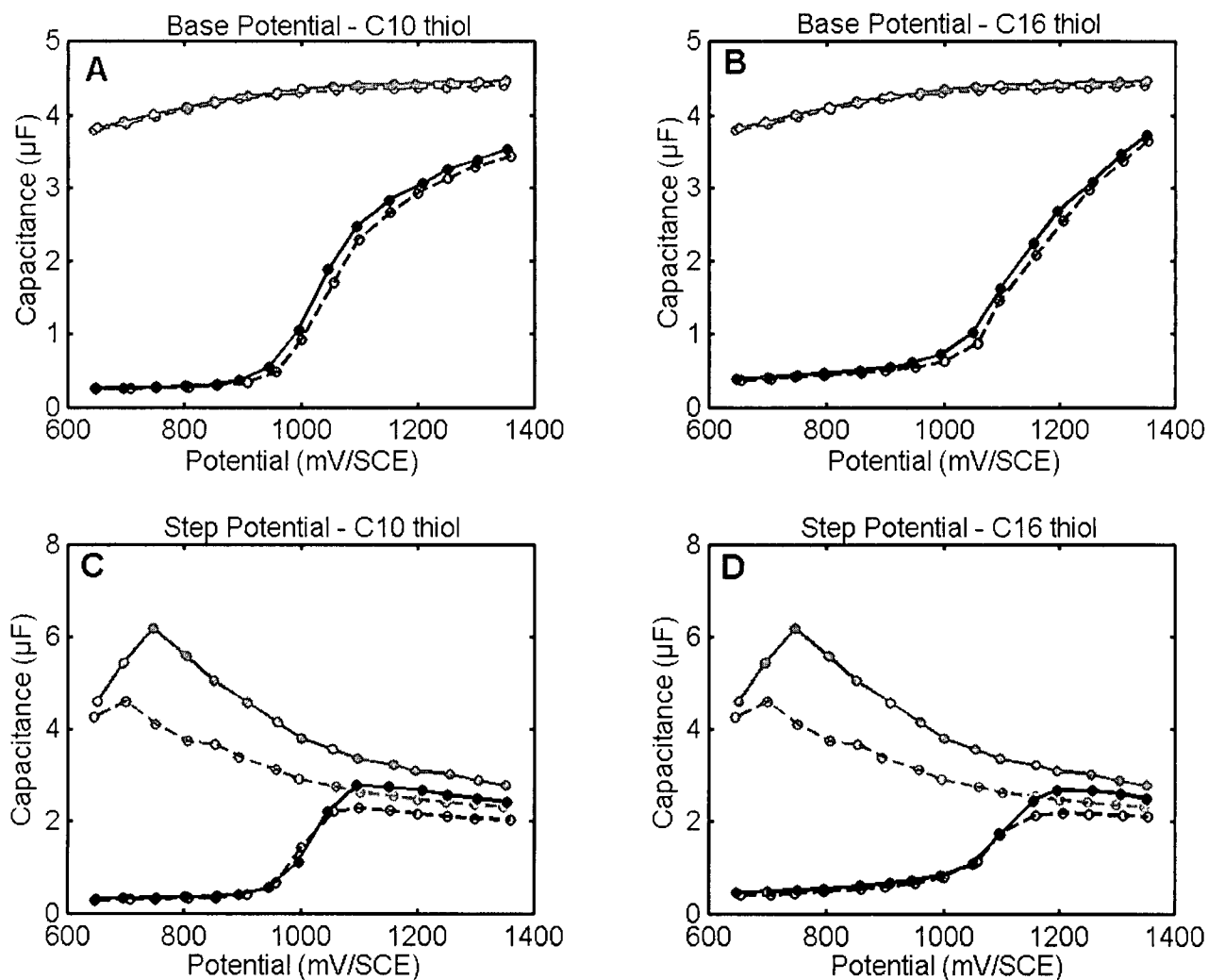
Figure 5-8 Capacitances from oxidative desorption of C10 (A,C) and C16 (B,D) thiols using pH 5±0.5 electrolyte. Black lines are capacitances from the thiol-modified electrodes, gray lines are from bare Au electrode. Solid lines and circles represent capacitance values from 5 seconds held at the potential, dashed lines with hollow circles represent capacitance values from 25 seconds.

89
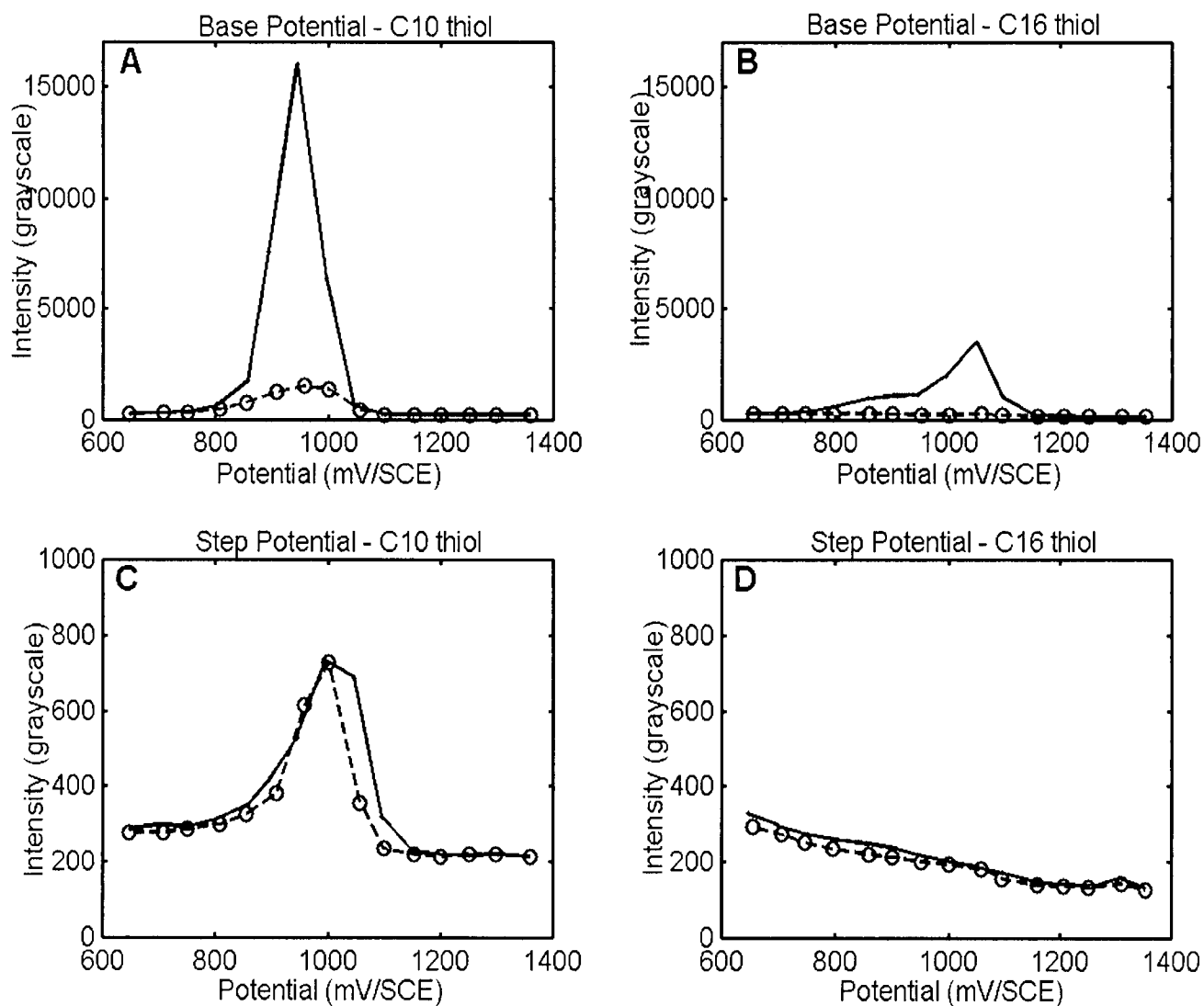
Figure 5-9 Fluorescence intensity from oxidative desorption of C10 (A,C) and C16 (B,D) thiol in pH 5±0.5 electrolyte, represented by average greyscale value of image (max= 65536). C10 images used a 0.5 sec exposure time, C16 images used 2 sec exposure time. All images were acquired with a gain of 2 and 1x1 binning. Solid lines represent intensities after 5 sec at the potential, dashed lines after 25 sec. See Appendix A for the images from which these measurements were derived.

~3.75 µF, suggesting that ~80% of the original thiol monolayer has been desorbed. The lack of complete desorption could be just that, or could be partially assignable to differences in electrode area between measurements and physical adsorption of oxidation products to the electrode surface. The shift in potential of the thiol removal versus the C10 thiol at the same pH is ~100 mV. An increase in potential is expected for the longer-chain thiol, as it is less soluble in aqueous media than the thiol with a shorter alkyl chain, and the relative difference in potential is roughly consistent with the shift observed at higher pH. The shift in oxidation potential of the C10 thiol at pH 5 vs pH 10 (~ +450 mV) does not correlate well with the potential shift predicted by the Nernst equation for the change in hydrogen ion concentration. However, it does agree well with the reports of Widrig [10] for propanethiol (Widrig: -79mV/pH, experimental: -80 mV/pH). The C16 thiol is more difficult to compare due to the small change in capacitance at pH 10 making it difficult to pinpoint exactly the onset of desorption.

5.3.2.2   Epi-Fluorescence Investigations

As in the investigations in alkaline electrolyte, fluorescence images were taken concurrently with the capacitance measurements. The same microscope settings and exposure times were used in the neutral media. Figure 5-9 (B), illustrating the fluorescence intensity from the C10 thiol at the step potential, shows that the fluorescence intensity begins to increase gradually from +750 mV/SCE, then increases more sharply beginning at+750 mV/SCE. The maximum of this increase corresponds to the center of the sharp rise in capacitance at the step potential, supporting the

correspondence of the change in capacitance with the visible removal of the thiol from the electrode surface. The value of the fluorescence intensity as the experiment time increases is also fairly steady, either equal to or slightly smaller at 25 seconds than the value after 5 seconds. This can be expected for a system where the fluorophores that are moving away from the electrode surface and out of the visible area are being replaced by newly desorbed fluorophores at nearly the same rate as they are moving out of view.

The fluorescence from the C10 thiol at the base potential, after remaining steady at the baseline value, begins to increase dramatically at +800 mV/SCE, rising to a maximum of ~11000 at +900 mV/SCE, then returning to the baseline value for step potentials above +1050 mV/SCE. The intensity after 25 seconds is much lower, indicating that the fluorophores are drifting out of the visible area faster than they are being replaced, as would be expected at a potential where no further oxidation of the thiols is occurring. This data also agrees with the hypothesis that the oxidation products are being held near the electrode at the step potentials, and subsequently released upon return to the base potential, likely through the mechanism of pH lowering with gold oxidation. The maximum intensity from the C10 thiol is much greater than that in alkaline electrolyte. This may be due to simply more thiol present in the SAM from a more well-formed layer, or the increase in fluorescence may be due to a greater pre-concentration of the thiols during the step potential. At higher pH, the combination of higher thiol solubility at the bulk solution pH and a higher pH at the electrode surface would result in a greater amount of the fluorophores being able to move away from the electrode surface during the step potential, despite the H^+ production at oxidizing potentials. At lower solution

92

pH, the oxidation product would be even less soluble at the step potential, and more product would remain near the electrode surface. The release of this concentrated collection of oxidized thiol on return to the base potential would result in a spike in the fluorescence intensity, which would be greater than the corresponding increase for the more alkaline media.

The C16 thiol has a much lower maximum fluorescence intensity overall than the C10 thiol. No appreciable increase in fluorescence is visible at the step potential. A low peak, starting at +800 mV/SCE , and increasing further from +900 mV/SCE to +1050 mV/SCE, then returning to the baseline by +1150 mV/SCE is visible. As with the C10 thiol, the maximum fluorescence intensity corresponds to the step potential in the middle of the rapid capacitance increase, though the fluorescence intensity does increase before a significant change in the capacitance is seen. The results thus support the pattern of both the correspondence of the change in capacitance to the actual release of the thiol from the electrode surface, and of the lowering of fluorescence intensity at the step potential.

5.3.3 Oxidation of Thiols in Acidic Electrolyte

Oxidation of the fluorescent thiols was carried out at another pH value for comparison to the previously obtained data. The method used was the same as for the neutral electrolyte, and the pH of the solution was adjusted with diluted perchloric acid to pH 2 ± 0.5.

5.3.3.1 Electrochemical Investigations

Capacitance measurements were obtained as for the previously described experiments, from +650 to +1350 mV/SCE. Figure 5-10 (C) shows the capacitance data for the C10-thiol modified electrode at the step potential. As with the measurements in neutral electrolyte, the capacitance began at a low initial value, then began to increase sharply, from ~0.2 µF at +950 mV/SCE to ~2.3 µF at +1150 mV/SCE. From +1150 mV/SCE and positive, the capacitance levels off, even decreasing slightly until +1350 mV/SCE. The leveling off of the capacitance indicates that little thiol is being removed from the electrode surface at these potentials, even though the capacitance is still below the value for the unmodified gold electrode (approx. 4.1 µF at +1150 mV/SCE). This depression in capacitance, as in the previous experiments, is most likely due to a decrease in the electrode area exposed to the electrolyte, with some possible contribution from unoxidized thiols and physically adsorbed oxidation products.

At the base potential (Figure 5-10 (A)), the capacitance again remains constant at the initial value ~0.2 µF, then increases sharply beginning at +950 mV/SCE to ~2.7 µF at +1350 mV/SCE, though the rate of increase appears to slow slightly positive of +1200 mV/SCE. As in the step potential, this capacitance is significantly lower than that of the bare gold measurements (about 60% of the bare gold capacitance), and the difference is likely due to similar reasons.

The capacitance of the C16-thiol modified electrode again follows the same general pattern as that from the C10 monolayer. At the step potential (Figure 5-10 (D)), the

94
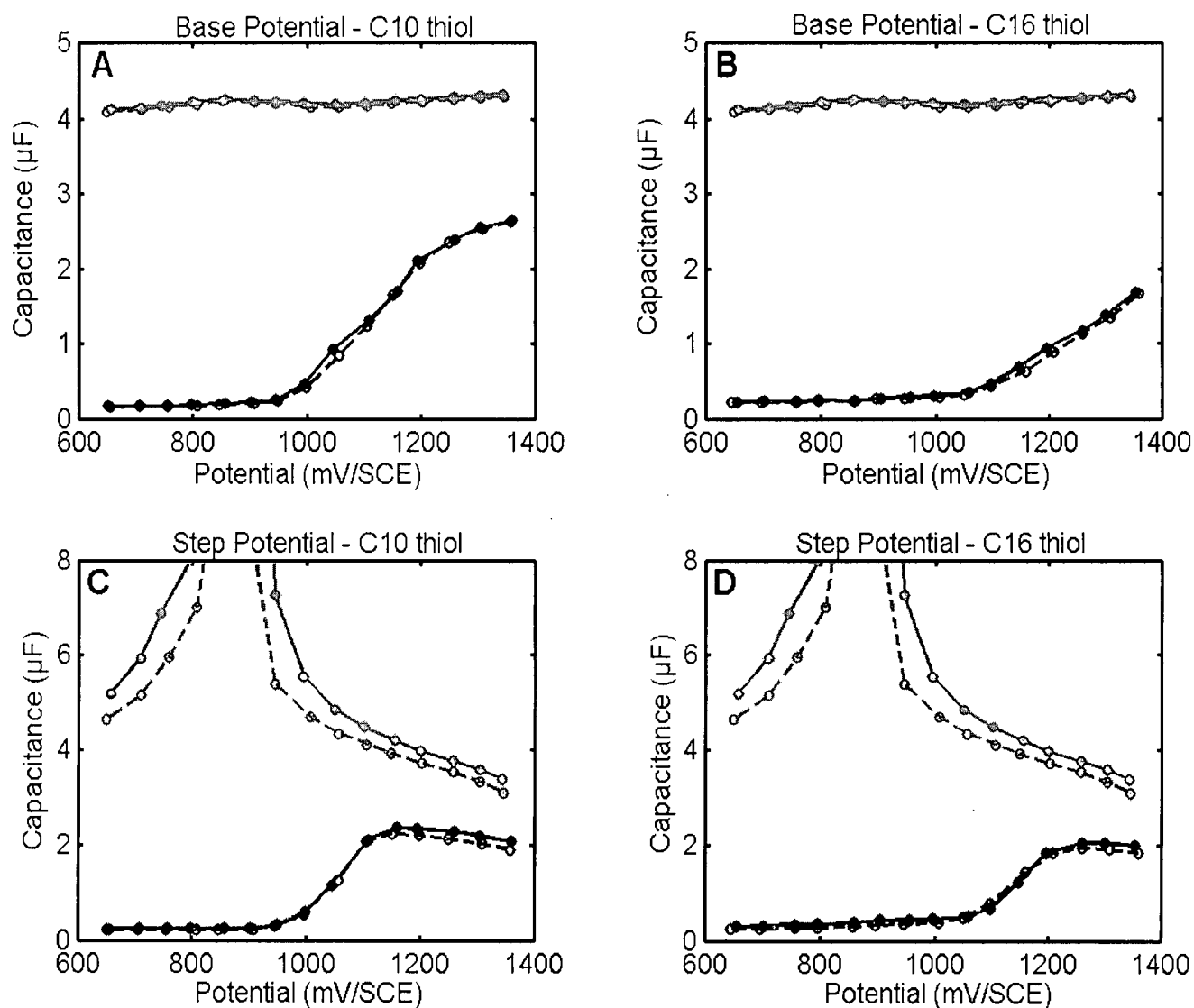
Figure 5-10 Capacitances from oxidative desorption of C10 (A,C) and C16 (B,D) thiols using pH 2±0.5 electrolyte. Black lines are capacitances from the thiol-modified electrodes, gray lines are from bare Au electrode. Solid lines and circles represent capacitance values from 5 seconds held at the potential, dashed lines with hollow circles represent capacitance values from 25 seconds.
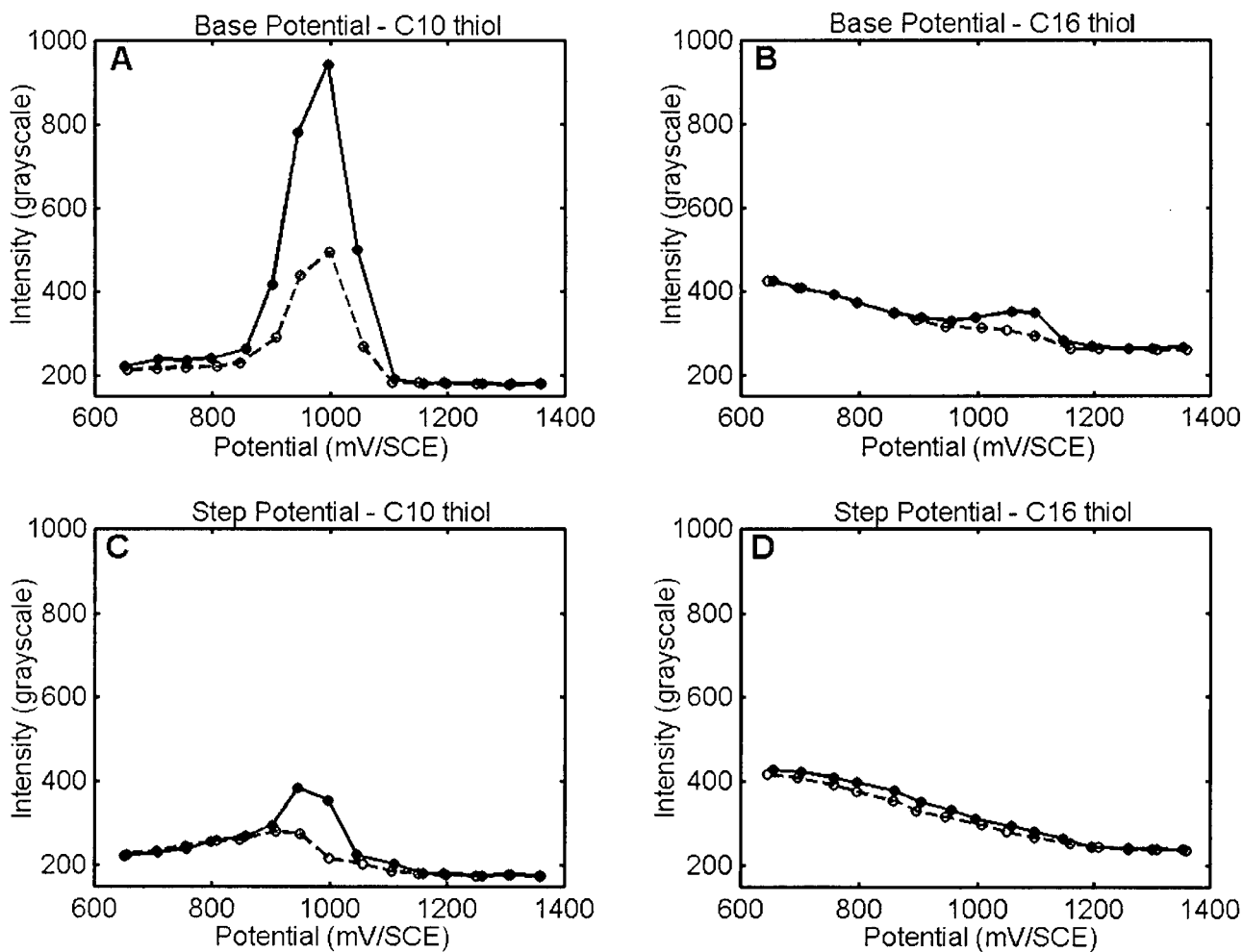
Figure 5-11 Fluorescence intensity from oxidative desorption of C10 (A,C) and C16 (B,D) thiol in pH 2±0.5 electrolyte, represented by average greyscale value of image (max= 65536). C10 images used a 0.5 sec exposure time, C16 images used 2 sec exposure time. All images were acquired with a gain of 2 and 1x1 binning. Solid lines represent intensities after 5 sec at the potential, dashed lines after 25 sec. See Appendix A for the images from which these measurements were derived.

initially low capacitance remains stable until +1050 mV/SCE. From +1050 mV/SCE to +1200 mV/SCE, the capacitance increases from ~0.3 µF to ~2 µF , then remains stable until +1350 mV/SCE and the end of the data collection. As with the previous experiments, the maximum capacitance of the thiol-modified electrode does not achieve the same capacitance as the unmodified electrode. Using the parallel-capacitors model, the change suggests that ~35% of the initial thiol monolayer was desorbed. This small capacitive increase could indicate either the presence of organic material on the surface (unoxidized thiol or physically adsorbed reaction product) or an inconsistency in the electrode area exposed to the electrolyte between the two experiments. At the step potential, it is also possible that differences in measured capacitances may arise from interference by the charge transfer current associated with the oxidation of gold.

At the base potential, the capacitance remains steady at the same initial value, gradually increasing at step potentials +1050 mV/SCE and beyond, increasing from ~0.3 µF to ~1.8 µF by +1350 mV/SCE. As in previous measurements, the final capacitance value of the thiol modified electrode is substantially lower than the value for the bare electrode, likely due to the same factors previously cited. The 100 mV increase in oxidation potential from the C10 to the C16 thiol is consistent with the increases between the two thiols at the other pH values measured. The increase in the oxidation potential of the thiols (~50mV) from pH 5 to pH 2 does not correspond to either a Nernstian relationship or the data reported from Widrig [10]. This may be due to the presence of two distinct regimes in Widrig's report: pH < 4 and pH >7. Though pH 5 lies between the two regimes, the difference between the two regimes is large enough that

comparison between a pH in one domain with one from another would result in an erroneous conclusion. A fourth point in the pH < 4 region is needed to determine if the results from this thesis correspond to the literature in both pH regimes.

5.3.3.2   Epi-fluorescence Investigations

Fluorescence measurements were taken along with the capacitance measurements, and are summarized in Figure 5-11. The fluorescence from the C10 thiol at the step potential, Figure 5-11 (C), is very low, as compared to the previous C10 fluorescence intensities, with only a small peak in fluorescence from +900 mV/SCE to +1050 mV/SCE. The background fluorescence also decreases slightly over the course of the experiment, a phenomenon possibly due to a small amount of fluorescence from physically adsorbed thiol not removed from the bead by sonication present on the electrode surface, which is desorbed along with the chemisorbed thiol monolayer. At the base potential, the same decrease in background fluorescence is evident, however the peak in fluorescence intensity is more pronounced. Beginning after the return from the step potential of +850 mV/SCE, the fluorescence intensity builds to a maximum of 975 counts at +1000 mV/SCE, the lowest by far of the three pH values, and returns to the baseline t +1100 mV/SCE. The C16 thiol has almost nonexistent fluorescence in the acidic electrolyte, showing no peak in fluorescence at the step potential at all, and only a small ~100 count peak at the base potential, from +850 mV to +1150 mV. The peaks from both thiols continue the trend of being centered at the beginning of the region of rapid change in capacitance, further support for the working hypothesis that the increase in capacitance was due to the thiol being removed from the electrode

98

surface, rather than some other reaction. As well, the trend of depressed fluorescence at the step potential is continued, reinforcing the need for a mechanism to explain this behavior. The decrease in the overall fluorescence is interesting, however, as the BODIPY fluorophore has been shown to have little pH dependency on its fluorescence intensity, and currently no explanation exists for this behavior.

5.3.4 Summary

The oxidative desorption of thiols was observed using the base-step potential profile, both by electrochemical and spectroelectrochemical measurements. Capacitance measurements indicate that the removal of the monolayer is incomplete, ranging from The C16-thiol monolayer consistently desorbed at a potential approximately 50 mV higher than that of the C10 thiol-modified electrode. An increase in solution pH is correlated with a decrease in the desorption potential for both thiols, though the relationship is not consistent across the pHs measured. Fluorescence is enhanced at the base potential relative to the step potential, perhaps due to a local pH effect on solubility.

6 Conclusions

The independence of the fluorescence of the C10- and C16-BODIPY-SH compounds to changes in solution pH was confirmed by *ex-situ* fluorescence measurements. The reductive desorption of C10 and C16 thiol SAMs was demonstrated and observed using epi-fluorescence microscopy. The increase in capacitance attributed to removal of the thiol monolayer from the electrode surface was correlated with the increase in measured fluorescence intensity as potentials were stepped in the negative direction. The use of an alternating base-step potential profile was established, and was then used to demonstrate the reductive desorption and oxidative readsorption of the C10 and C16 thiol SAMs. Though the fluorescence images were clouded both by desorbed thiolates remaining in the visible area and by oxidatively readsorbed thiols re-desorbing in subsequent steps, the selective nature of the reductive desorption was confirmed.

The base-step potential profile was then used to examine the oxidative desorption of the C10 and C16 thiol SAMs, and evidence of oxidative desorption was confirmed by use of epi-fluorescence microscopy. The increase in capacitance due to the oxidative removal of the adsorbed thiol monolayer was considered alongside the fluorescence intensity at the same potential. Fluorescence intensity was greater at the base potential than at the step potential, though the thiol was actually desorbed at the step potential (as indicated by the capacitance measurements). This unexpected behavior is attributed to a local decrease in pH near the electrode surface at oxidizing potentials. The proposed oxidation products will be less soluble in the acidic medium into which they desorb, causing them to aggregate and remain close to the electrode surface.

Fluorescence is quenched by the metal, so will only be observed from the fraction of molecules that do diffuse far enough away from the electrode.

On return to the base potential, the solution pH near the electrode is returned to the pH of the bulk solution, in which the oxidation products are more soluble. This allows more of the products to move away from the electrode and into a region where their fluorescence is observable, resulting in an increase in the fluorescence intensity even though no further thiol is being removed from the surface.

The electrolyte pH was found to have an effect on both the desorption potential and the fluorescence intensity. Generally, as the pH increased, the desorption potential decreased. The change in desorption potential (as measured by capacitance) with solution pH (-80 mV/pH) agreed with previous measurements [10] on alkanethiols at the two higher pH values. A fourth pH point is required to correctly determine if the pH response below 4 also agrees. Fluorescence measurements were correlated with the capacitance measurements for three pH values, and confirmed that desorption is occurring at the potentials when capacitance increases rapidly, and that the oxidation products are able to move away from the electrode surface.

The experiments were performed on thiols with two alkyl chain lengths, ten- and sixteen- carbons. The desorption potential required for the C16 thiol was consistently 50-100 mV larger than that for the C10 thiol. This behavior was expected, and may be attributed to the need for greater energy to disrupt the intermolecular forces binding the monolayer together in order to initiate oxidation (or reduction). Depending on the

mechanism, it is believed that a water or OH⁻ molecule is required for the oxidation reaction to occur, and it would need to penetrate the monolayer in order to reach the electrode surface and participate in the reaction. A greater energy required to draw a molecule through the monolayer, or create a defect from which the reaction may begin, would correspond to a larger (greater positive or greater negative) potential to be applied. The roughness of the electrode may also play a part in the value of the desorption potential: it has been suggested[82][83] that thiols desorb from defects and crystal edges first; thus a rougher electrode will behave differently than a smooth one with fewer edges. The electrode used in these studies was unpolished, and after several cycles of thiol adsorption and desorption developed pits related to the formation of the thiol monolayers. The electrode was not re-melted, in order to provide consistency in the crystal structure of the facet under study, so the evolving roughness of the electrode may slightly affect the desorption potentials.

The length of the alkyl chain also had a marked effect on the fluorescence of the desorbing monolayers. The C16 thiol had a consistently lower fluorescence intensity than the C10 at the same pH. This could be due either to the monolayers simply containing fewer molecules of the C16 thiol, or to a difference in solubility between the two thiols. The C16 thiol (and its reaction products) are expected to be less soluble in aqueous solution due to the longer alkyl chain, and thus may tend to aggregate and remain near the electrode-solution interface. This could reduce the measured fluorescence, either through self-quenching of the BODIPY fluorophore for molecules near to each other or, alternately, by quenching through coupling with the metal surface. Though both of these factors would also affect the C10 thiol, they are expected

102

to show a smaller effect due to the less hydrophobic nature of the shorter alkyl chain. The effect of pH on the C16 thiol was also greater than for the C10 thiol. Presumably, since the solubility of the C16 thiol (and thus its oxidation products) should be smaller, a decrease in the solution pH, causing a further decrease in the solubility of the product, would have a greater effect on the measured fluorescence.

The studies of the oxidative behavior of thiol monolayers at a gold electrode surface open the doors for many future investigations into the deeper nature of this behavior, including studies of the nature of the oxidation products.

7   Suggestions for Future Work

The oxidation of thiol SAMs is an underexplored branch of electrochemistry, and many interesting avenues of investigation remain related to the work presented in this thesis. Surface analysis (FTIR, for example) of the electrode could be used to great advantage to determine if the depression of the final capacitance after oxidative desorption is due to organic material on the surface, and if so, what material that is. As well, an improved electrode design with a more reproducible surface area, such as the hanging meniscus style used in previous work [16][17], could be used to eliminate the uncertainty in the electrolyte contact area.

There has been debate in the literature as to the product of electrochemical oxidation of thiols, viz. whether the C-S bond is broken, or solely the S-Au bond is broken on oxidation. Various spectroscopic techniques could be used to analyze the products in solution to determine their structure. FTIR has already been exploited for this [25][27], though the results so far are conflicting. A more exotic analysis could use the developing technique of X-ray absorption spectroscopy to probe the oxidation state of the sulfurous products and extrapolate the structure.

The mobility of the oxidative and reductive products could also be analyzed. Particularly of interest for the reduction products, it may be possible to use electroosmotic flow of the product to migrate it from one electrode to another, where it could be oxidatively readsorbed. The ability to manipulate the thiol in such a way would have numerous uses in sensor development and other applications. This could be carried out with some

104

modification of the current setup, all that is needed is two electrodes that can be brought very close together, and independent potential control over both of them.

As well, the interesting effect that solution pH appears to have on the fluorescence intensity could be investigated. If it is due to the behavior, such as micelle formation, of the oxidation product, then knowing its structure, as suggested above, will aid in solving this problem. Properties of the products themselves should also be investigated, such as the likelihood of the product to aggregate or form a disulfide, and if formation of such a product would affect fluorescence via self-quenching. An IR or Raman study would be appropriate to determine the formation of disulfides in the BODIPY-tagged thiols, or nonfluorescent analogues. Since even a small amount of fluorescence will interfere with the Raman spectrum, the use of a nonfluorescent analogue of the thiols used in this thesis would be advisable. Simple visible-spectrum fluorescence spectroscopy, as carried out for this thesis, would determine if the fluorescence is affected by various conditions.

Atomic force microscopy studies could also be used to examine the behavior of the thiol monolayers as desorption occurs. This would help elucidate whether aggregates form at the surface, if the desorption proceeds from defects and spreads outwards, or if it occurs from random sites throughout the layer. However, to ensure that as little as possible of the desorbed product adsorbs onto the tip surface, care would have to be taken in choosing tip coatings.

References

1. J D Swalen, *J Mol Electron* **1986**, *2*, 155.

2. D K Schwartz, *Annu Rev Phys Chem* **2001**, *52*, 107.

3. J C Love, L A Estroff, J K Kriebel, R G Nuzzo, G M Whitesides, *Chem Rev* **2005**, *105*, 1103.

4. Y-C Yang, Y-P Yen, L-Y O Yang, S-L Yau, K Itaya, *Langmuir* **2004**, *20*, 10030.

5. D-S Kong, S-L Yuan, Y-X Sun, Z-Y Yu, *Surf Sci* **2004**, *573*, 272.

6. P E Laibinis, G M Whitesides, D L Allara, Y-T Tao, A N Parikh, R G Nuzzo, *J Am Chem Soc* **1991**, *113*, 7152.

7. K J Stevenson, M Mitchell, H S White, *J Phys Chem B* **1998**, *102*, 1235.

8. M Borsari, M Cannio, G Gavioli, *Electroanalysis* **2003**, *15*, 1192.

9. J J Gooding, D B Hibbert, *Trend Anal Chem* **1999**, *18*, 525.

10. C A Widrig, C Chung, M D Porter, *J. Electroanal. Chem.* **1991**, *310*, 335.

11. M G Sullivan, H Uotomo, P J Fagan, M D Ward, *Anal Chem* **1999**, *71*, 4369.

12. M Reipl, V M Mirsky, O S Wolfbeis, *Mikrochim Acta* **1999**, *131*, 29.

13. J L Shepherd (2005): *Electro-Fluorescence Characterization Of Insoluble Surfactants Adsorbed On Solid Electrodes*. Ph.D. Dissertation, University of British Columbia, Vancouver, BC. 233 p.

14. J L Shepherd, A Kell, E Chung, C W Sinclair, M S Workentin, D Bizzotto, *J Am Chem Soc* **2004**, *126*, 8329.

15. A J Bard and L R Faulkner, *Electrochemical methods. fundamentals and applications*. John Wiley and Sons: New York, 2001: 833 p..

16. J L Shepherd, D Bizzotto, *J Phys Chem B* **2003**, *107*, 8524.

17. J Shepherd, Y Yang, D Bizzotto, *J Electroanal Chem* **2002**, *524*, 54.

18. C D Bain, E B Troughton, Y Tao, J Evall, G M Whitesides, R G Nuzzo, *J Am Chem Soc* **1989**, *111*, 321.

19. K Shimazu, I Yagi, Y Sato, K Uosaki, *Langmuir* **1992**, *8*, 1385.

20. R Yamada, H Sakai, K Uosaki, *Chem Lett* **1999**, , 667.

21. T W Schneider, D A Buttry, *J Am Chem Soc* **1993**, *115*, 12391.

22. D E Weisshaar, B D Lamp, M D Porter, *J Am Chem Soc* **1992**, *114*, 5860.

23. H O Finklea, S Avery, M Lynch, *Langmuir* **1987**, *3*, 409.

24. W H Mulder, J J Calvente, R Andreu, *Langmuir* **2001**, *17*, 3273.

25. D-F Yang, H Al-Maznai, M Morin, *J. Phys. Chem. B* **1997**, *101*, 1158.

26. V M Mirsky, *Trends Anal Chem* **2002**, *21*, 439.

27. A-Z Yu, S Ye, H L Zhang, K Uosaki, Z-F Liu, *Langmuir* **2000**, *16*, 6948.

28. P W Atkins, *Physical chemistry*. Oxford University Press: Oxford, 1982: .

29. L M Raff, *Principles of physical chemistry*. Prentice-Hall: New Jersey, 2001: .

30. F W D Rost, *Fluorescence microscopy*. Cambridge University Press: New York, 1992: .

31. K H Drexhage, *J Luminescence* **1970**, *1/2*, 693.

32. K H Drexhage, H Kuhn, F P Schäfer, *Ber Bunsenges Physik Chem* **1968**, *72*, 329.

33. K H Drexhage, M Fleck, H Kuhn, F P Schäfer, W Sperling, *Ber Bunsenges Physik Chem* **1966**, *70*, 1179.

34. D H Waldeck, A P Alivisatos, C B Harris, *Surf Sci* **1985**, *158*, 103.

35. W H Weber, C F Eagen, *Opt Letters* **1979**, *4*, 236.

36. R M Amos, W L Barnes, *Physical Review B* **1997**, *55*, 7249.

37. W L Barnes, *J Modern Optics* **1998**, *45*, 661.

38. BODIPY is a registered trademark of Molecular Probes, Inc.

39. http://probes.invitrogen.com/handbook/tables/0726.html.

40. J Karolin, L B- Johansson, L Strandberg, T Ny, *J Am Chem Soc* **1994**, *116*, 7801.

41. M Baruah, W Qin, N Basarić, W M De Borggraeve, N Boens, *J Org Chem* **2005**, *70*, 4152.

42. T Gareis, C Huber, O Wolfbeis, J Daub, *Chem Commun* **1997**, , 1717.

43. R A Bissell, A P de Silva, H Q N Gunaratne, P L M Lynch, G E M Maguire, K R A S Sandanayake, *Chem Soc Rev* **1992**, , 187.

44. C S Chen, O C Martin, R E Pagano, *Biophys J* **1997**, *72*, 37.

45. B P Wittmershaus, J J Skibicki, J B McLafferty, Y-Z Shang, S Swan, *J Fluor* **2001**, *11*, 119.

46. X D Song, B I Swanson, *Anal Chim Acta* **2001**, *442*, 79.

47. I Mikhalyov, S T Bogen, L B A Johansson, *Spectrochim Acta A* **2001**, *57*, 1839.

48. R C M Reis, M H F Sorgine, T Coelho-Sampaio, *Eur J Cell Biol* **1998**, *75*, 192.

49. A T Da Poian, A M O Gomez, T Coelho-Sampaio, *J Virol Method* **1998**, *70*, 45.

50. http://www.chroma.com/products/index.php?doPrintSet=yes&sSetID=41004.

51. http://www.olympusmicro.com/primer/microscopy.pdf.

52. Y Sato, S Ye, T Haba, K Uosaki, *Langmuir* **1996**, *12*, 2726.

53. M J Esplandiu, H Hagenström, D M Kolb, *Langmuir* **2001**, *17*, 828=838.

54. J J Calvente, Zuzana Kováčová, M D Sanchez, R Andreu W Ronald Fawcett, *Langmuir* **1996**, *12*, 5696.

55. D-F Yang, C P Wilde, M Morin, *Langmuir* **1997**, *13*, 243.

56. F Ma, R B Lennox, *Langmuir* **2000**, *16*, 6188.

57. M Schweizer, H Hagenstrom, D M Kolb, *Surf Sci* **2001**, *490*, L627.

58. T Sawaguchi, Y Sato, F Mizutani, *Phys Chem Chem Phys* **2001**, *3*, 3399.

59. D W Wang, F Tian, J G Liu, *J Vac Sci Technol B* **2002**, *20*, 60.

60. O Azzaroni, M E Vela, G Andreasen, P Carro, R C Salvarezza, *J Phys Chem B* **2002**, *106*, 12267.

61. H Wano, K Uosaki, *Langmuir* **2001**, *17*, 8224.

62. D Hobara, K Miyake, S Imabayashi, K Niki, T Kakiuchi, *Langmuir* **1998**, *14*, 3591.

63. H Hagenström, M A Schneeweiss, and D M Kolb, *Langmuir* **1999**, *15*, 2435.

64. C Schönenberger, J A M Sondag-Huethorst, J Jorritsma, L G J Fokkink, *Langmuir* **1994**, *10*, 611.

65. E Boubour, R B Lennox, *Langmuir* **2000**, *16*, 7464.

66. J Kim, H Uchida, N Honda, N Hashizume, Y Hashimoto, H Kim, K Nishimura, M Inoue, *Jpn J Appl Phys* **2003**, *42*, 4770.

67. C B Gorman, R L Carroll, Y He, F Tian, R Fuierer, *Langmuir* **2000**, *16*, 6312.

68. M S Lewis, C B Gorman, *J Phys Chem B* **2004**, *108*, 8581.

69. T Wilhelm, G Wittstock, *Mikrochim Acta* **2000**, *133*, 1.

70. J R Lakowicza, Y Shena, S D'Auriaa, J Malickaa, J Fangb, Z Gryczynskia I Gryczynskia, *Analytical Biochemistry* **2002**, *301*, 261.

71. J F Lacowicz, J Malicka, I Gryczynski, Z Gryczynski, C D Geddes, *J Phys D: Appl Phys* **2003**, *36*, R240.

72. K H Drexhage, *Sci Am* **1970**, *222*, 108.

73. R R Chance, A Prock, R Silbey, *Adv Chem Phys* **1978**, *37*, 1.

74. G W Ford, W H Weber, *Phys Rep* **1984**, *113*, 195.

75. D Bizzotto, J Lipkowski, *J Electroanal. Chem.* **1996**, *409*, 33.

76. D Bizzotto, B Pettinger, *Langmuir* **1999**, *15*, 8309.

77. R Stoodley, D Bizzotto, *Analyst* **2003**, *128*, 552.

78. E Chung, J L Shepherd, D Bizzotto, M O Wolf, *Langmuir* **2004**, *20*, 8270.

79. J Richer (1990): . Ph.D. Dissertation, University of Guelph, Guelph, ON.

80. D Bizzotto (1996): *Characterization Of The Adsorption Of Insoluble Surfactants Onto An Electrified Interface*. Ph.D. Dissertation, University of Guelph, Guelph, ON. 238 p.

81. George L. Gaines, Jr., *Insoluble monolayers at liquid-gas interfaces*. Interscience Publishers: New York, New York, 1966: .

82. M J Hostetler, A C Templeton, R W Murray, *Langmuir* **1999**, *15*, 3782.

83. B M Quinn, K Kontturi, *J Am Chem Soc* **2004**, *126*, 7168.

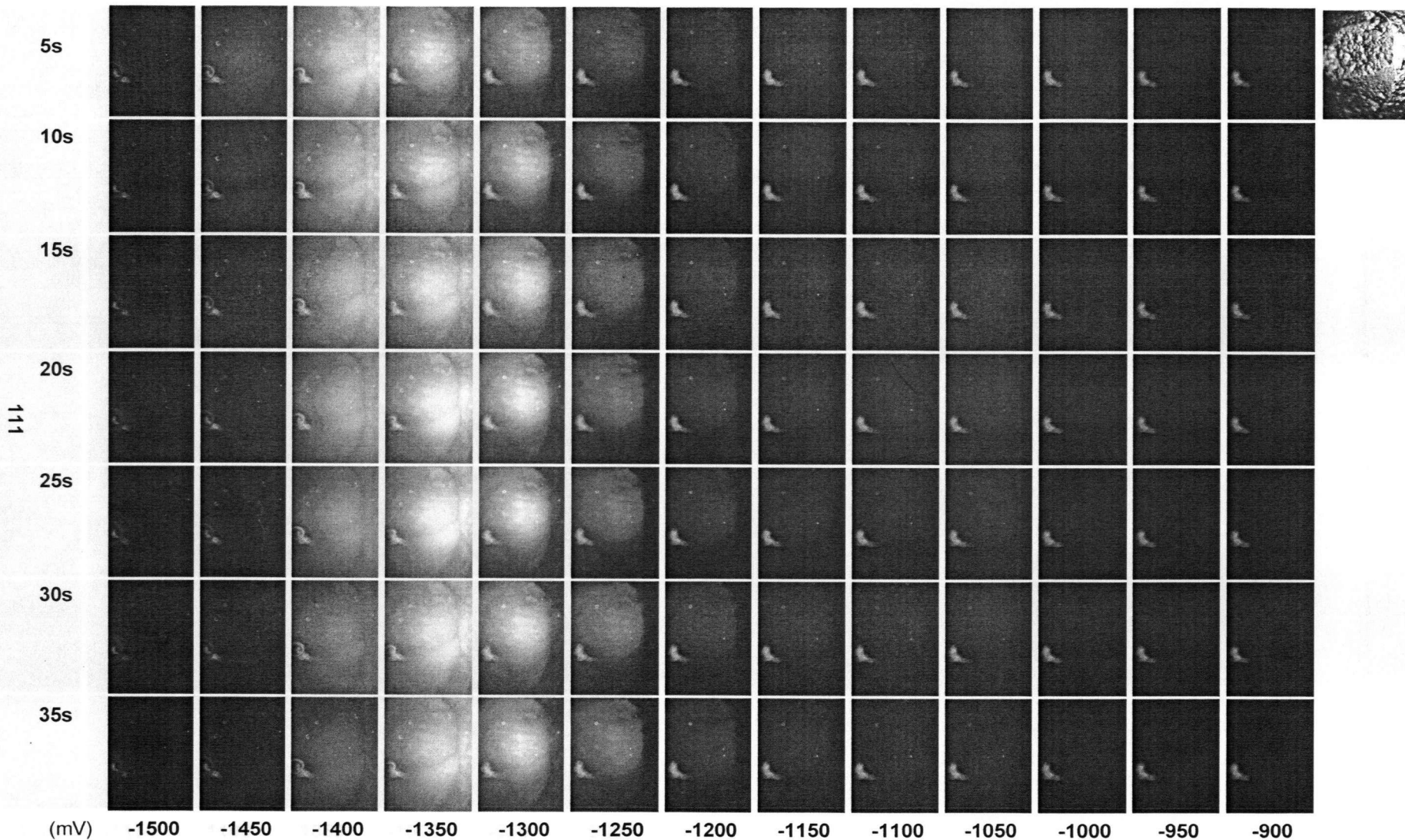# Appendix A:

Fluorescence Images

Figure A-1 Fluorescence images for reductive desorption of C10 thiol with 'sweeping' potential profile. A brightfield image of the electrode for orientational reference is included on the right. Images have been enhanced for clarity. Modifications to grayscale may not be linear.
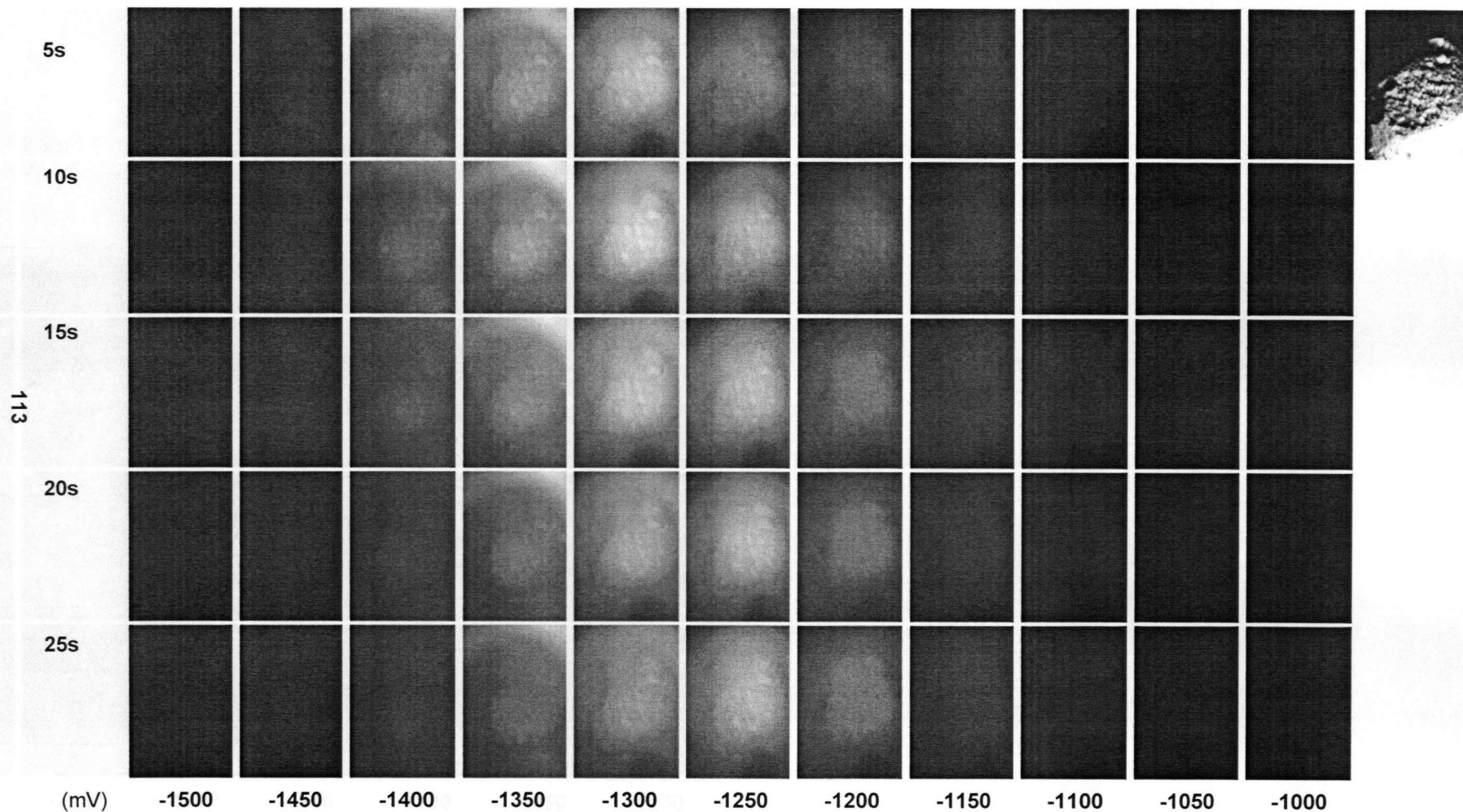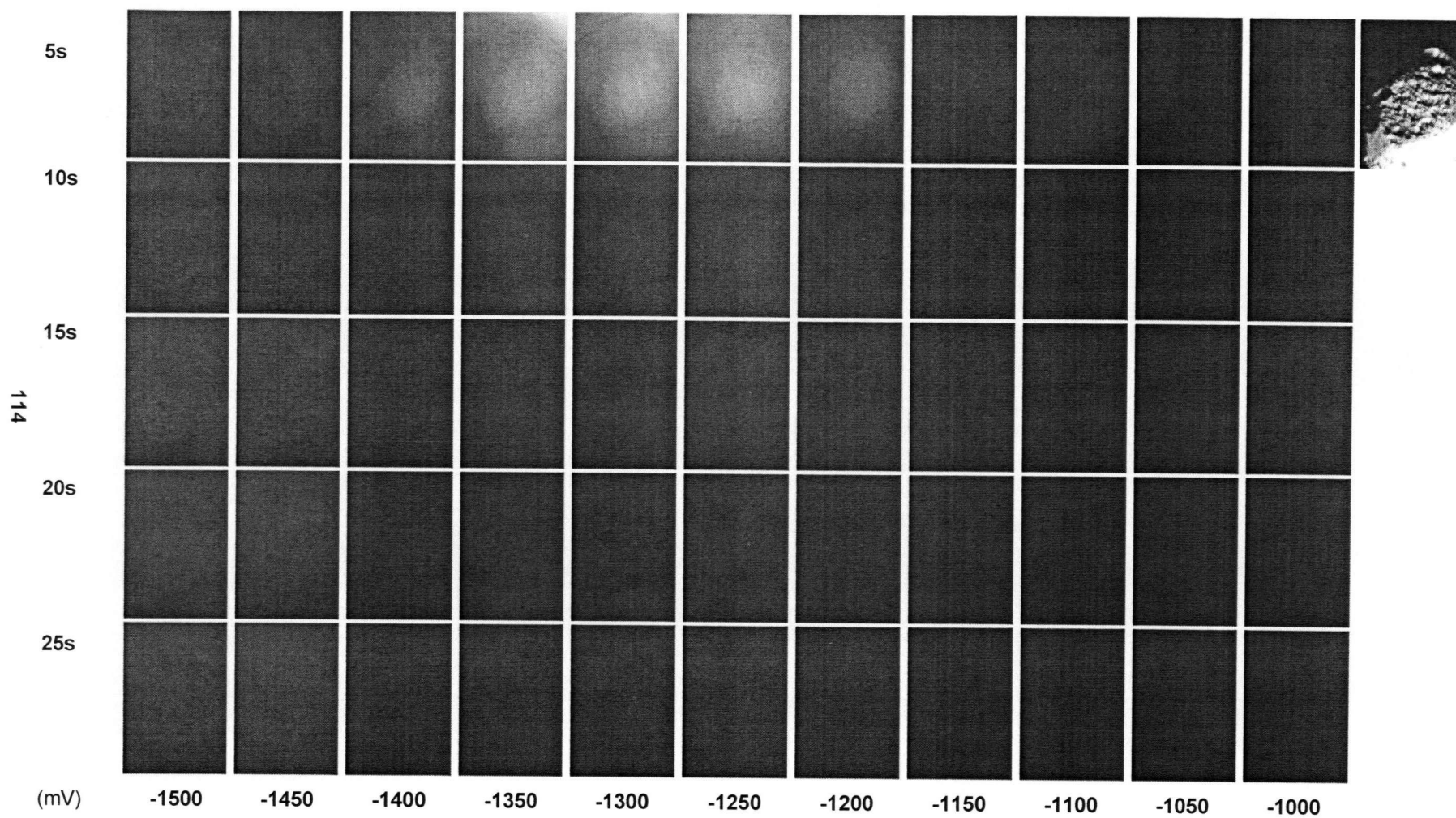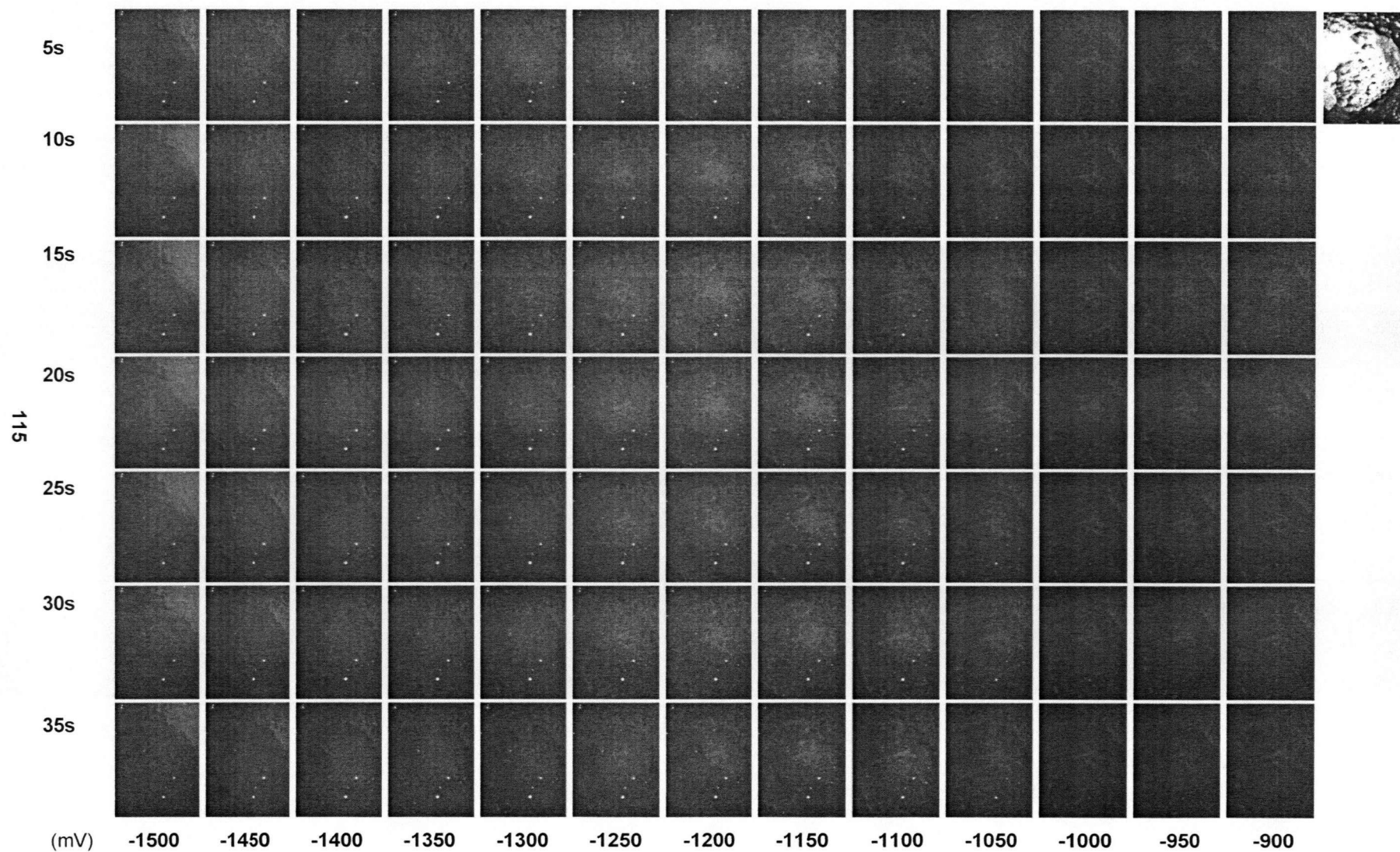
Figure A-3 Fluorescence images at step potential for reductive desorption of C10 thiol with 'base-step' potential profile. A brightfield image of the electrode for orientational reference is included on the right. Images have been enhanced for clarity. Modifications to grayscale may not be linear.

113

Figure A-4 Fluorescence images at base potential for reductive desorption of C10 thiol with 'base-step' potential profile. A brightfield image of the electrode for orientational reference is included on the right. Images have been enhanced for clarity. Modifications to grayscale may not be linear.
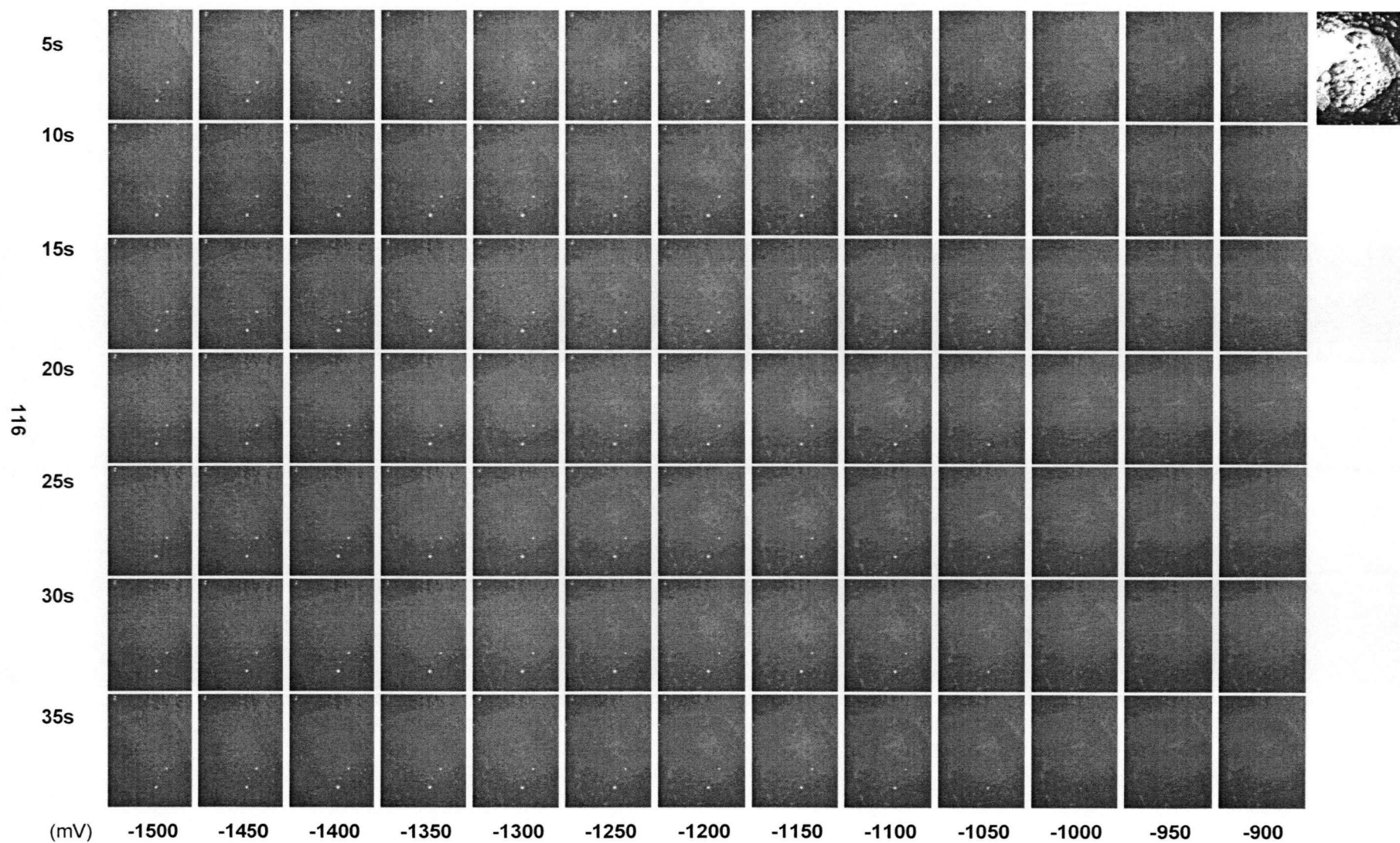
114

Figure A-5 Fluorescence images at step potential for reductive desorption of C16 thiol with 'base-step' potential profile. A brightfield image of the electrode for orientational reference is included on the right. Images have been enhanced for clarity. Modifications to grayscale may not be linear.
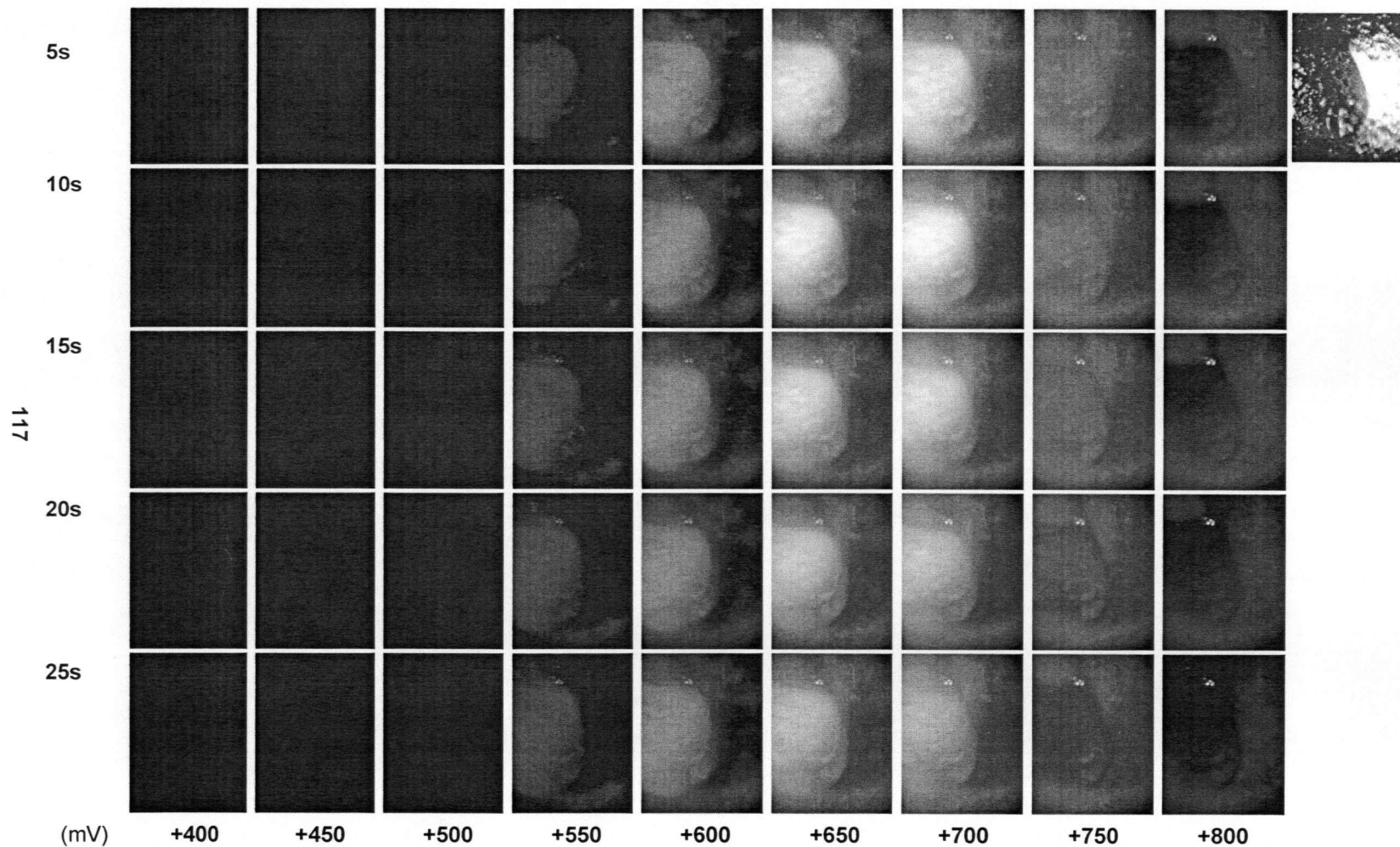
115

Figure A-6 Fluorescence images at base potential for reductive desorption of C16 thiol with 'base-step' potential profile. A brightfield image of the electrode for orientational reference is included on the right. Images have been enhanced for clarity. Modifications to grayscale may not be linear.
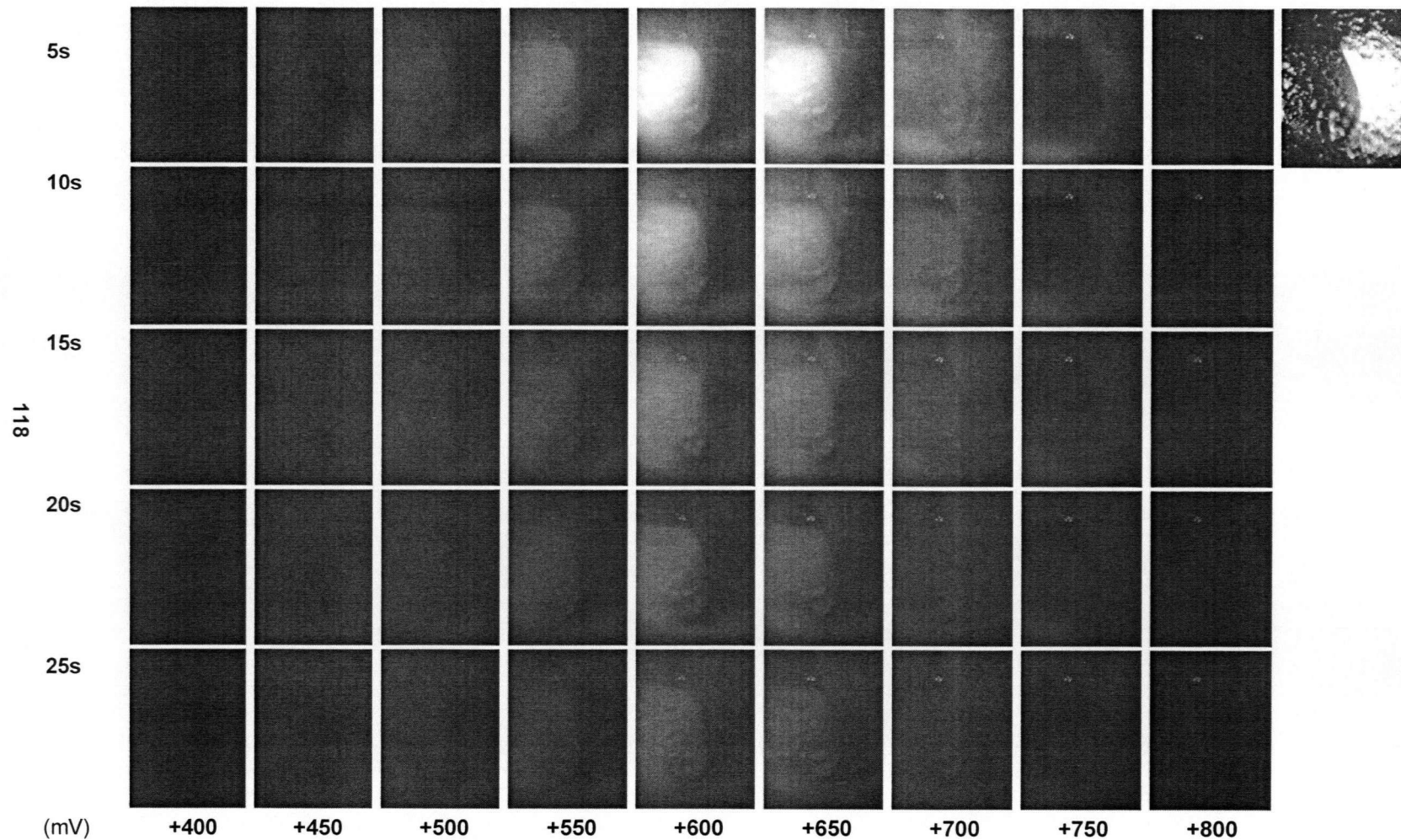
Figure A-7 Fluorescence images at step potential for oxidative desorption of C10 thiol at pH 10±1. A brightfield image of the electrode for orientational reference is included on the right. Images have been enhanced for clarity. Modifications to grayscale may not be linear.
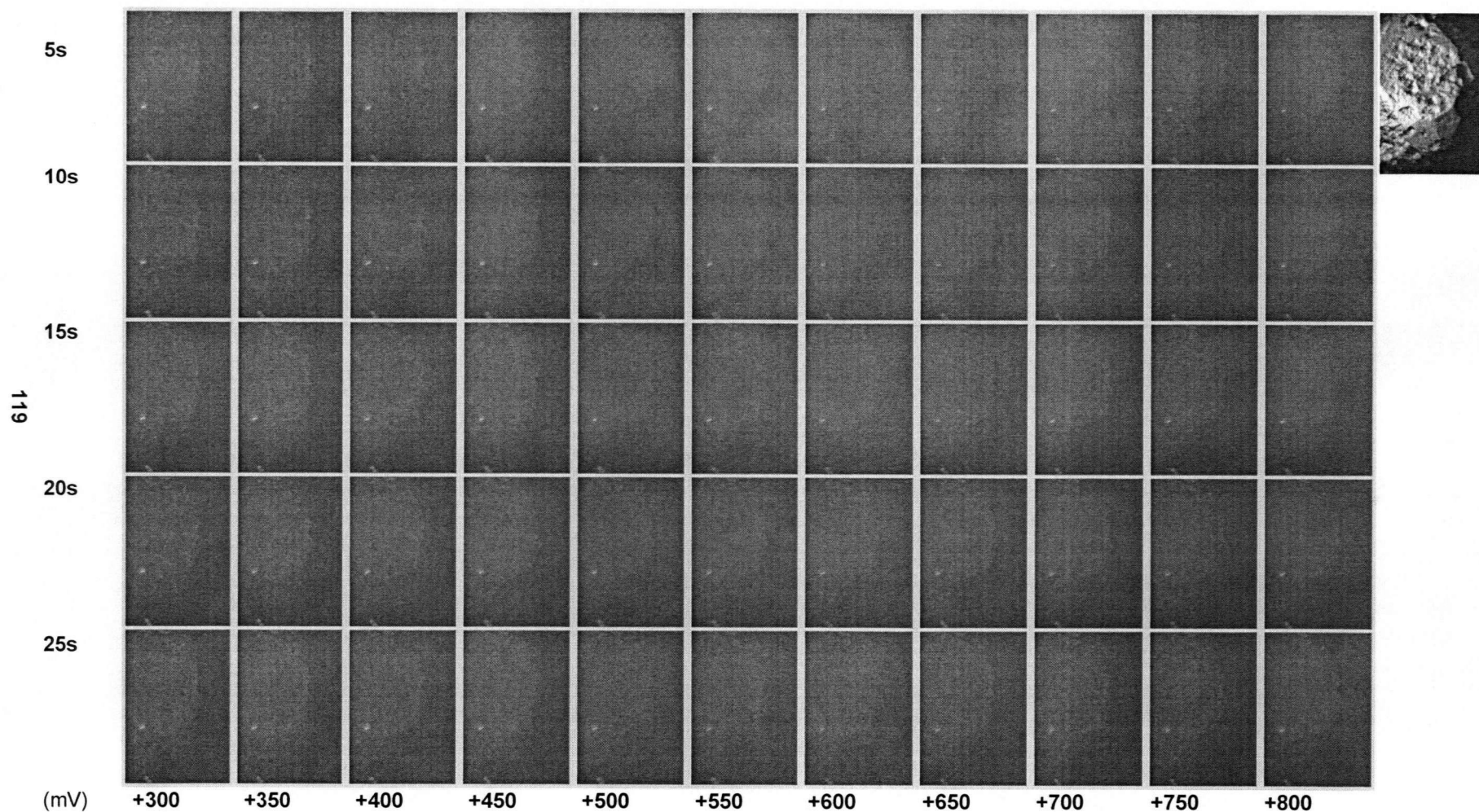
Figure A-8 Fluorescence images at base potential for oxidative desorption of C10 thiol at pH 10±1. A brightfield image of the electrode for orientational reference is included on the right. Images have been enhanced for clarity. Modifications to grayscale may not be linear.

Figure A-9 Fluorescence images at step potential for oxidative desorption of C16 thiol at pH 10±1. A brightfield image of the electrode for orientational reference is included on the right. Images have been enhanced for clarity. Modifications to grayscale may not be linear.
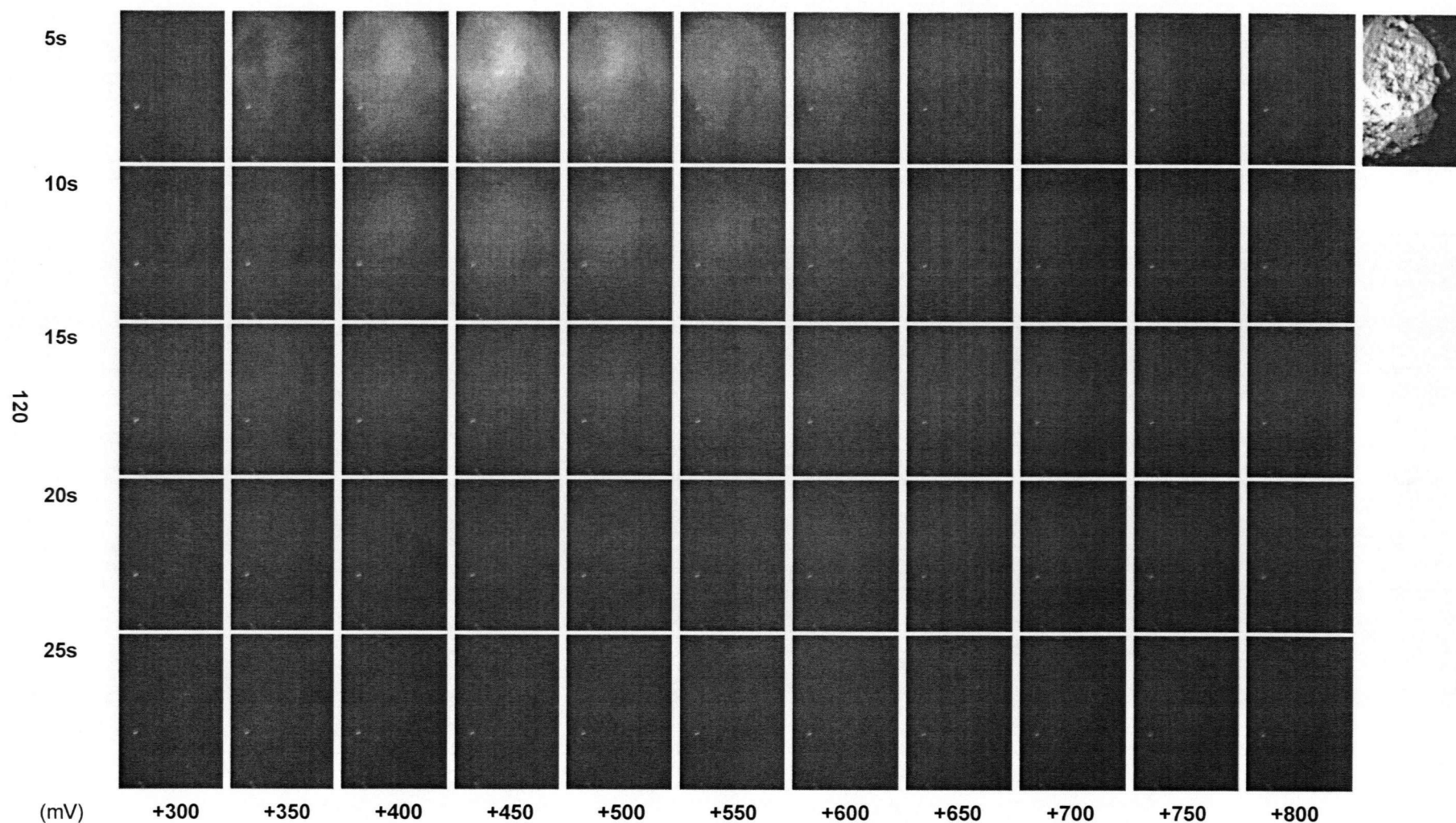
Figure A-10 Fluorescence images at base potential for oxidative desorption of C16 thiol at pH 10±1. A brightfield image of the electrode for orientational reference is included on the right. Images have been enhanced for clarity. Modifications to grayscale may not be linear.
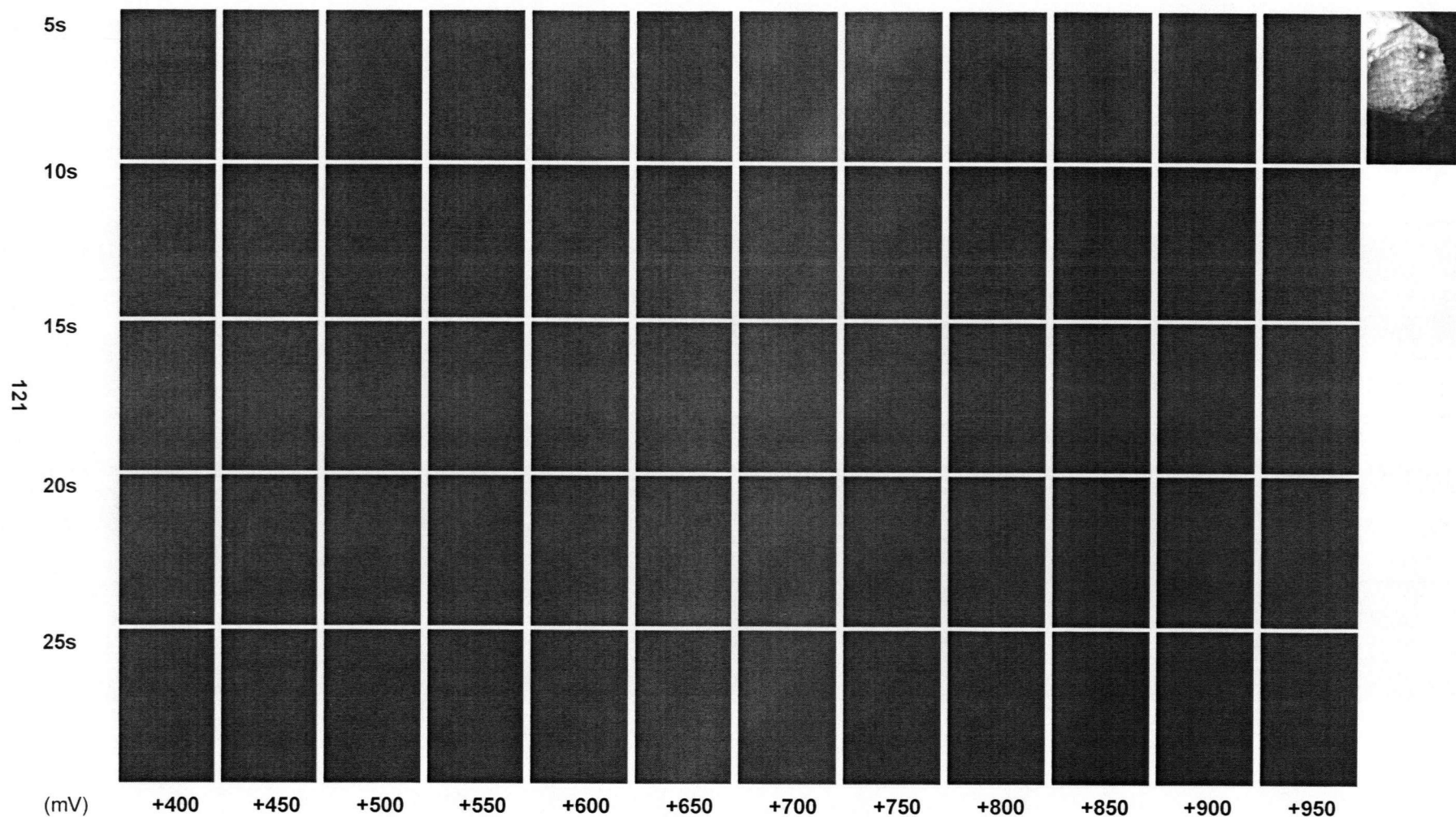
Figure A-11 Fluorescence images at step potential for oxidative desorption of C10 thiol at pH 5±0.5. A brightfield image of the electrode for orientational reference is included on the right. Images have been enhanced for clarity. Modifications to grayscale may not be linear.

Figure A-12 Fluorescence images at base potential for oxidative desorption of C10 thiol at pH 5±0.5. A brightfield image of the electrode for orientational reference is included on the right. Images have been enhanced for clarity. Modifications to grayscale may not be linear.
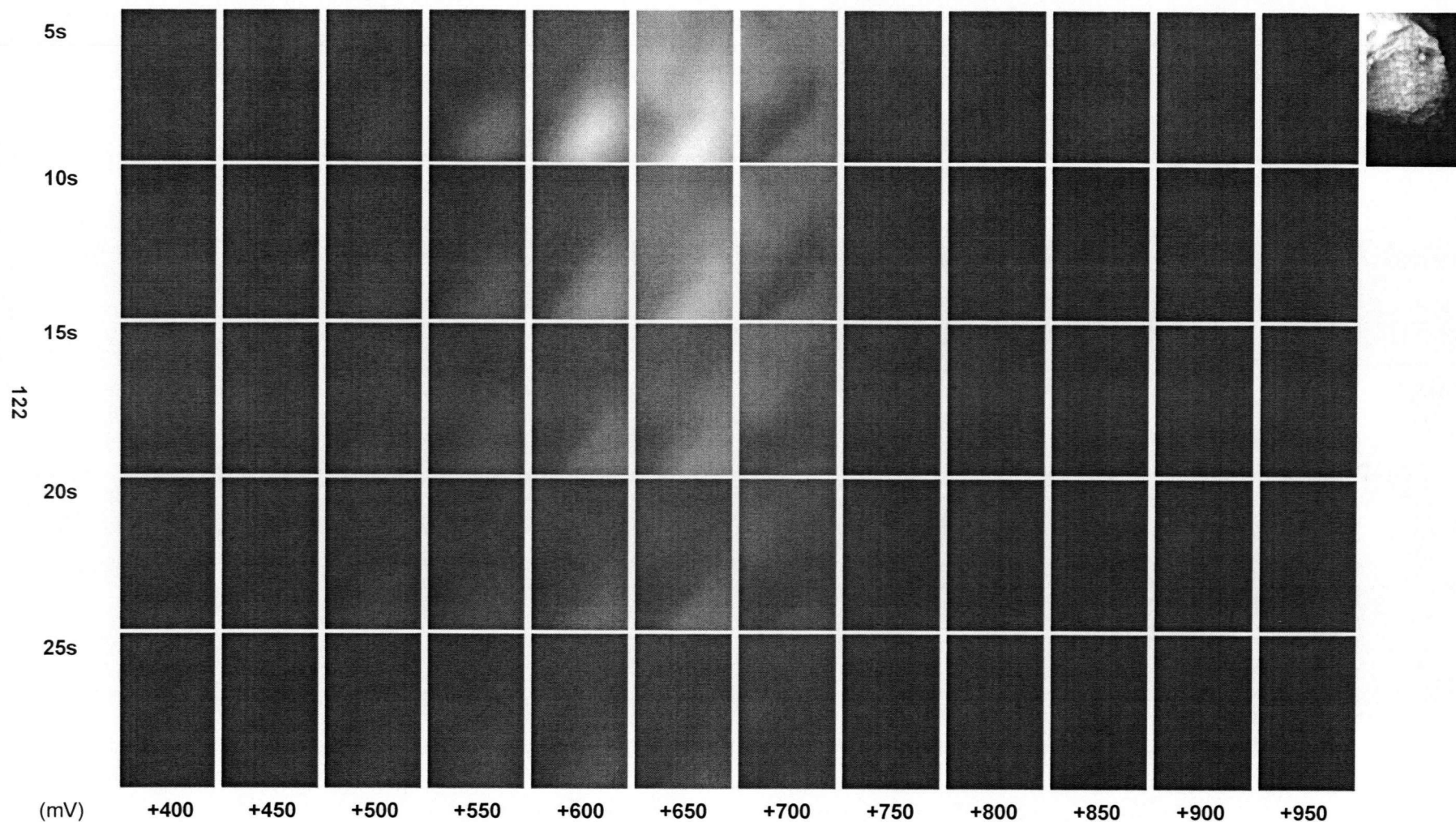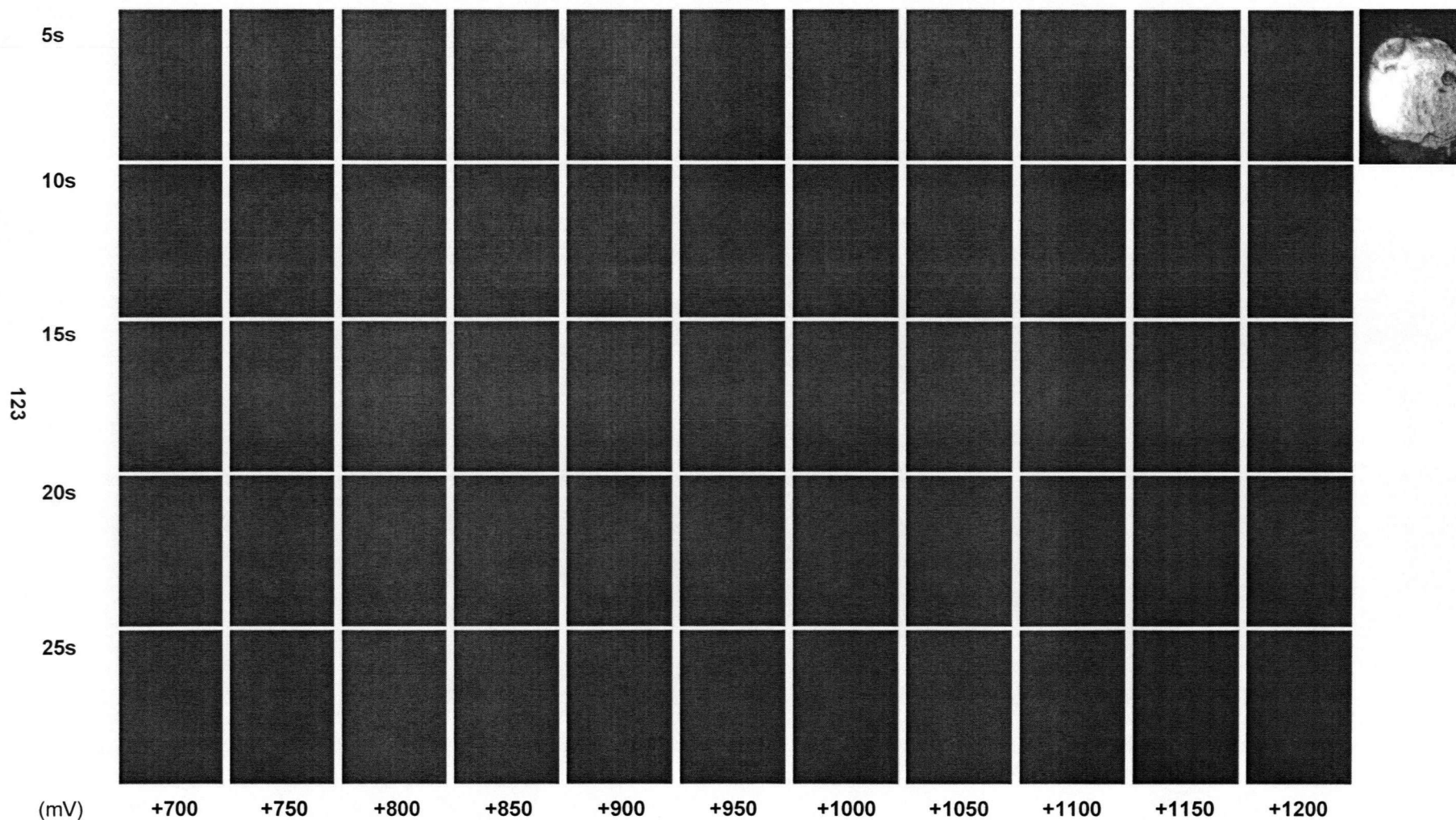
	+700	+750	+800	+850	+900	+950	+1000	+1050	+1100	+1150	+1200
5s											
10s											
15s											
20s											
25s											

(mV)

Figure A-13 Fluorescence images at step potential for oxidative desorption of C16 thiol at pH 5±0.5. A brightfield image of the electrode for orientational reference is included on the right. Images have been enhanced for clarity. Modifications to grayscale may not be linear.
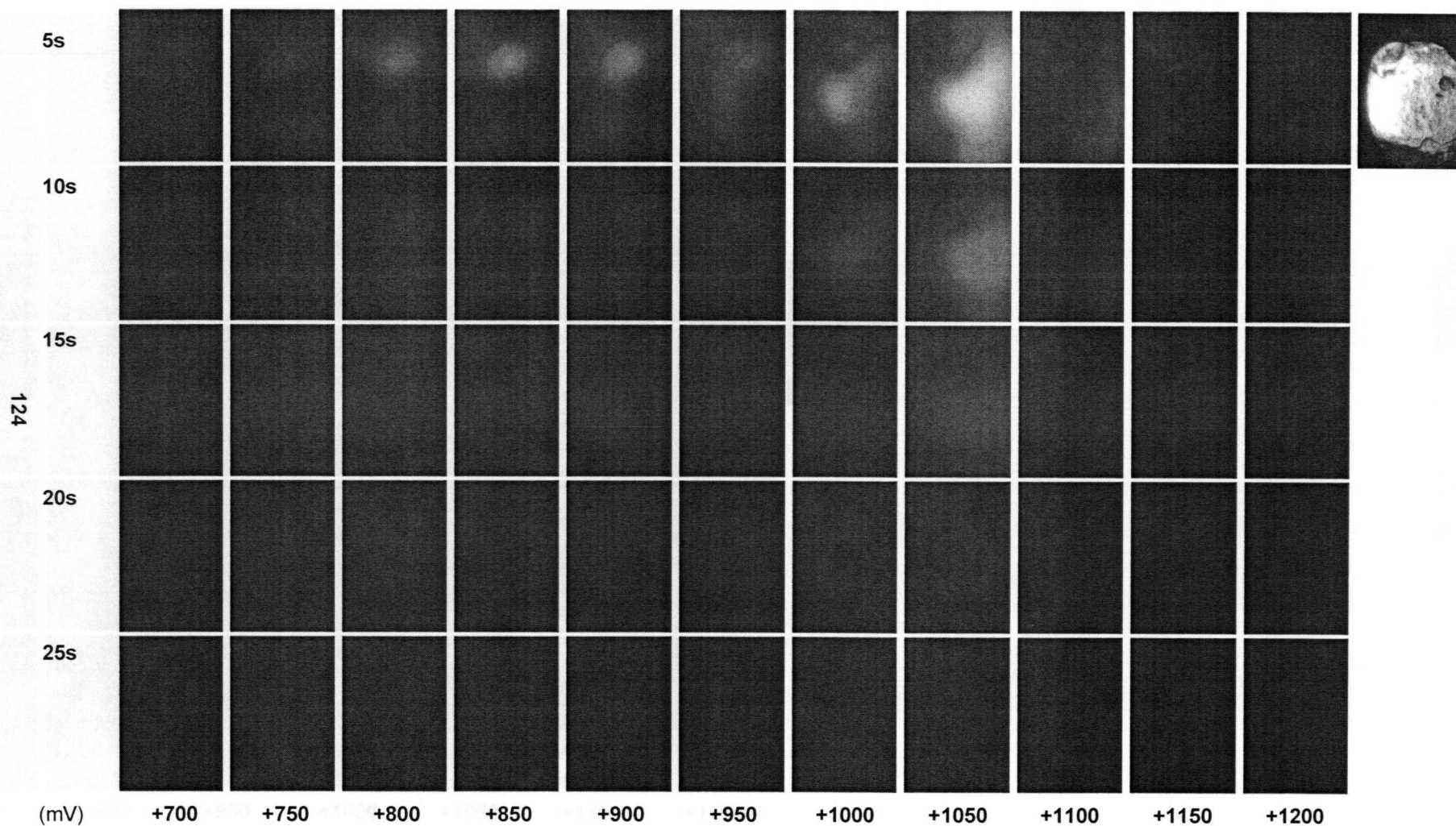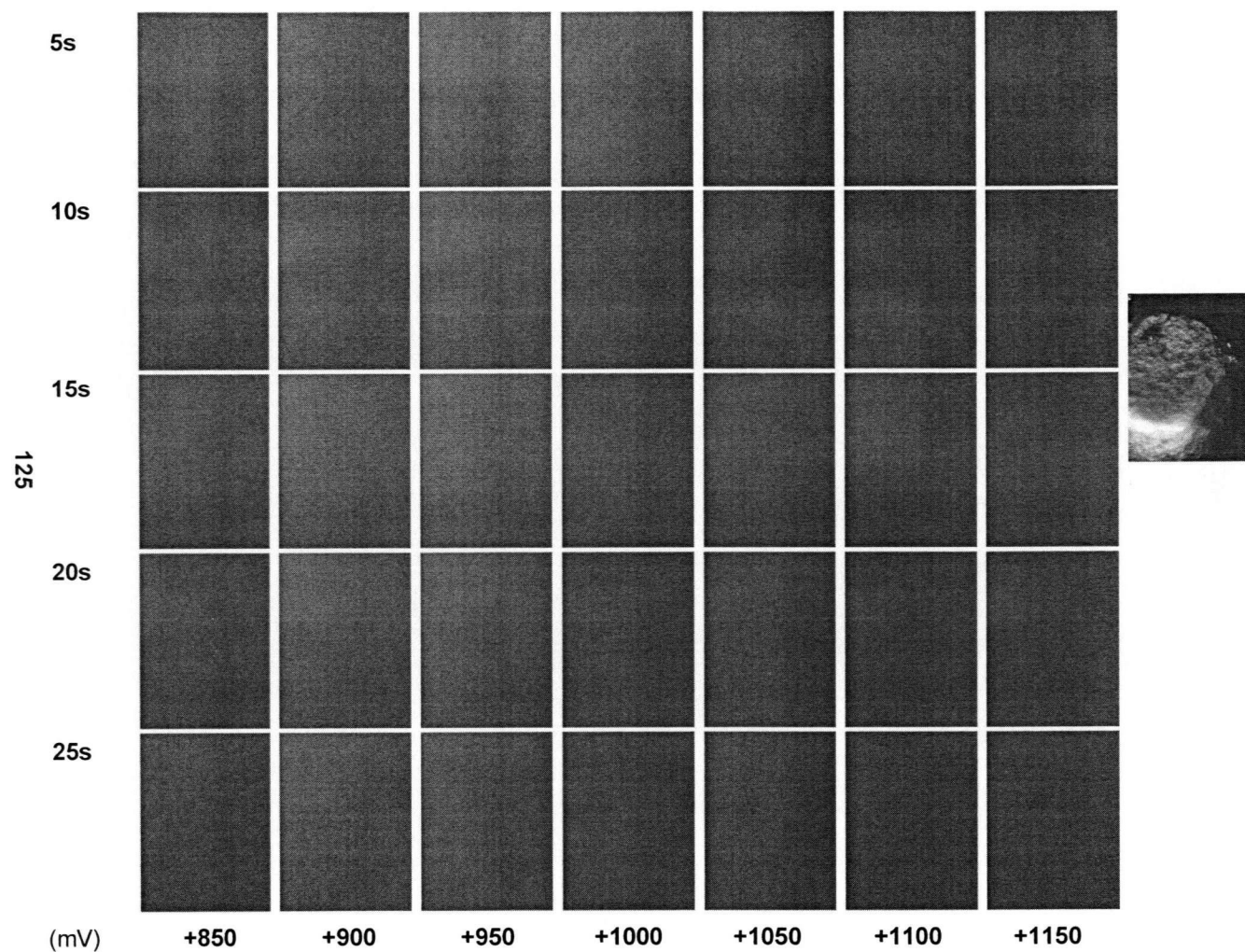
123

Figure A-14 Fluorescence images at base potential for oxidative desorption of C16 thiol at pH 5±0.5. A brightfield image of the electrode for orientational reference is included on the right. Images have been enhanced for clarity. Modifications to grayscale may not be linear.

Figure A-15 Fluorescence images at step potential for oxidative desorption of C10 thiol at pH 2±0.5. A brightfield image of the electrode for orientational reference is included on the right. Images have been enhanced for clarity. Modifications to grayscale may not be linear.
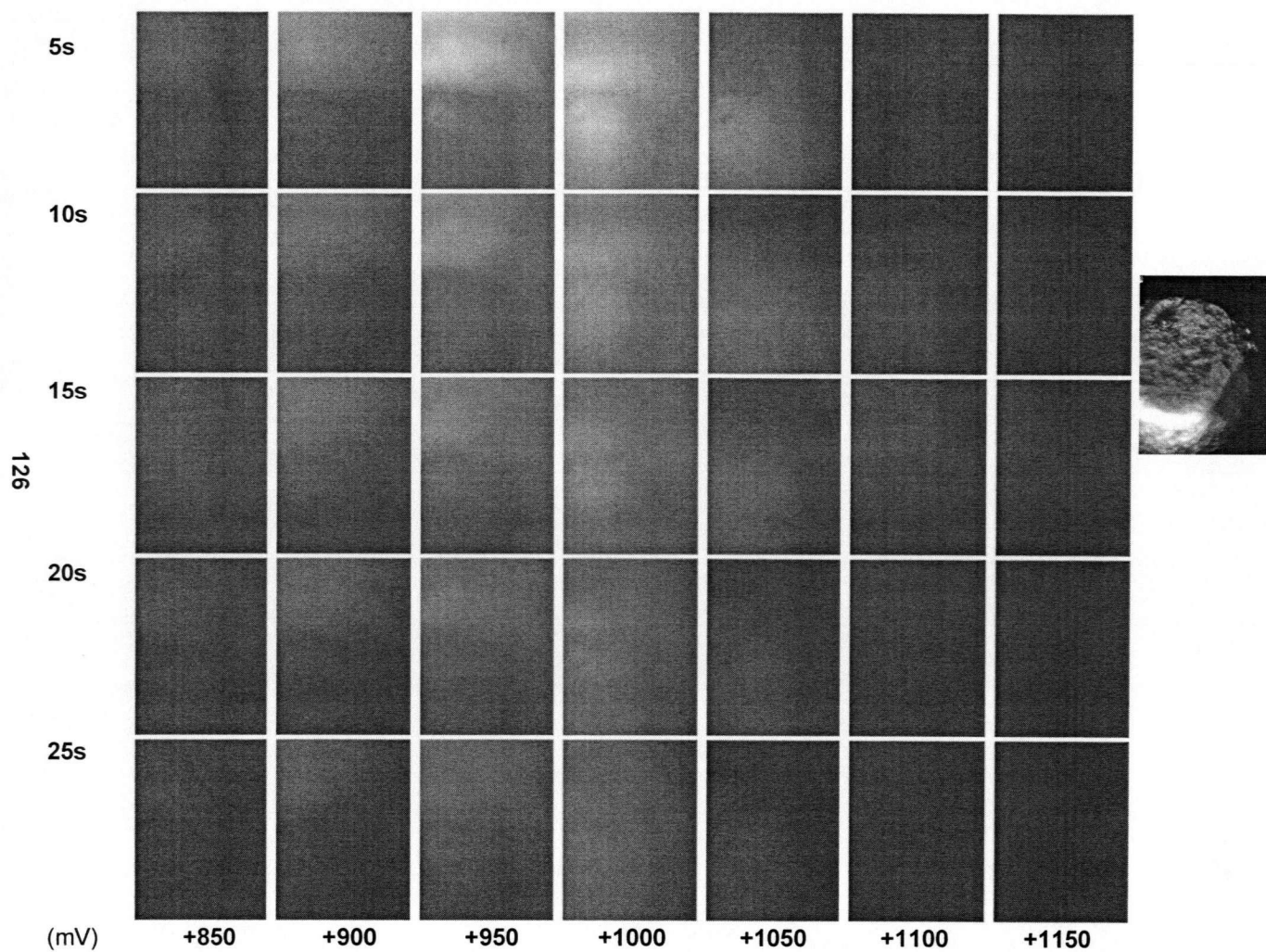
Figure A-16 Fluorescence images at base potential for oxidative desorption of C10 thiol at pH 2±0.5. A brightfield image of the electrode for orientational reference is included on the right. Images have been enhanced for clarity. Modifications to grayscale may not be linear.
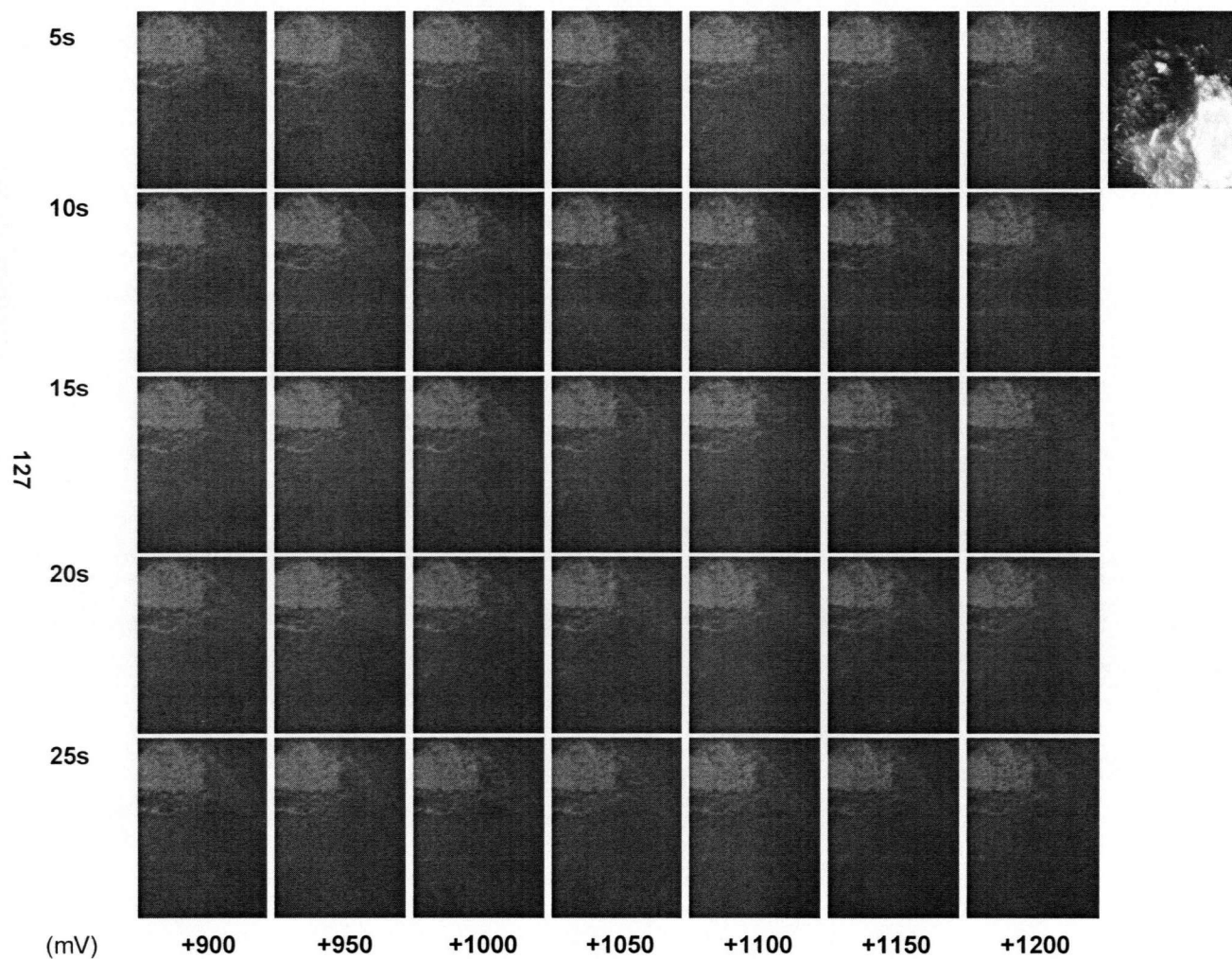
Figure A-17 Fluorescence images at step potential for oxidative desorption of C16 thiol at pH 2±0.5. A brightfield image of the electrode for orientational reference is included on the right. Images have been enhanced for clarity. Modifications to grayscale may not be linear.
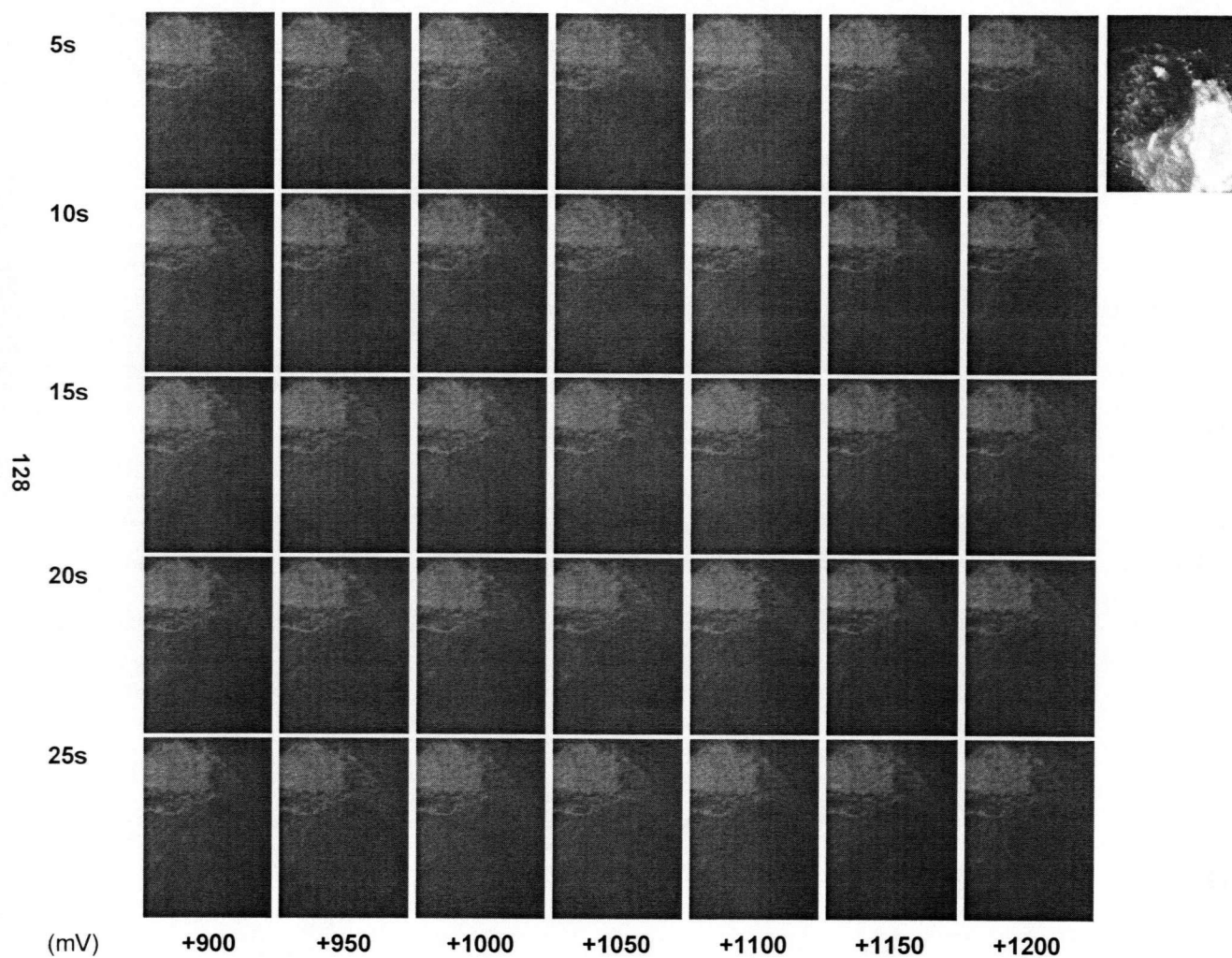
Figure A-18 Fluorescence images at base potential for oxidative desorption of C16 thiol at pH 2±0.5. A brightfield image of the electrode for orientational reference is included on the right. Images have been enhanced for clarity. Modifications to grayscalemay not be linear.